S.S. SAMATAR

EXTERNAL STEEL BRACE STRENGTHENING OF RC BUILDINGS HAVING REMOVED COLUMNS

THE GRADUATE SCHOOL OF NATURAL AND APPLIED SCIENCES
OF
ATILIM UNIVERSITY

SULAIMAN SALAD SAMATAR

A MASTER OF SCIENCE THESIS
IN
THE DEPARTMENT OF CIVIL ENGINEERING

OCTOBER 2023

ATILIM UNIVERSITY 2023

EXTERNAL STEEL BRACE STRENGTHENING OF RC BUILDINGS HAVING REMOVED COLUMNS

A THESIS SUBMITTED TO
THE GRADUATE SCHOOL OF NATURAL AND APPLIED SCIENCES
OF
ATILIM UNIVERSITY

BY

SULAIMAN SALAD SAMATAR

IN PARTIAL FULFILLMENT OF THE REQUIREMENTS
FOR
THE DEGREE OF MASTER OF SCIENCE
IN
THE DEPARTMENT OF CIVIL ENGINEERING

OCTOBER 2023

Approval of the Graduate School of Natural and Applied Sciences, Atılım University.

_____

Prof. Dr. Ender KESKİNKILIÇ
Director

I certify that this thesis satisfies all the requirements as a thesis for the degree of **Master of Science in Civil Engineering Department, Atılım University**.

_____

Prof. Dr. Yakup DARAMA
Head of Department

This is to certify that we have read the thesis "External Steel Brace Strengthening of RC Buildings Having Removed Columns" submitted by SULAIMAN SALAD SAMATAR and that in our opinion it is fully adequate, in scope and quality, as a thesis for the degree of Master of Science.

_____

Assist. Prof. Dr. Halit Cenan MERTOL
Supervisor

Examining Committee Members:

Prof. Dr. Tolga AKIŞ
Civil Eng. Department, Atılım University _____

Assist. Prof. Dr. Halit Cenan MERTOL
Civil Eng. Department, Atılım University _____

Assoc. Prof. Dr. Rıza Secer Orkun KESKİN
Civil Eng. Department, TED University _____

Date: *9th of October, 2023*

I hereby declare that all information in this document has been obtained and presented in accordance with academic rules and ethical conduct. I also declare that, as required by these rules and conduct, I have fully cited and referenced all material and results that are not original to this work.

Name, Last Name: Sulaiman Salad SAMATAR

Signature:

ABSTRACT

EXTERNAL STEEL BRACE STRENGTHENING OF RC BUILDINGS HAVING REMOVED COLUMNS

Samatar, Sulaiman Salad
M. S., Department of Civil Engineering
Supervisor: Asst. Prof. Halit Cenan Mertol
October 2023, 132 pages

The vertical load carrying members (columns) in a building may be damaged by earthquakes or other sources during the service life. Users of these buildings may also remove those structural members to get more space in plan-view. These deficient buildings (buildings having less columns than they were designed for) shall be strengthened economically and fast to avoid collapse during a future earthquake if not collapsed.

The objective of this study is to evaluate the performance of an economical and fast strengthening method, namely external steel bracing strengthening, of RC buildings which had lost some of its columns due to any reason. For this purpose, models of RC buildings having varying story numbers, specifically 3, 6, 9, and 12 were produced. These buildings were initially properly designed based on current specifications used in Turkey. Some of the columns of the models were removed and the buildings became deficient. These deficient buildings were then strengthened using two different configurations of external steel braces (inverted V- and X-Type) to achieve a sufficient building under the applied loads. The efficiency of this strengthening method was assessed using three different analysis methods, namely equivalent earthquake load, pushover analysis, and time-history analysis method. The results indicated that the deficient building models could be strengthened using external steel braces and modelled effectively by all three models except for the 12-story model results were conflicting for pushover analysis method.

Keywords: Reinforced concrete buildings, loss of columns, strengthening using external steel braces, equivalent earthquake load method, pushover analysis, time-history analysis.

ÖZ

KOLONLARI KESİLMİŞ BETONARME BİNALARIN ÇAPRAZ ÇELİK PROFİLLERLE GÜÇLENDİRİLMESİ

Samatar, Sulaiman Salad
Yüksek Lisans, İnşaat Mühendisliği Bölümü
Tez Yöneticisi: Dr. Öğr. Üyesi Halit Cenan Mertol
Ekim 2023, 132 sayfa

Bir binadaki düşey yük taşıyan elemanlar (kolonlar), binanın kullanım ömrü boyunca deprem veya diğer nedenlerden dolayı hasar görebilir. Bu tip binaların kullanıcıları, plan alanını büyütmek amaçlı, bu yapısal elemanları da kaldırmış olabilirler. Bu eksik binalar (tasarlandığındaki kolonlardan daha az sayıda kolona sahip binalar), yıkılmadıkları takdirde, ileride meydana gelebilecek bir depremde yıkılmalarını önlemek için, ekonomik ve hızlı bir şekilde güçlendirilmelidir.

Bu çalışmanın amacı, herhangi bir nedenden dolayı kolonlarının bir kısmını kaybeden betonarme binaların, ekonomik ve hızlı bir güçlendirme yöntemi olan dıştan çelik çaprazlarla güçlendirilmesinin performansının değerlendirilmesidir. Bu amaçla 3, 6, 9, 12 olmak üzere farklı kat sayılarına sahip betonarme binaların modelleri hazırlanmıştır. Bu binalar başlangıçta Türkiye'de kullanılan mevcut yönetmeliklere göre uygun şekilde tasarlanmıştır. Modellerin bazı kolonları kaldırılarak, binalar yetersiz hale getirilmiştir. Bu yetersiz binalar, iki farklı dış çapraz çelik profil konfigürasyonu (ters V ve X Tipi) kullanılarak güçlendirilmiştir. Bu güçlendirme yönteminin verimliliği, eşdeğer deprem yükü, itme analizi ve zaman tanım alanı analizi yöntemi olmak üzere üç farklı analiz yöntemi kullanılarak değerlendirilmiştir. Sonuçlar, yetersiz bina modellerinin dış çelik çaprazlar kullanılarak güçlendirilebileceğini ve 12 katlı model sonuçlarının itme analizi yöntemi için çelişkili olması dışında her üç modelle de etkili bir şekilde modellenebileceğini göstermiştir.

Anahtar Kelimeler: Betonarme binalar, kolon kaybı, dış çapraz çelik profillerle güçlendirme, eşdeğer deprem yükü yöntemi, itme analizi, zaman tanım alanında deprem yer hareketi analizi.

ACKNOWLEDGMENTS

I would like to express my heartfelt gratitude to my supervisor, Assist. Prof. Dr. Halit Cenan Mertol, for his patience and unwavering support throughout my journey to complete my thesis. Without him, this would not be possible.

Also, I would like to express my appreciation to my mother and siblings for their support and encouragement throughout the academic journey.

And finally, my special thanks to all my teachers and lecturers who their knowledge and guidance have been invaluable.

TABLE OF CONTENTS

LIST OF FIGURES

LIST OF TABLES

CHAPTER 1

INTRODUCTION

1.1 Problem Statement

A crucial load-bearing component like column may fail as a result of an intense loading event, a gas explosion in the building like the Ronan Point apartment in 1968 Pearson and Delatte [1] or attack on building like Murrah Federal Building attack in 1995 Lu and Wu [2]. Column loss due to a disastrous event may happen based on a variety of reasons. One of the reasons for this loss may be due to the devastating impact of earthquakes.

Turkey frequently experiences earthquakes due to its orientation on several seismic fault lines as shown in Figure 1.1. Over the past century alone, there have been hundreds of earthquakes and aftershocks, 15 of which were of greater magnitude than 7 AFAD [3]. As a result, Turkey is among the world nations with the severest earthquakes. Recently, in February 2023 Kahramanmaraş earthquake of 7.8 and 7.5 magnitude shook central and southern provinces of Turkey. The devastation caused by these earthquakes led to tragic loss of many human lives as well as inflicting severe damage upon infrastructure and particularly buildings. The earthquakes had extensive effects on buildings. A total of 704,281 buildings were affected across the 11 provinces. The damage levels ranged from lightly damaged to collapse AFAD [3]. A total of 1,031.9 billion TRY which is equal to 54.7 billion USD, was lost solely due to the damage and collapse of the buildings AFAD [3]. In the earthquake affected regions, 86.7% of those buildings were reinforced concrete (RC) buildings AFAD [3]. Buildings constructed using RC are commonly used throughout the world, due to the low cost and wide availability of required materials. These structures, if designed accordingly, can resist various types of loads such as dead, live, snow, wind, earthquake, etc. At extreme loading conditions, the RC buildings may suffer damage at different levels. These buildings shall be strengthened before use or demolished

based on economic considerations. One example of a building damaged during Kahramanmaraş earthquakes is shown in Figure 1.2.

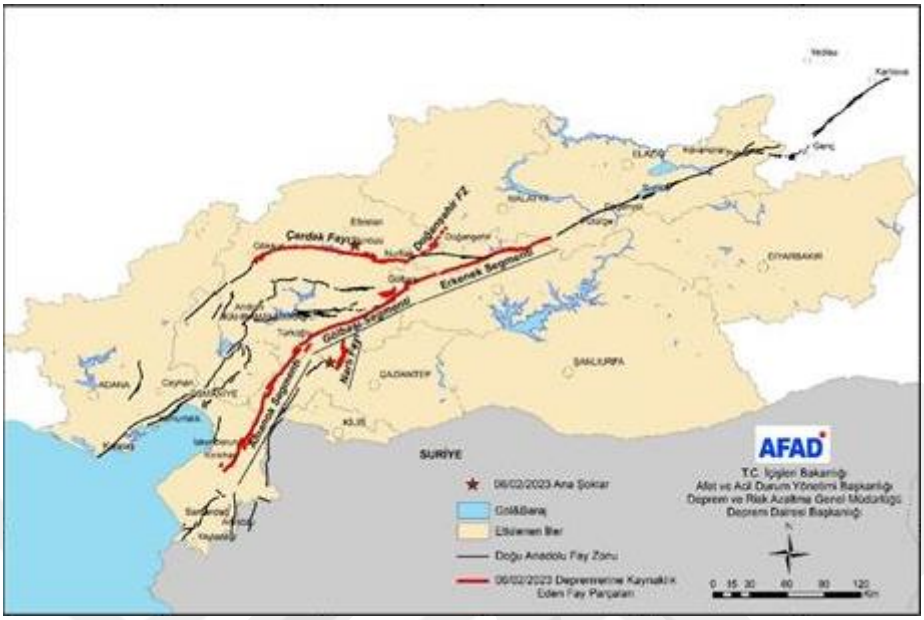

Figure 1.1 Fault Lines in Turkey, AFAD [3]

Figure 1.2 Damaged Building By Earthquake in Kahramanmaraş Province, TRTHABER [4]

Considering the substantial number of damaged buildings in an earthquake, the scarcity of time, and high cost of reconstructing them all, there is a need for a fast, effective, and economical seismic strengthening method for these buildings. Many studies were performed to evaluate the most effective method to strengthen damaged

buildings. One of the feasible solutions is to strengthen these buildings using steel braces on the faces of the buildings.

This study focuses on strengthening RC buildings using external steel braces that experienced column loss due to any reason. Esmaeili et al. [5] concluded that proper external bracing designs may improve lateral resistance and reduce the effects of internal forces on beams and columns.

1.2 Objective and Scope

The main load carrying members (column) in a building may be damaged by earthquakes or other sources during the service life. Users of these buildings may also remove those structural members to get more space in plan-view. These deficient buildings (buildings having less columns than they were designed for) shall be strengthened economically and fast to avoid collapse during a future earthquake if not collapsed. The objective of this study is to evaluate the performance of an economical and fast strengthening method, namely external steel bracing strengthening, of RC buildings which had lost some of its columns due to any reason.

The models of RC buildings used in the research had varying story numbers, specifically 3, 6, 9, and 12. These buildings were initially properly designed based on current specifications used in Turkey. Some of the columns of the models were removed and the buildings became deficient. These deficient buildings were strengthened using external steel braces to achieve a sufficient building under the applied loads. SAP2000 Structural Software [23]-[24] was used for the analysis and design of these buildings to evaluate the performance of the steel bracing strengthening method. The efficiency of this strengthening method was assessed using three different analysis methods, namely equivalent earthquake load, pushover analysis, and time-history analysis method. The steel bracing system was designed according to AISC 360-10 [6].

1.3 Organization Of The Dissertation

This thesis is composed of 5 chapters. Chapter 1 outlines the need for a fast and economic strengthening method for RC buildings. The objective of this thesis is also summarized in this chapter.

A comprehensive literature review on the past studies related to strengthening using external steel braces is discussed in Chapter 2.

In Chapter 3, the building models, loadings, and analysis methods used in the research are explained in detail. The designs of the proper, deficient, and strengthened buildings are also performed in this chapter.

The results of the analysis of strengthening method based on equivalent earthquake load, pushover analysis, and time-history analysis method are explained in Chapter 4. This chapter also includes a detailed discussion of these results.

The final chapter, Chapter 5, supplies a summary of this research, discusses the findings of analysis, and recommends guidelines for future research related to the application of external steel braces as an effective tool for strengthening purposes.

CHAPTER 2

LITERATURE REVIEW

Maheri and Sahebi [7] tested four RC frames strengthened using various steel diagonal bracing arrangements to determine the effectiveness of strengthening for in-plane shear. Proper connection details related to steel braces and the concrete frame were also considered. The test results indicated that significant improvement was achieved in in-plane shear strength of strengthened frames. X-bracing system performed a better behavior than that of single diagonal brace. The failure of the X-braced test specimen initiated by the failure of tension brace and then with the compression brace. The connection between the steel brace and RC frame played an important role on the overall efficiency of the bracing system. It was concluded that the X-bracing system might strengthen RC-framed structures effectively.

Esmaeili et al. [5] performed analyses to evaluate the seismic performance of steel moment-resisting frames (MRF) combined with RC shear walls and steel MRF coupled with concentrically X-braced frames. The models were analyzed using pushover analysis with both the uniform nonlinear static and triangular nonlinear static procedures. Two models were used in this study namely, a 30-story residential building constructed with RC shear walls and special steel MRF and a 30-story residential building with special steel MRF and concentrically steel x-braced frames. The models had composite RC slabs and secondary steel beams. It was concluded that special steel MRF accompanied with RC shear wall system performed better than special steel MRF accompanied with concentrically steel x-braced frames.

Nandi and Hiremath [8] performed a parametric study to investigate the effects of eccentric Y-type steel bracing system on non-ductile RC buildings. Pushover analysis was performed on 2-D 10-, 15-, and 20-story 5-bay RC building models using SAP2000 Structural Software [23]-[24]. Variables such as distribution of steel bracing over the height of RC frame and link length of eccentric bracing were studied. The results were evaluated based on energy absorption capacity, stiffness of frame and

ductility. Analysis results indicated that eccentric-braced frames absorbed more energy compared to bare frames. It was concluded that eccentrically braced frames were suitable for up to 15-story buildings in seismic regions to reduce the seismic hazards efficiently. However, the importance of choosing the right seismic strengthening configurations to balance stiffness, ductility, and energy absorption capacity was also emphasized.

Yu et al. [9] conducted a study to investigate the progressive collapse resistance of RC frames retrofitted with steel bracing. A retrofitting approach using steel braces for improving robustness of RC bare frames was proposed. The finite element models of this approach were constructed using Opensees Software and calibrated using the results of experiments performed by Qian et al. [22]. The calibrated models were used to investigate the effects of the constraints of braces, the locations of the braced story, and the removed column(s) (single-column removal and two-adjacent-column removal scenarios) on the progressive collapse resistance of the planar frames. The results indicated that it was necessary to strengthen the bare frame using steel bracing when two-adjacent-column were removed. The design procedure of steel bracing with eccentric x-braces was proposed. It was concluded that eccentric x-braces shall be used in the design of the top story. These retrofitted frames had shown strong resistance to progressive collapse.

Boru and Aydin [10] investigated the effect of different types of steel braces specified in TBEC [15] on strengthening regular RC buildings against earthquake forces. A 2-D 9-storey RC frame model having three spans was produced and was strengthened using diagonal, X-, inverted V-, V-, and K-type bracings. Circular and rectangular steel sections were used for bracing systems. Pushover analyses of the models were conducted using SAP2000 Structural Software [23]-[24] to determine the most effective braces on seismic behavior. The findings were compared in terms of stiffness, interstory drift, and displacement values. The results indicated that X- and K-bracing types produced the most rigid models compared to other types. The lowest displacement demands were obtained in circular section K-braced model. When interstory drift values were compared, circular hollow steel sections used in bracing

systems provided the lowest drift ratios in all the models compared to rectangular steel sections.

Erpek [11] conducted a parametric study to examine the effectiveness of external strengthening using steel braces for existing deficient RC buildings. Four 3-D building models having 3, 6, 9, and 12 stories having column deficiencies were strengthened using two different configurations of bracing system. The models were analyzed using Equivalent Static Earthquake Load, Pushover Analysis, and Time History Analysis Method. The results indicated inverted V-type external bracing system might be used to effectively strengthen the deficient buildings up to 12 stories. X-type bracing system was efficient for buildings up to 9 stories.

CHAPTER 3

DESCRIPTION OF MODELS

3.1 General

This chapter describes the properties of the models used in this study to evaluate the performance of external steel bracing system in RC buildings with column failure or loss due to any reason. Four models were produced having different number of stories (3, 6, 9, and 12). These number of stories were selected since 90.5% of the buildings in Turkey had a number of stories less than 10 according to TurkStat [12]. Therefore, this study is focused on low- to mid-rise buildings.

All the building models had a uniform story height of 3 meters. The total heights of the building models with 3, 6, 9, and 12 stories were 9, 18, 27, and 36 m, respectively. The models had a square plan view having 30 m in length in both directions. There were 5 bays having equal lengths (6 m) in both x- and y-directions. The plan view area per story was 900 m^2 for all the models. The plan view of the models is shown in Figure 3.1.

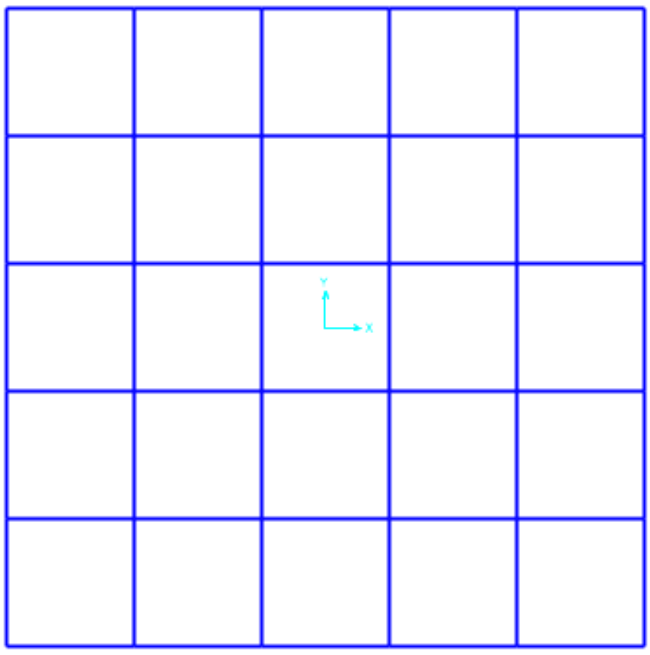

Figure 3.1 Plan View of the Model

3.2 Assumptions

The following assumptions were made in this study:

- Üsküdar, İstanbul was selected as the location of the building models. This location was selected to obtain a large level of earthquake loads to better evaluate the effectiveness of external steel braces.
- ZC site class was selected for the type of soil under the building models. This type of site class represents very dense soil and soft rock.
- Connections between reinforced concrete beam-column connections and external structural steel sections were assumed to be rigid.
- The moment of inertias of the RC structural members in the analysis were not reduced. As a result, the deflection of the deficient building decreased. For the strengthened buildings, the deflection of was controlled by the steel braces. Therefore, it can be concluded that the unreduced moment of inertia did not have any significant effects in the analysis and design.
- All the stories of the building models were modelled as rigid diaphragms. The distributed seismic loads obtained from equivalent earthquake load method were applied at the mass center of each story.
- The foundations of the building models were assumed to be fully fixed. Joints of the models at the foundation level were assigned as fixed and restrained in all directions.

3.3 Materials

3.3.1 RC

To simulate the behavior of an existing building constructed before 2000's, low strength concrete and steel were used in this study. Concrete class C16 having a compressive strength of 16 MPa and S220 steel type having a yield tensile strength of 220 MPa (both for transverse and longitudinal reinforcement) was used in all the models. The characteristics of concrete and steel reinforcement used in the building models are shown in Table 3.1 and Table 3.2. The unit weight of the combination of these two materials was equal to 25 kN/m^3 in all the models.

Table 3.1 Concrete Characteristics of Model

Concrete Class	Characteristic Compressive Strength f_{ck} (MPa)	Equivalent Cube Compressive Strength (MPa)	Characteristic Tensile Strength f_{ctk} (MPa)	Elastic Modulus E_c (MPa)
C16	16	20	1.4	27000

Table 3.2 Steel Reinforcement Characteristics of Model

Mechanical Characteristics	Values (MPa)
Characteristic Yield Strength, f_{yk}	220
Ultimate Strength, f_{su}	340
Elastic Modulus, E_s	200000

3.3.2 Steel Braces

A992Fy50 grade steel was used for the material of external steel braces. The characteristics and properties of this material were obtained from ASTM A992 [13] as shown in Table 3.3. Three different steel sections were used for steel braces based on the results of the design iterations. H400×237 steel section was used for beams and columns of the bracing system. HE160A and HE180A were used for the diagonal elements of the system. Dimensional properties of these steel sections are shown in

Table 3.4.

Table 3.3 External Steel Characteristics

Mechanical Characteristics	Values (MPa)
Modulus of elasticity, E=	200000
Minimum Yield Stress=	345
Minimum Tensile Stress=	448

Table 3.4 Steel Braces Properties

Section	t_3 (m)	t_2 (m)	t_f (m)	t_w (m)	t_{2b} (m)	t_{fb} (m)
H400×237	0.381	0.395	0.0305	0.0185	0.395	0.0305
HE160A	0.152	0.16	0.009	0.006	0.16	0.009
HE180A	0.171	0.18	0.0095	0.006	0.18	0.0095

3.4 Section Properties

In this section, the properties related to the beam, column, and slab sections are explained.

3.4.1 Beams

Initial dimensions of the beams were selected using the information provided in TS500 [14] shown in the Table 3.5. The selected dimensions were checked using the SAP2000 Structural Software [23] and final dimensions of the beams were determined as shown Table 3.6. The beam dimensions were varying in models since these dimensions were also affected by the column dimensions. The beam widths were determined to be smaller or equal to the least dimension of column in the building model.

Table 3.5 Beam Dimensions Criteria in TS 500 [14]

Member	Simple Span	Exterior Span	Interior Span	Cantilever
One-way Slab	L/20	L/25	L/30	L/10
Two-way Slab	L/25	L/30	L/35	-
Joist Slab	L/15	L/18	L/20	L/8
Beam	L/10	L/12	L/15	L/5

Table 3.6 Column Dimensions of Each Model

Model	Depth (mm)	Width (mm)
301	70	30
601	65	45
901	65	50
1201	65	50

3.4.2 Columns

The columns in the models of the buildings were defined based on their location in the building as corner, edge, and inner columns. All columns in the models were square in shape and their sizes vary depending on their location in the building. Corner columns had the smallest cross-sectional area whereas inner columns had the largest cross-sectional area. The dimensions of the columns were determined using the expression (Equation 3-1) provided by the TBEC [15]. In this equation, A_c is defined as the column cross-sectional area, N_{dm} is defined as the largest axial load effect under the vertical and earthquake loads, and f_{ck} is defined as the characteristic concrete compressive strength. The dimensions of the columns in the building models are shown in Table 3.7.

$$A_c = N_{dm}/(0.4 \times f_{ck}) \quad \text{Equation 3-1}$$

Table 3.7 Cross-Section Dimensions of Columns in Building Models

Building Models	Cross-sectional Dimensions (mm×mm)		
	Corner Columns	Edge Columns	Inner Columns
3-Story Building	300×300	450×450	600×600
6-Story Building	450×450	650×650	800×800
9-Story Building	600×600	800×800	1000×1000
12-Story Building	750×750	950×950	1200×1200

3.4.3 Slab

Equation 3-2 specified in TS500 [14] was used to determine the slab thickness. The slab thickness was calculated as 150 mm for all the building models as shown in Table 3.8.

$$h \geq \frac{l_{sn}}{15 + \left(\frac{20}{m}\right)} \times \left(1 - \frac{\alpha_s}{4}\right) \geq 80\ mm \qquad \text{Equation 3-2}$$

Where h is the slab thickness, l_{sn} is the span length of the slab in short direction, m is the ratio of the long side length to the short side length of the slab, and α_s is the summation of the continuous sides divided by the perimeter of the slab.

Table 3.8 Beam Dimensions Criteria Based on TS 500 [14]

Slab	α_s	m	l_{sn} (mm)	h (mm)	Used h (mm)
Corner Slabs	0.5	1	6000	150	150
Edge Slabs	0.75	1	6000	139	
Inner Slabs	1	1	6000	128	

3.5 Loads

In the analysis of the models, 5 types of loads were used namely, dead, live, snow, wind, and earthquake loads. The procedures explained in TS498 [16] and TBEC [15] were used to calculate these loads. Details of these calculations are explained in this section.

3.5.1 Dead Loads

The dead loads of structural component such as beams, columns, and slabs were calculated using their volume and the unit weight of RC (γ_{RC}=2.5 kN/m^3). The analysis software used in this research calculated these loads automatically when section dimensions were defined. A superimposed dead load was applied on slabs representing additional dead load due to floor covering and plaster. On top of the RC slab, 50 mm of plain concrete and 20 mm of marble was used. A plaster was applied under the slab which was also considered in calculation of superimposed dead loads. These calculations are shown in Table 3.9. The unit weights of the materials below were obtained from TS ISO9194 [17]. The application of superimposed dead load on slabs is shown in Figure 3.2.

Table 3.9 Calculation of Superimposed Dead Load on Slab

Material	**Thickness (m)**	**Unit Weights (kN/m^3)**	**Calculated Load (kN/m^2)**
Plain Concrete	0.05	22	1.1
Marble	0.02	27	0.54
Plaster	0,02	20	0.4
		Total=	**2.04**

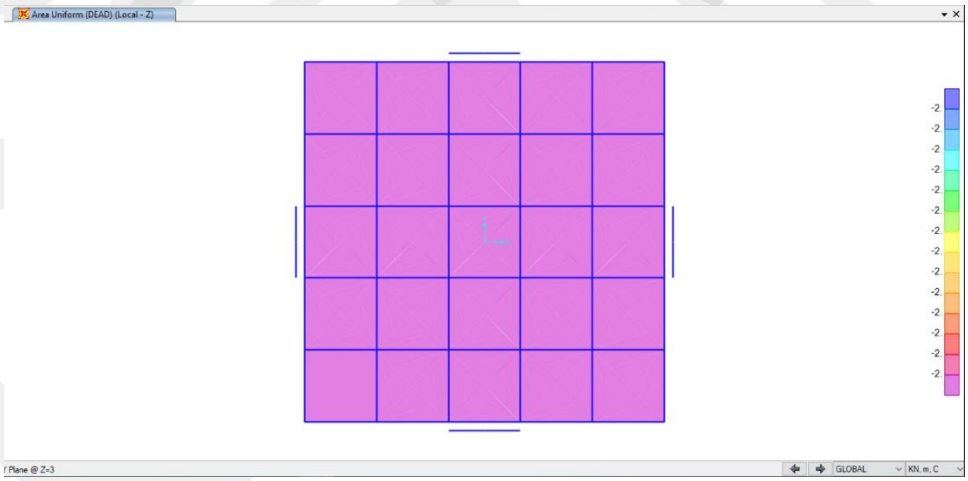

Figure 3.2 Application of Dead Load on Slabs

The walls used in the models consisted of three different types, namely, outer walls, inner walls, and parapet walls. Each wall in the model had a different brick and plaster thickness. The inner walls, also called partition or separator walls, consisted of bricks having 200 mm width and plaster of 24 mm on both sides. The outer wall had 300 mm wide bricks. The plaster thicknesses of the outer walls were 30 and 24 mm for outside

and inside, respectively. One-meter-high parapet walls surrounded the perimeter of the roof. Parapet walls were built using bricks having 300 mm width and they were plastered on both sides using 6 mm layer. Calculations related to dead loads of walls are shown in Table 3.10. The unit weights of the materials below were obtained from TS ISO9194 [17]. The application of superimposed dead load on slabs is shown in Figure 3.3.

Table 3.10 Calculation of Dead Loads of Walls

Wall Type	Material	Thickness (m)	Width (m)	Unit Weights (kN/m^3)	Calculated Load (kN/m)
Outer	Brick Wall	0.3	2.4	9.8	7.056
	Plaster (Outer)	0.03	3	19.6	1.764
	Plaster (Inner)	0.02	2.85	19.6	1.1172
				Total=	9.94
Inner	Brick Wall	0.2	2.4	9.8	4.704
	Plaster (Outer)	0.02	2.85	19.6	1.1172
	Plaster (Inner)	0.02	2.85	19.6	1.1172
				Total=	6.94
Parapet	Brick Wall	0.3	1	9.8	2.94
	Plaster (Outer)	0.02	2.85	19.6	1.1172
	Plaster (Inner)	0.02	2.85	19.6	1.1172
				Total=	5.17

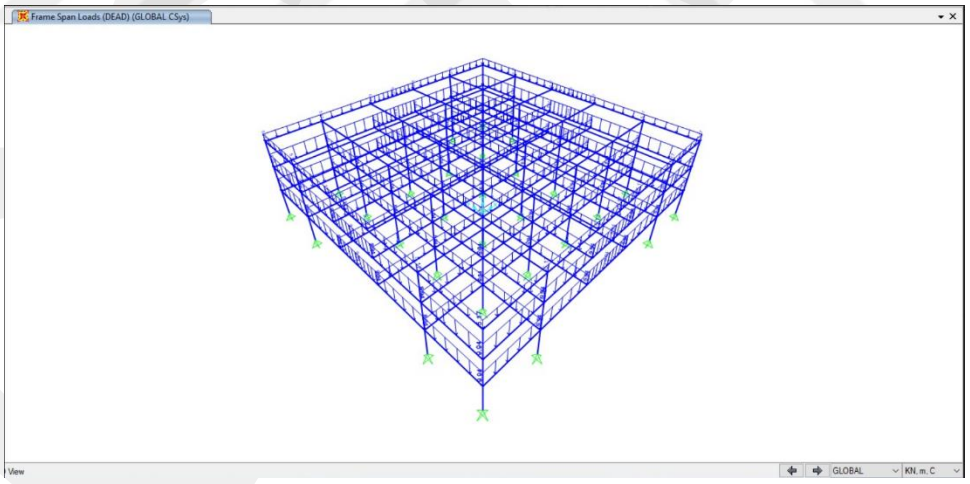

Figure 3.3 Application of Wall Loads on Slabs

3.5.2 Live Loads

The live loads of the models were obtained from TS498 [16]. A uniform live load of 2 kN/m^2 was applied on all the stories of all the models. The application of live loads on slabs is shown in Figure 3.4.

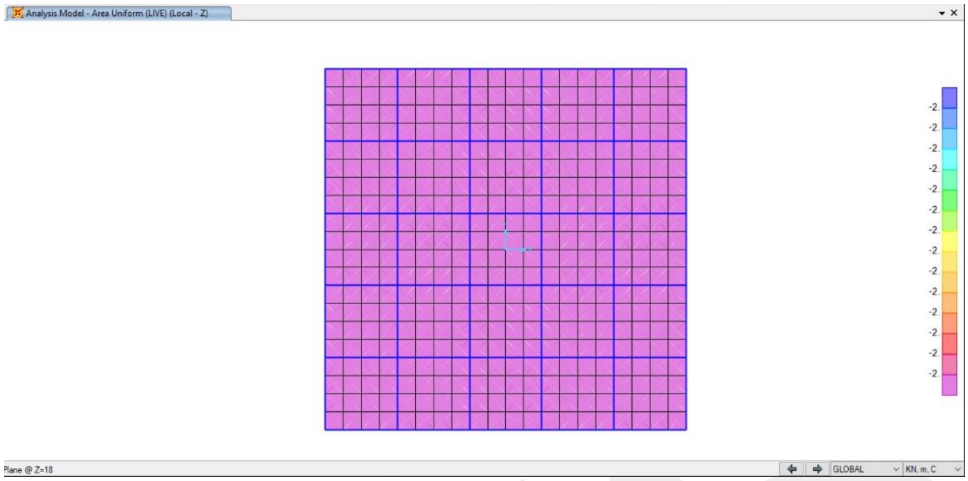

Figure 3.4 Application of Live Load

3.5.3 Snow Loads

The snow load on the models was calculated using TS498 [16]. The equation in this specification is shown below:

$$P_k = m \times P_{k0} \qquad \text{Equation 3-3}$$

Using the procedure in the specification and the selected location (Üsküdar), the value of the snow load was calculated as 0.75 kN/m^2. Snow load is only applied on the roof slab of the models. The application of snow load is shown in Table 3.9.

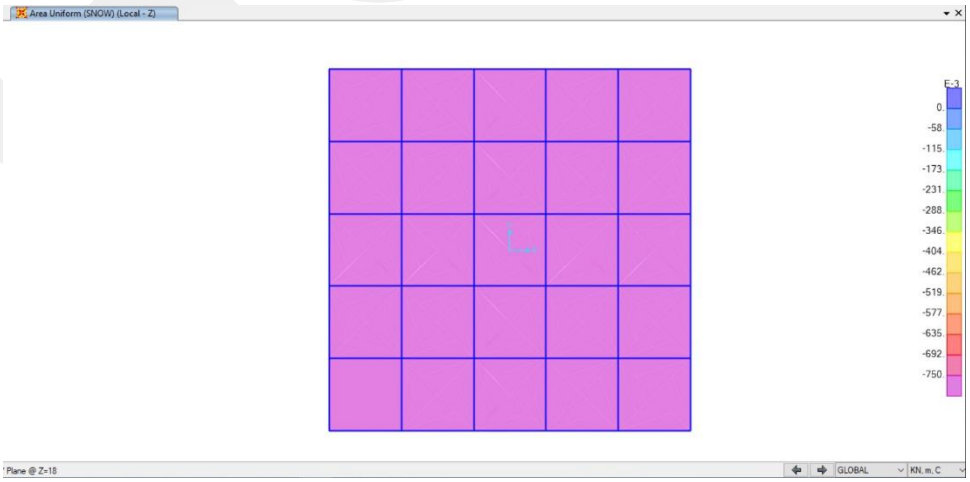

Figure 3.5 Application of Live Load

3.5.4 Wind Loads

The procedure specified by TS498 [16] was used to determine the effect of wind loads on the building models. Table 3.11 and Figure 3.6 illustrate the relevant calculations and coefficients for wind load. The calculated wind loads for x- and y-directions were applied to the building models as shown in Figure 3.7 and Figure 3.8.

Table 3.11 Suction and Pressure of Winds on Buildings Height, TS498 [16]

Height from Ground (m)	Suction, q (KN/m^2)
0-8	0.5
9-20	0.8
21-100	1.1
>100	1.3

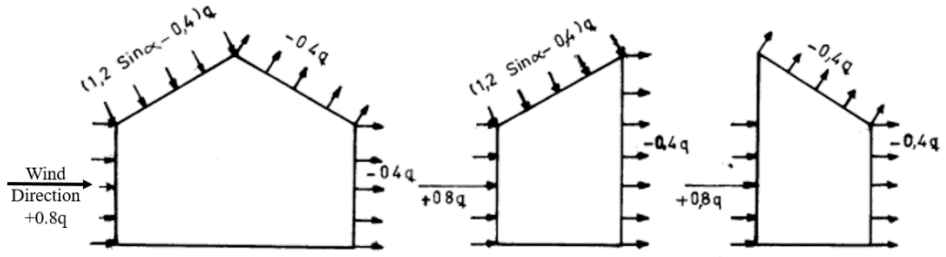

Figure 3.6 Suction and Pressure of Wind Load Coefficients and Calcultions, TS498 [16]

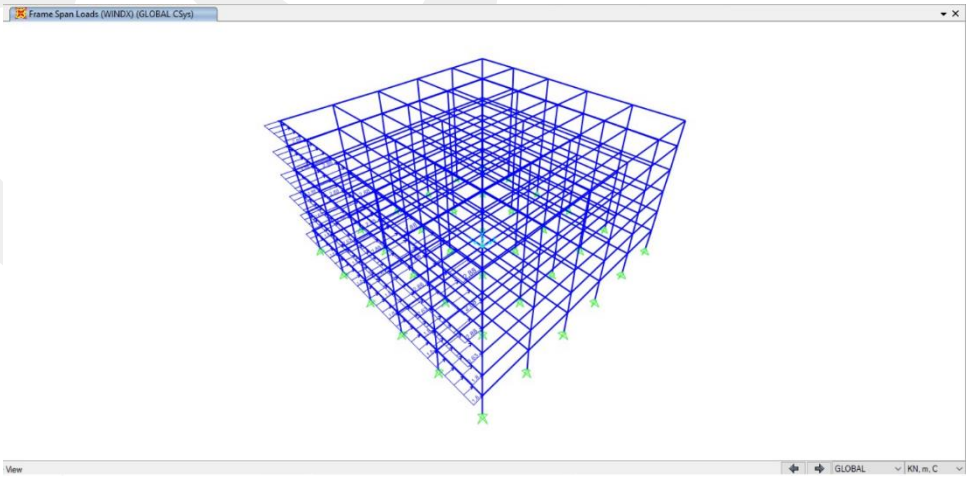

Figure 3.7 Application of Wind Loads in X-Direction

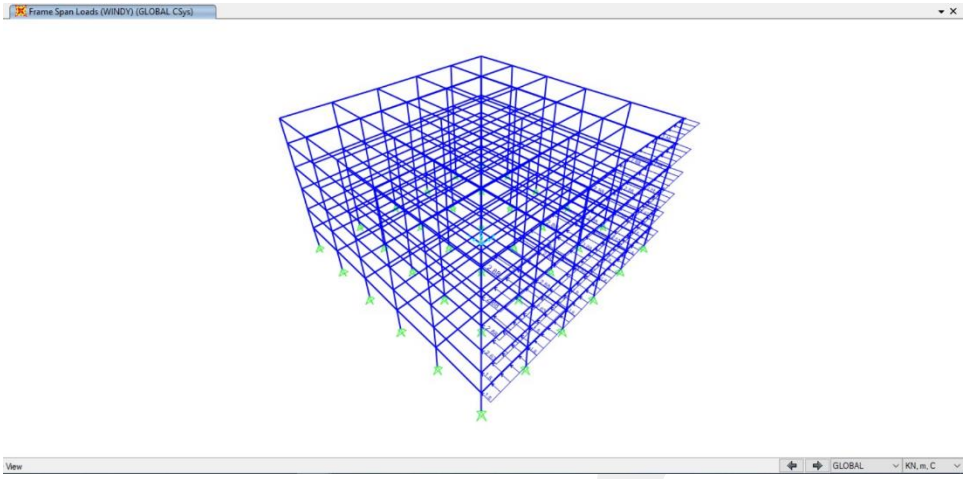

Figure 3.8 Application of Wind Loads in Y-Direction

3.5.5 Earthquake Loads

Three different analysis methods were used to calculate the effects of earthquake loads on the models. These methods were Equivalent Earthquake Load, Pushover Analysis and Time History Analysis Method. TBEC [15] was used to determine the corresponding seismic forces. The analysis of the models was performed for each method and the results of these methods were compared in the following chapters.

3.5.5.1 Equivalent Earthquake Load Method

The Equivalent Earthquake Load Method is used to calculate the equivalent lateral static forces that shall be applied on various stories of the structure to simulate earthquake effects. A total base shear was calculated and distributed to story levels. The distribution had an inverted triangular shape, simulating the first mode of the dynamic response (zero at the bottom level and maximum at the top level). The calculated story forces were applied at the mass center of each story.

The procedure explained in TBEC [15] was used to calculate the total base shear. The earthquake forces were calculated based on many factors such as the seismic hazard of the location where the building shall be constructed, type of soil, importance of building, building load-resisting system, the seismic coefficient, etc.

The location of the structure was selected as Üsküdar, İstanbul, Turkey as shown in Figure 3.9. For the building models used in this research, DD2 earthquake ground motion level was used in all the calculations. The map spectral acceleration coefficient in short-period range (S_s) and map spectral acceleration coefficient at 1.0 second period (S_1) for DD2 earthquake ground motion level were obtained as 0.885 and 0.246, respectively, using the Turkish Seismic Risk Map [18]. The soil class was selected as ZC. These coefficients were modified to calculate the design values based on the soil type under the building models. Design spectral acceleration coefficient in short-period range (S_{DS}) and design spectral acceleration coefficient at 1.0 second period (S_{D1}) for DD2 earthquake ground motion level were obtained as 1.062 and 0.369, respectively. These coefficients, peak ground acceleration and peak ground velocity are shown in Table 3.12.

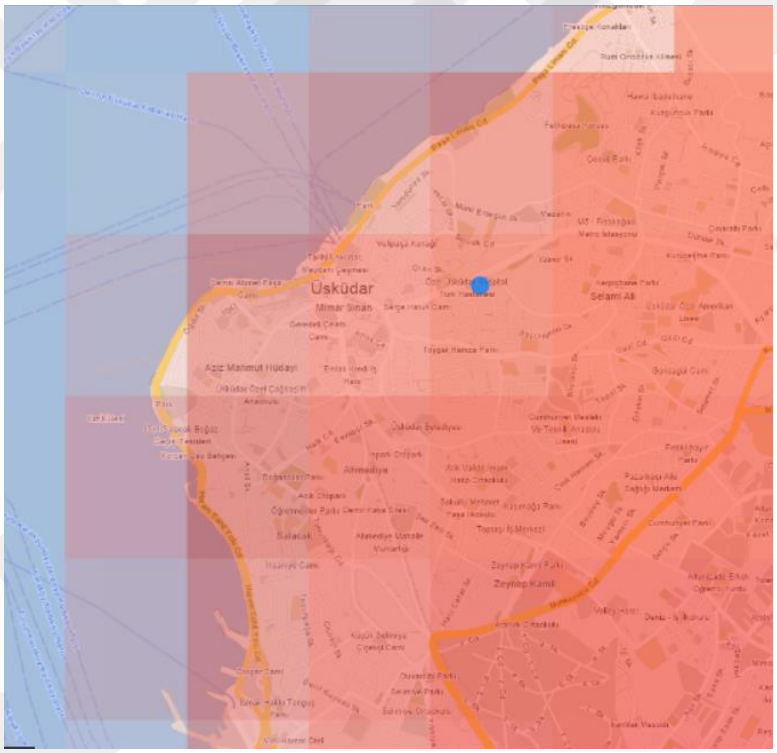

Figure 3.9 Location of Building Models

Table 3.12 Spectral Acceleration Coefficients, Peak Ground Acceleration, and Peak Ground Velocity of Location of Building Models for DD2 Earthquake Ground Motion Level

Definition	Value
Map Spectral Acceleration Coefficient in Short-Period Range (S_s)	0.885
Map Spectral Acceleration Coefficient at 1.0 Second Period (S_1)	0.246
Design Spectral Acceleration Coefficient in Short-Period Range (S_{DS})	1.062
Design Spectral Acceleration Coefficient at 1.0 Second Period (S_{D1})	0.369
Peak Ground Acceleration (PGA) (g)	0.363
Peak Ground Velocity (cm/c^2)	22.542

The horizontal elastic response spectrum is the graph that shows the acceleration response of a structure as a function of its natural period of vibration. Given the local soil conditions and seismic danger, the maximum acceleration response that a structure will experience during an earthquake can be determined. The horizontal elastic response spectrum shown in Figure 3.10 was used in this study. The horizontal axis in this spectrum is the period of the structure (T) and the vertical axis is the acceleration coefficient ($S_{ae}(T)$). The values of T_A and T_B are calculated as 0.069 and 0.347, respectively using the equations shown below. T_L is defined as 6 s according to TBEC [15]. This spectrum was modified using the selected soil type (ZC) and earthquake ground motion level (DD2) for the building models used in this study. The modified horizontal elastic response spectrum is shown in Figure 3.11.

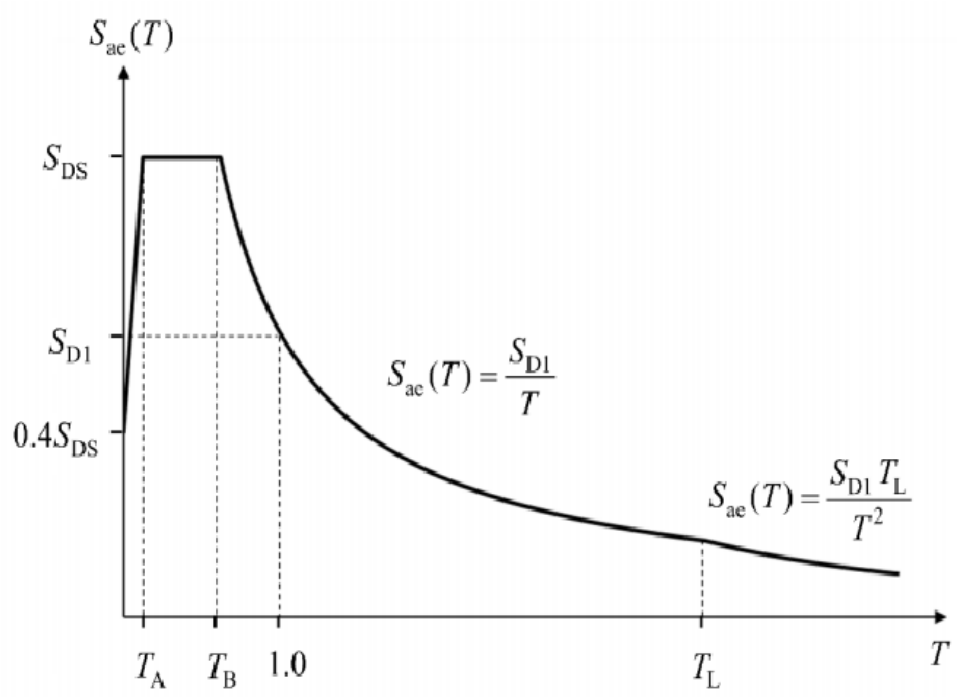

Figure 3.10 Horizontal Elastic Response Spectrum, TBEC [15]

$$T_A = 0.2\frac{S_{D1}}{S_{DS}}$$ Equation 3-4

$$T_B = \frac{S_{D1}}{S_{DS}}$$ Equation 3-5

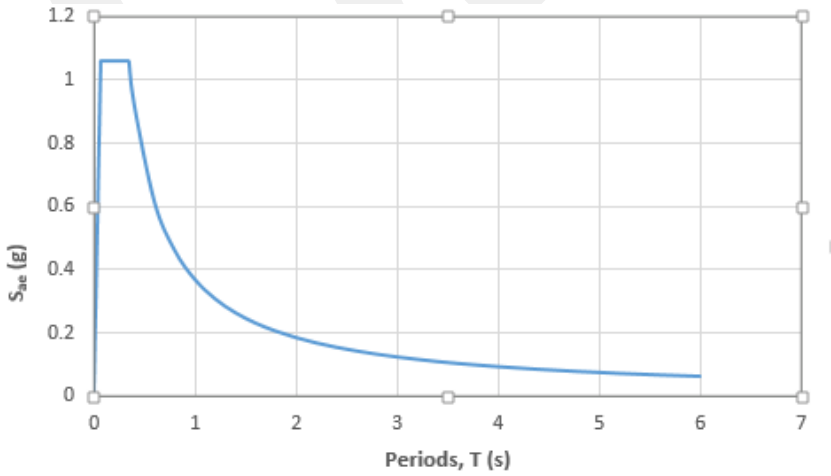

Figure 3.11 Horizontal Elastic Response Spectrum used in Analysis

The seismic weight of the models ($w_j^{(S)}$) is calculated using some fraction of the live load ($w_{Q,j}^{(S)}$) and full dead load ($w_{G,j}^{(S)}$) based on TBEC [15]. The equation is shown below:

$w_j^{(S)} = w_{G,j}^{(S)} + n \times w_{Q,j}^{(S)}$ Equation 3-6

The live load participation factor (n) for the building models used in this study was defined as 0.3 in TBEC [15] as shown in Table 3.13.

Table 3.13 Live Load Participation Factor based on TBEC [15]

Purpose of Occupancy of Building	Live Load Participation Factor, n
Residence, office, hotel, hospital, etc.	0.3

The importance factor (I) is one of the input parameters used in calculation of the earthquake loads. Since all the building models considered in this study were residential buildings, the importance factor was defined as 1 according to TBEC [15].

The structural performance of buildings during an earthquake was determined using the structural behavior coefficient (R) and over-strength factor (D) as shown in Table 3.14. When calculating the structural behavior of the strengthened structures for the models in this study, the coefficient of structural behavior and over-strength factor were chosen as 8 and 3, respectively. It was assumed that the strengthened structures had a high level of ductility. In the other hand the defected structures values were assumed to be 4 and 2.5.

Table 3.14 R and D Coefficients for Structural Behavior, TBEC [15]

Building Structural System	Coefficient of Structural Behavior, R	Over Strength Factor, D
High ductility level building in which seismic loads are fully resisted by frames	8	3
Limited ductility level building in which seismic loads are fully resisted by frames	4	2

The earthquake load reduction factor, $R_a(T)$ is calculated using R, D coefficients and period of the structure (T) using following equations:

$R_a(T) = \frac{R}{I}$ $T > T_B$ Equation 3-7

$R_a(T) = D + \left(\frac{R}{I} - D\right)\frac{T}{TB}$ $T \leq T_B$ Equation 3-8

The $S_{aR}(T)$ value is defined as the reduced acceleration spectrum based on the building's structural characteristics. $S_{aR}(T)$ is calculated using the equation below:

$$S_{aR} = \frac{Sae(T)}{Ra(T)} \qquad \text{Equation 3-9}$$

Once all the variables were calculated, the following equations were used to determine the total base shear.

$$V_{tE}^{(H)} = m_t \times S_{aR}(T_p^{(H)}) \qquad \text{Equation 3-10}$$

The base shear is then distributed to all the story levels of the building as shown in Figure 3.12. The following equations were used to calculate necessary variables.

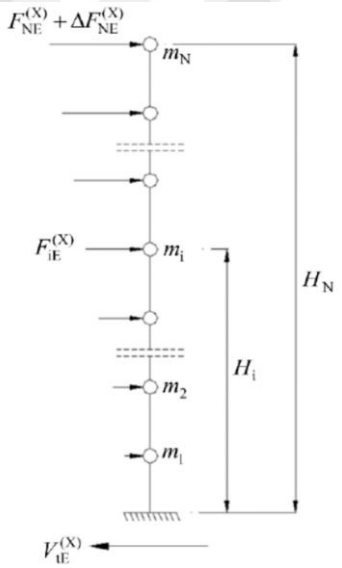

Figure 3.12 Distribution of Total Base Shear to Story Levels

$$F_{iE}^{(H)} = (V_{tE}^{(H)} - \Delta F_{NE}^{(H)}) \times \frac{mi \times Hi}{\sum_{j=1}^{N} mj \times Hj} \qquad \text{Equation 3-11}$$

$$V_{tE}^{(H)} = \Delta F_{NE}^{(H)} + \Sigma F_{iE}^{(H)} \qquad \text{Equation 3-12}$$

$$\Delta F_{NE}^{(H)} = 0{,}0075 \times N \times V_{tE}^{(H)} \qquad \text{Equation 3-13}$$

3.5.5.1.1 Application of Constraints in SAP2000 Structural Software

Diaphragms were defined as diaphragm constraints at all the joints of each story level of the building models. Diaphragms of each story were named differently. In this study, the diaphragms were named with the letter "S" and the story number. As an example, "S1" diaphragm constraint was defined to be used for the first story joints. The

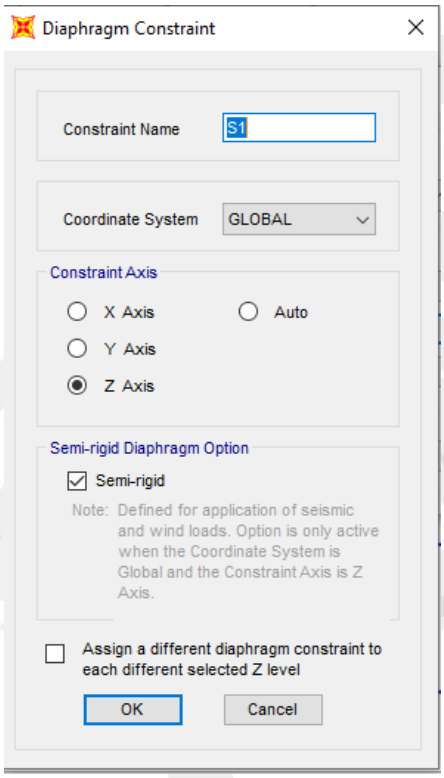

Figure 3.13 Definition of Diaphragm Constraint in SAP2000 Structural Analysis Software

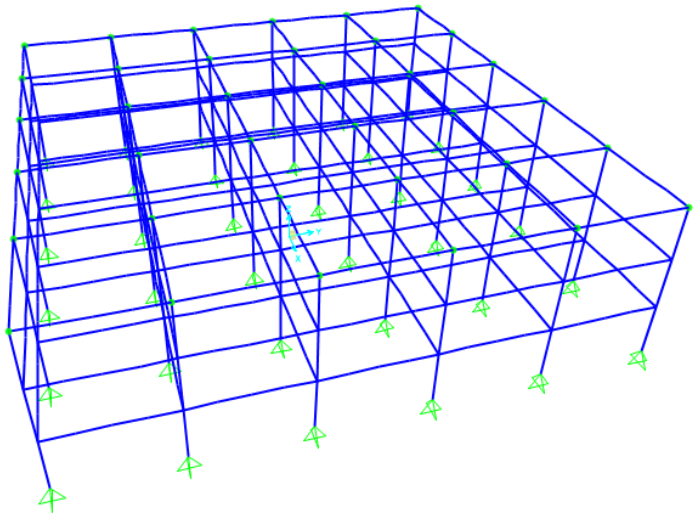

Figure 3.14 Assignment of Diaphragm Constraint (S3) in SAP2000 Structural Analysis Software

Body constraints were used to provide a fully rigid connection between the reinforced concrete beam-column connections and external structural steel sections.

3.5.5.2 Pushover Analysis Method

Pushover analysis is a static nonlinear analysis method that includes applying progressively increasing lateral loads on a structure until it fails or displaces to a predetermined range. Pushover analysis is less computationally intensive and less time consuming than more sophisticated dynamic analysis methods.

The first mode shape is usually used as the initial input for the pushover analysis. Using the mode shape, the behavior of the lateral force-resisting system of the structure is determined under a uniformly increased load. The building was anticipated to predominantly deform into this shape. The load-deformation diagram of the structure is achieved at the end which shows the behavior under lateral load.

The pushover analysis helps to determine the vulnerability of structure and perform design changes using the information provided related to the behavior of the building.

3.5.5.2.1 Capacity Spectrum Method (CSM)

The CSM process includes the construction of a capacity spectrum that shows the lateral force resistance of a structure as a function of its basic. The performance of the structure (capacity curve) is calculated using the pushover analysis and drawn as a function of period. The demand of the earthquake is also drawn as a function of period. The intersection point of these two curves (performance and demand curves) is known as the performance point of the structure as shown in Figure 3.15.

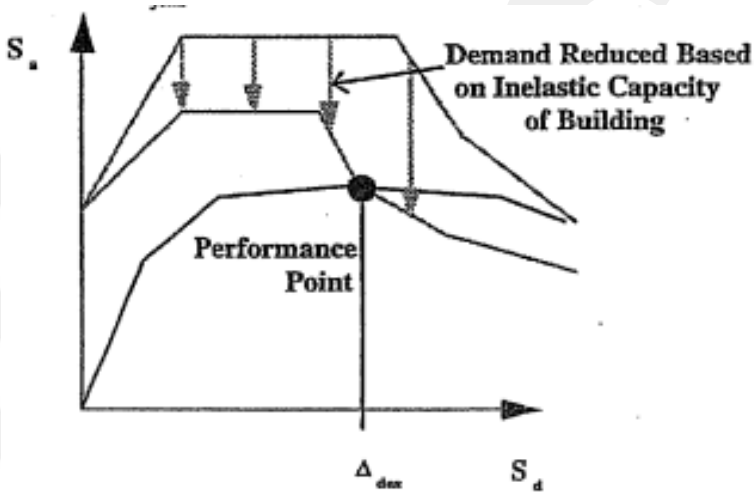

Figure 3.15 Representation of Performance Point, ATC-40 [19]

The capacity curve in pushover analysis is a graphic representation of the nonlinear behavior of the structure and the building response to increasing lateral forces or displacements. It offers a way to evaluate the performance of a structure under seismic effects and helps determine its ultimate capacity and possible failure modes. The capacity curve is usually represented by a plot of the base shear or lateral force (y-axis) against the corresponding displacement or roof drift (x-axis). At any selected location of interest, such as the roof or a certain floor level, the displacement can be measured.

The demand curve shown in Figure 3.16 from ATC-40 [19] was used to produce the demand of the structure. The coefficients, C_A and C_V, were calculated using the equations below. The values of S_{DS} and S_{D1}, shown in Table 3.12, were used to calculate C_A and C_V.

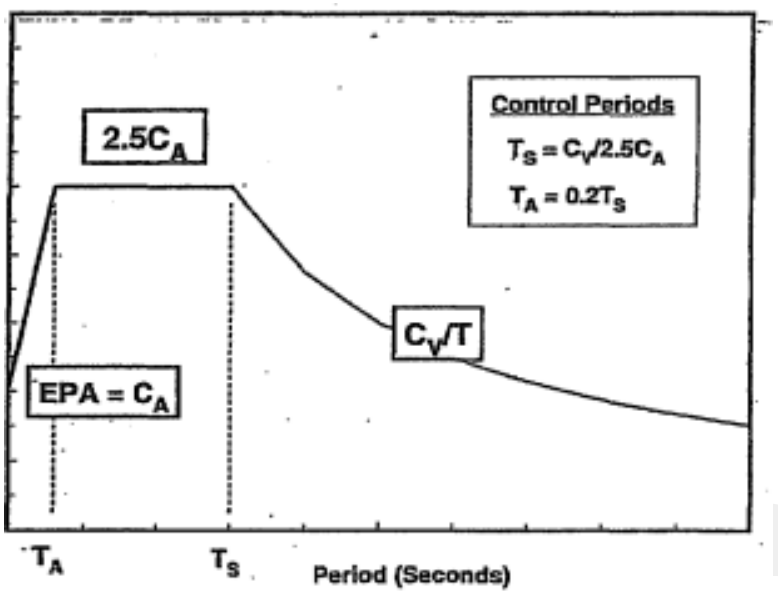

Figure 3.16 Demand elastic response spectrum, ATC-40 [19]

$C_A = 0{,}4 \times S_{DS}$ Equation 3-14

$C_V = S_{D1}$ Equation 3-15

The produced demand spectrum of the building models used in this research was defined in SAP2000 Structural Software [23] as shown in Figure 3.17.

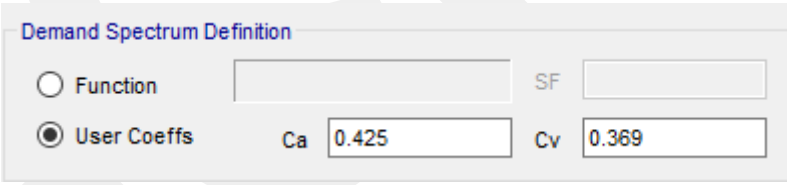

Figure 3.17 Definition of Demand Spectrum in SAP2000 Structural Software

3.5.5.2.2 Performance-Based Design

The behavior of the structure obtained using pushover analysis may be drawn in various diagrams. The most used behavior representation diagram is load-deflection curve which relates base shear to roof displacement. When this diagram is obtained, some performance levels are defined based on the damage to the structure. The performance points defined by Kalibhat et al. [20] were used in this study. These performance points are shown in Figure 3.18. Section AB is the elastic section in this figure meaning the structure will return to original shape without any residual

deformation. At performance point B, the structure starts to behave plastically. Up to the point IO which means Immediate Occupancy, some damage occurs to the structure which does not affect the safely-usage of the structure. The performance point LS (Life Safety) indicates that the structure undergoes significant damage without partial or full collapse. Beyond this point, the structure shall not be inhabited. The next performance point, CP (Collapse Prevention), is the point when structure will experience partial- or full-collapse (CP), if more load is applied. At performance point C, the structure collapses and reaches performance point D. After collapse, the structure reaches performance point E when maximum deformation capacity is reached. Definition of these performance points helps designers to establish goals for various levels of laterally applied loads. As an example, for a high lateral load (such as DD1 earthquake ground motion level based on TBEC [15], the structures may reach a maximum performance point of collapse prevention. This type of design is called performance-based design.

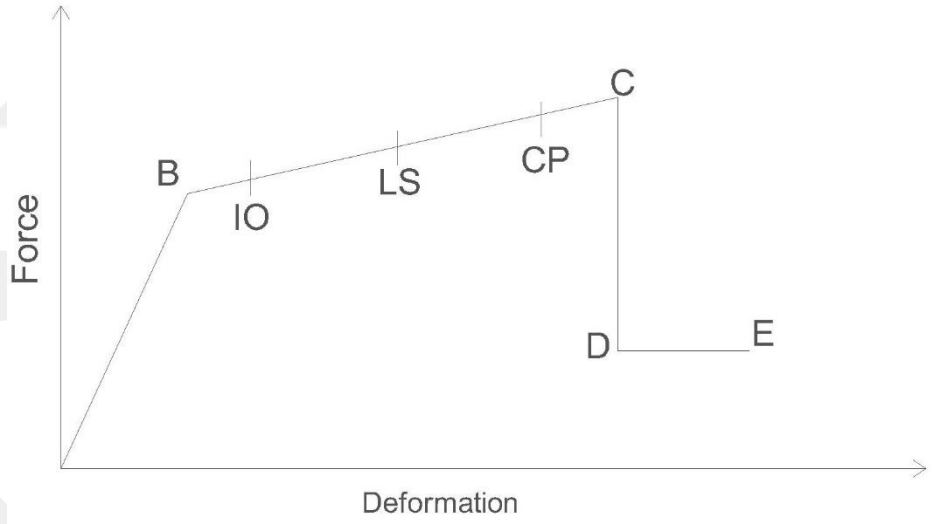

Figure 3.18 Pushover Curve with Performance Level Points by Kalibhat et al. [20] 2014)

3.5.5.2.3 Definitions for Pushover Analysis in SAP2000 Analysis Software

The models of the buildings were produced using SAP2000 Structural Software [23]. Initially load case data for the structure was defined. The structure was first analyzed under the gravity loads which used the seismic weight of the structure including full

dead load and 30% of the live and snow loads. Nonlinear analysis was performed on top of the gravity analysis case as shown in Figure 3.19.

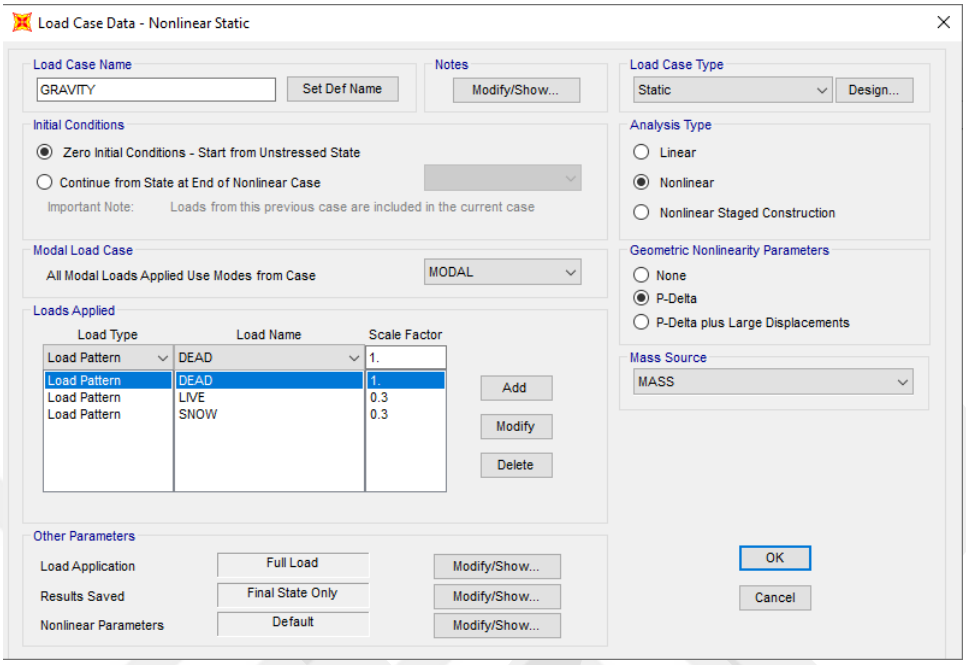

Figure 3.19 Definition of Nonlinear Static Load Case (Gravity)

P-delta effects were considered in the pushover analysis to capture the full nonlinear behavior of the structure. Therefore, the effect of gravitational loads on the laterally displaced structure was also accounted for using this geometric nonlinearity parameter.

The next step was the definition of load cases Push-X and Push-Y. These load cases were produced to apply the lateral forces on the structure gradually. In the pushover load case, a lateral load was gradually increased up to a predetermined displacement or target performance level. As explained earlier, the pushover load case starts from the end of the analysis of gravity loads. The definitions of these load cases (Push-X and Push-Y) are shown in Figure 3.20 and Figure 3.21.

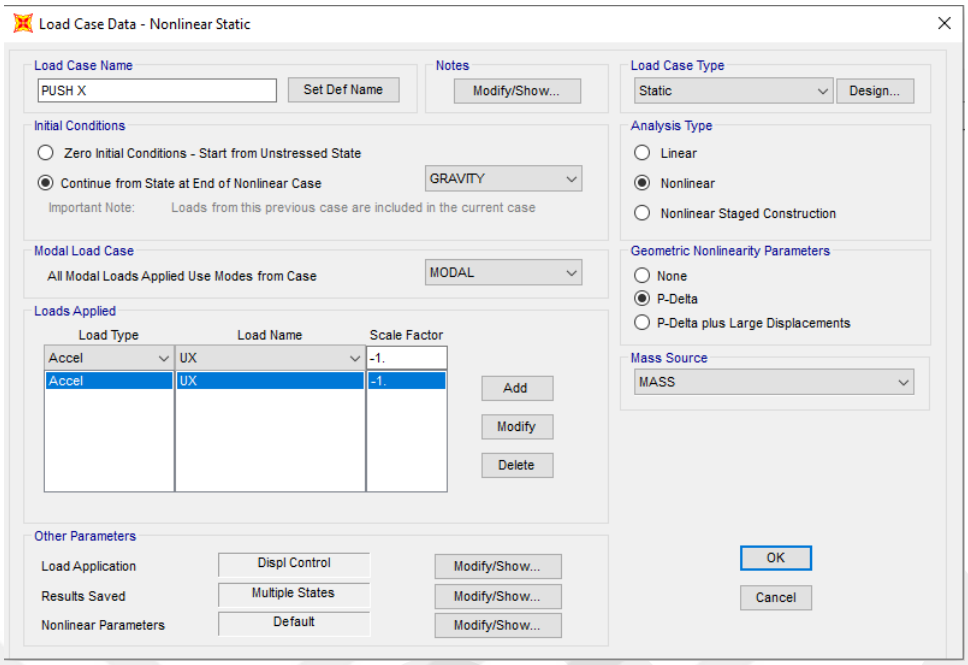

Figure 3.20 Definition of Nonlinear Static Load Case, Push-X

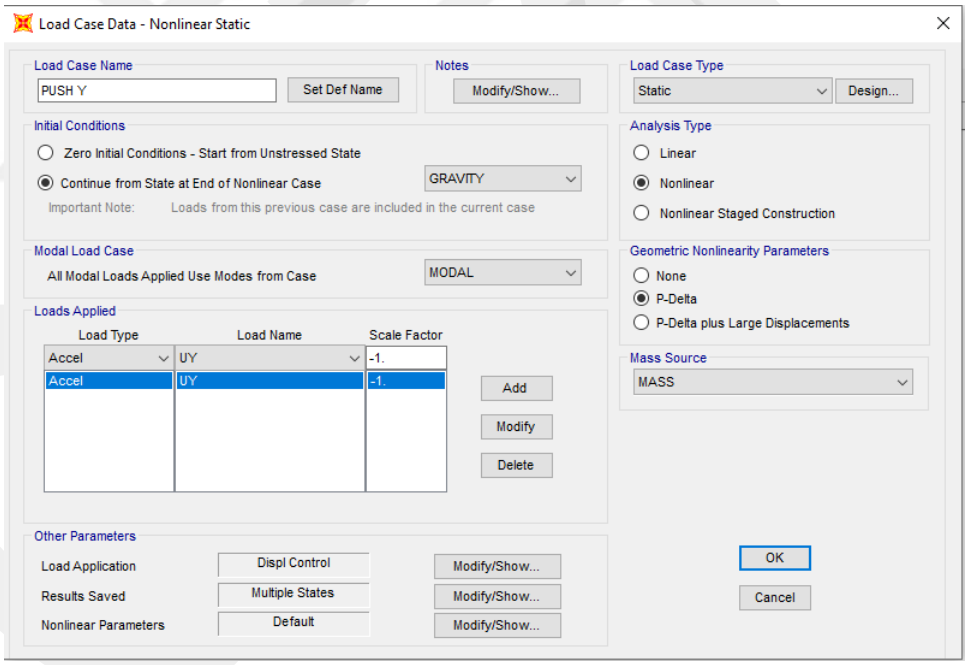

Figure 3.21 Definition of Nonlinear Static Load Case, Push-Y

The load application control for pushover analysis were defined as displayed in Figure 3.22 and Figure 3.23. The pushover load case was specifically selected as a displacement-controlled load case to monitor the specified value of displacement at the control joint. The control joint in this study was taken as the midpoint of the edge

of the roof level. The degree of freedom selected in the model for the pushover analysis in x-direction was U1. This degree of freedom represented the displacement along x-axis. Similarly, U2 was selected as the degree of freedom for the pushover analysis in y-direction. This degree of freedom represented the displacement along the y-axis.

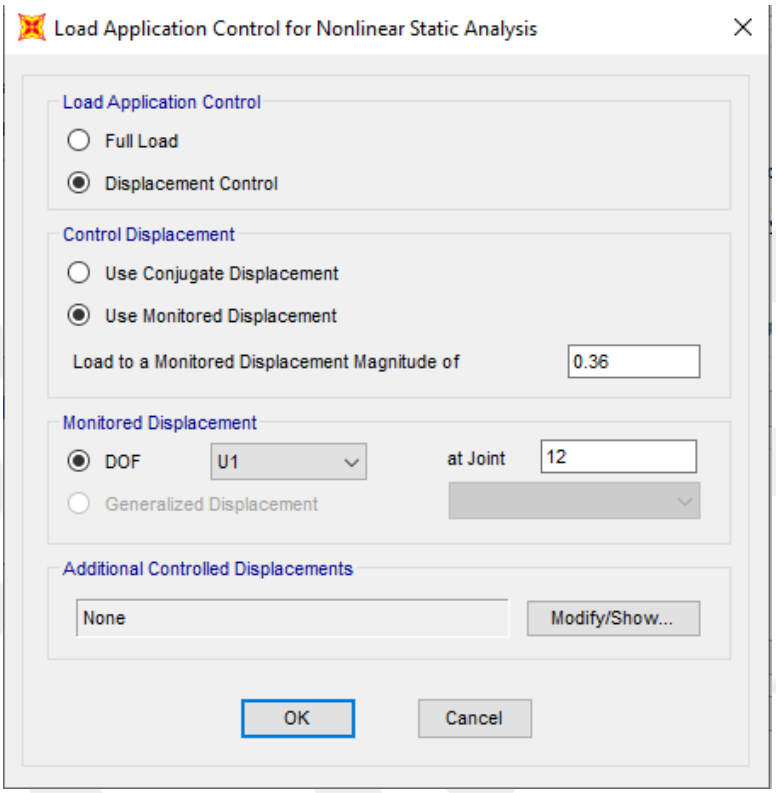

Figure 3.22 Selecting Load Application Criteria for Push-X And Push-Y Load

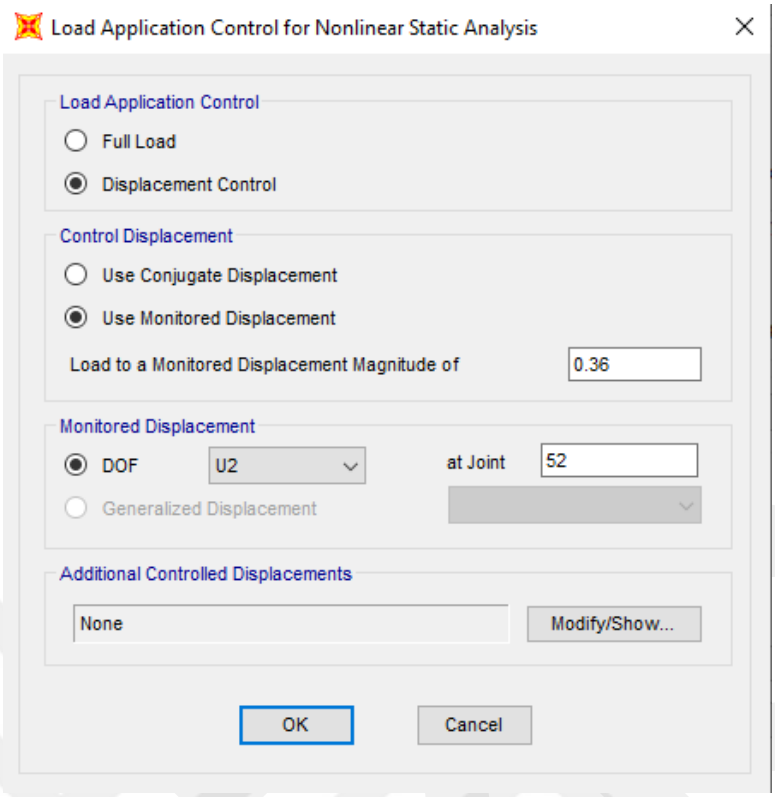

Figure 3.23 Selecting Load Application Criteria for Push-Y Load

SAP2000 Structural Software [23] may provide results of both the “final state” and “multiple states” of the pushover analysis as shown in Figure 3.24. By selecting the “final state” option, the force-deformation analysis final findings will only be saved. An overview of the results of force-deformation behavior at the final state can only be seen by the user. Details (steps of the analysis) may only be reviewed if “multiple states” option is selected. This option gives more specific information, enabling a thorough analysis of the findings.

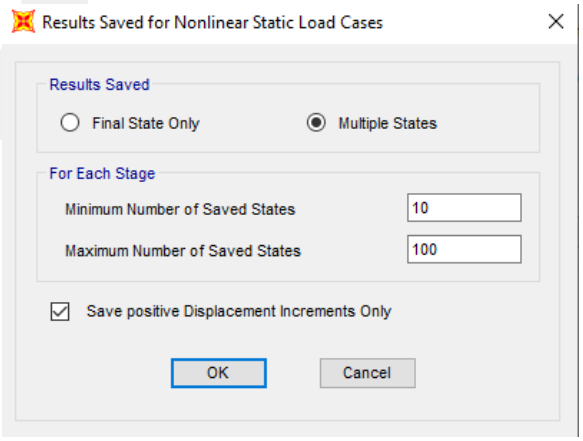

Figure 3.24 Analysis Save Options for Nonlinear Static Load

During the pushover analysis of the structure, the ends of the structural elements such as beams and columns are converted to hinges. In SAP2000 Structural Software [23], hinge properties of each structural member can be defined for the nonlinear behavior. The moment-rotation relationships (properties related to initiation and development of plasticity of the hinge) of each structural element are defined TBEC [15]. The locations of plastic hinges were selected at the ends of columns and beams. The hinge property assignments of structural elements used in the analysis are shown in figures from Figure 3.25 to Figure 3.28. Figures from Figure 3.29 to Figure 3.32 show hinge property data for RC and steel beams and moment rotation data for RC and steel columns.

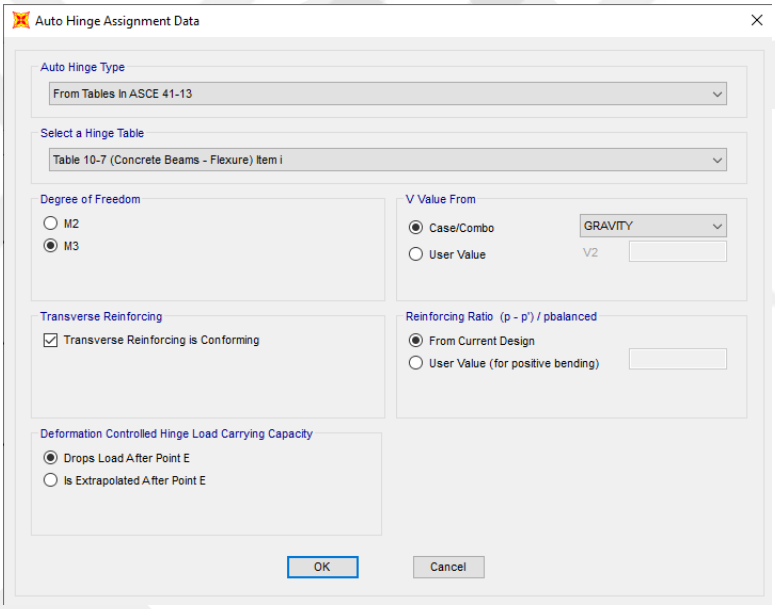

Figure 3.25 Definition of Hinge Properties for RC Beams

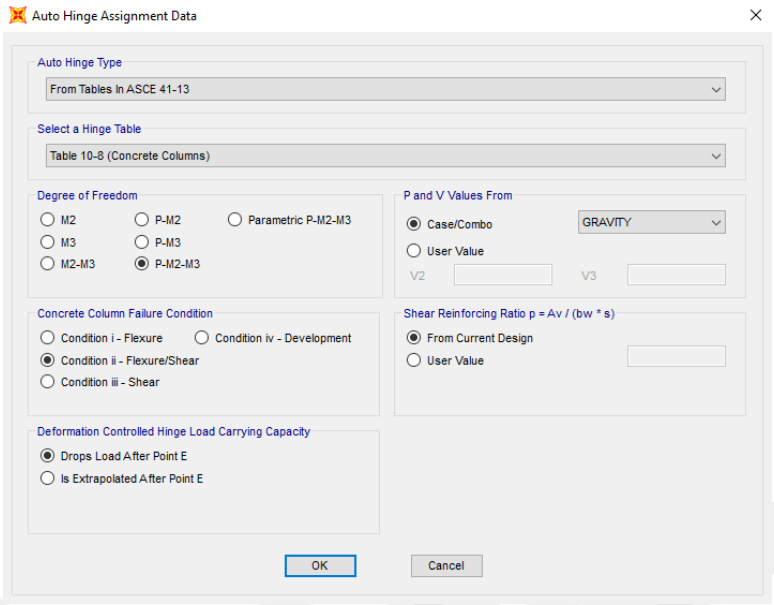

Figure 3.26 Definition of Hinge Properties for RC Columns

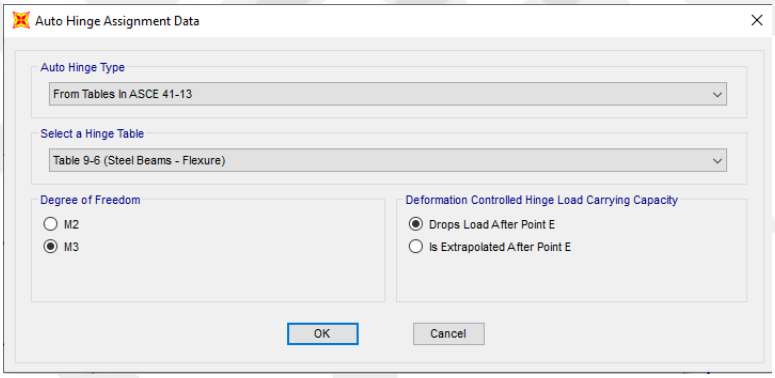

Figure 3.27 Definition of Hinge Properties for Steel Beams

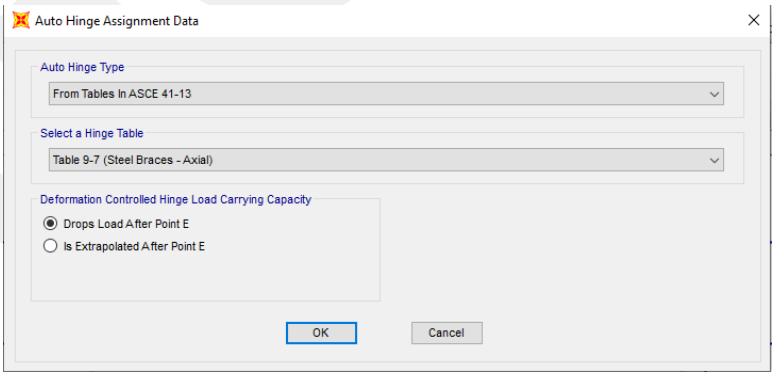

Figure 3.28 Definition of Hinge Properties for Steel Braces

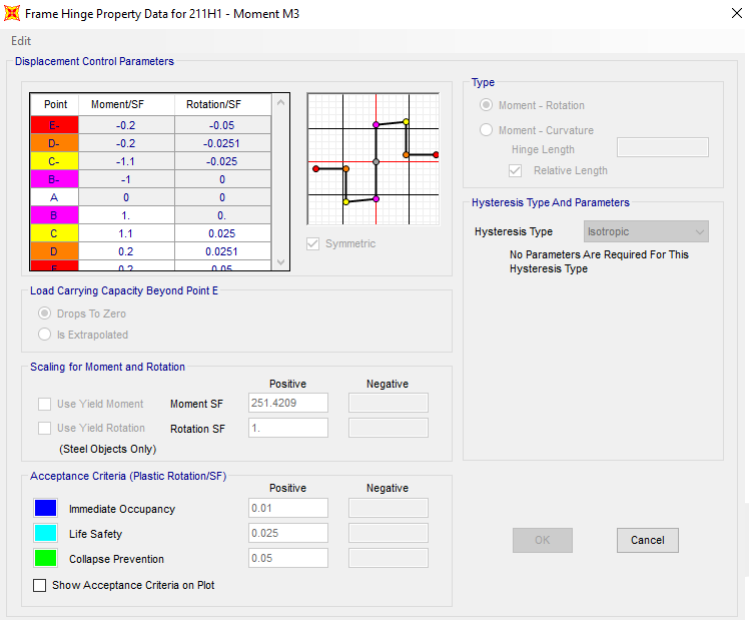

Figure 3.29 Hinge Property Data for RC Beams

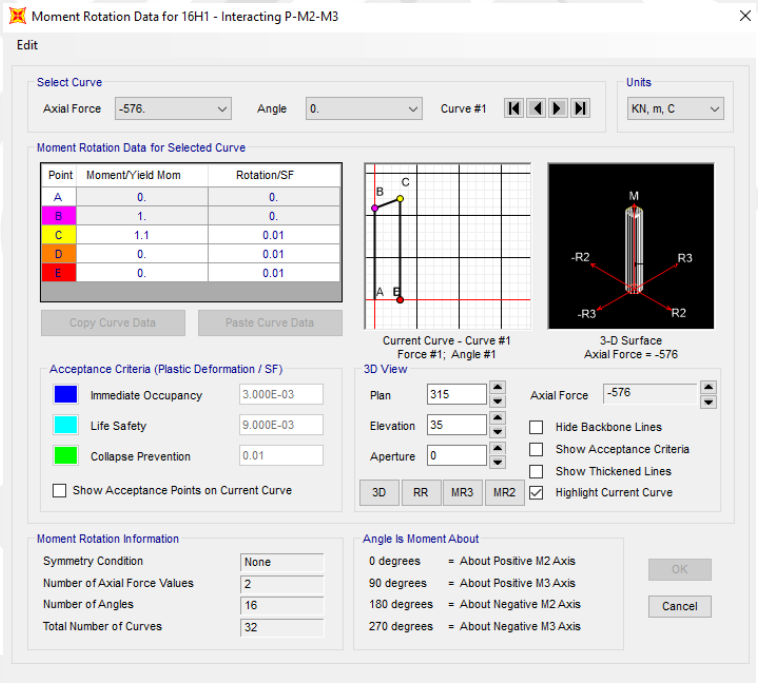

Figure 3.30 Moment Rotation Data for RC Columns

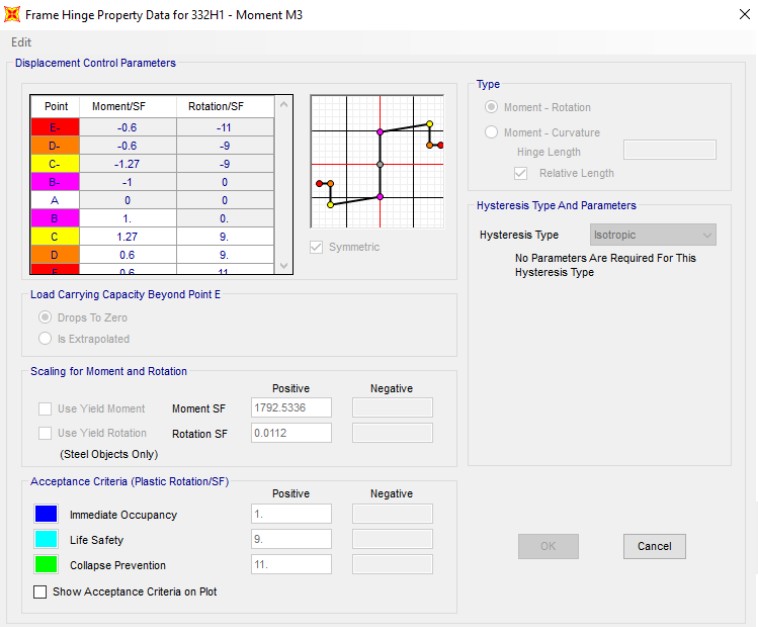

Figure 3.31 Hinge Property Data for Steel Beams

Figure 3.32 Moment Rotation Data for Steel Columns

3.5.5.3 Time-History Analysis Method

As a dynamic analysis technique, time-history analysis method predicts and evaluates the response of a structure to time-varying loads or ground motions. In this method the behavior of the structure is obtained using a step-by-step process in which the loads and response are evaluated at smaller time increments. This method is the most effective and complete analysis method for assessing the nonlinear seismic response of buildings Lee [21]. This method initially requires the selection of the ground motion records. In this study, the earthquake ground motion records were selected from the Earthquake Engineering Research Ground Motion Database [25]. Eleven different earthquake time-history data sets were used in the time-history analysis, in accordance with TBEC [15]. The selected earthquake ground motion records are listed in Table 3.15. The acceleration vs. time graphs of these earthquake ground motion records as shown in figures from Figure 3.33 to Figure 3.43. These records are raw records which shall be scaled to match the earthquake effects of the horizontal elastic response spectrum used in this study (Figure 3.11).

Table 3.15 Selected Earthquake Motions

Earthquake	Station	Year	Magnitude (M_w)	PGA(g)
San Fernando-01	Pearblossom Pumb	1971	6.61	0.0545
San Fernando-02	Santa Anita Dam	1971	6.61	0.0597
Imperial Valley	Superstition Mountains	1979	6.53	0.0801
Loma Prieta-01	APEEL 7 - Pulgas	1989	6.93	0.0641
Loma Prieta-02	APEEL 9 - Crystal Spring Res	1989	6.93	0.0487
Loma Prieta-03	Fremont - Mission San Jose	1989	6.93	0.0809
Loma Prieta-04	Palo Alto – SLAC Lab	1989	6.93	0.0907
Northridge-01	Lake Hughes	1994	6.69	0.0789
Northridge-02	Pasadena	1994	6.69	0.1536
Northridge-03	San Gabriel - E Grande Ave	1994	6.69	0.0756
Düzce	Lamont 1061	1999	7.14	0.0531

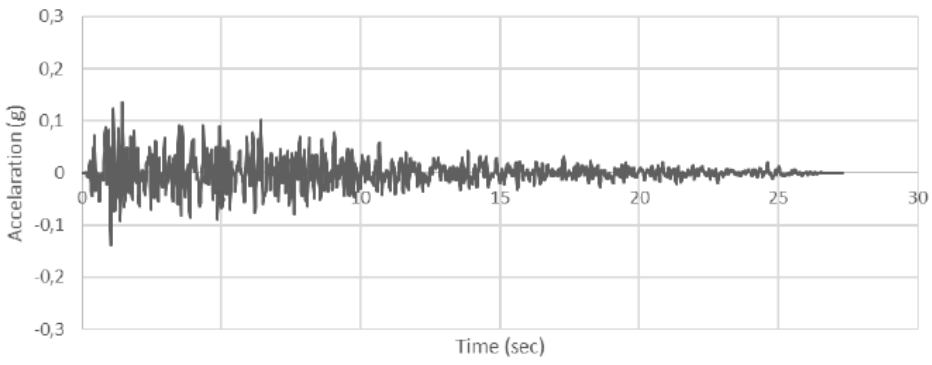

Figure 3.33 San Fernando-01 EQ1

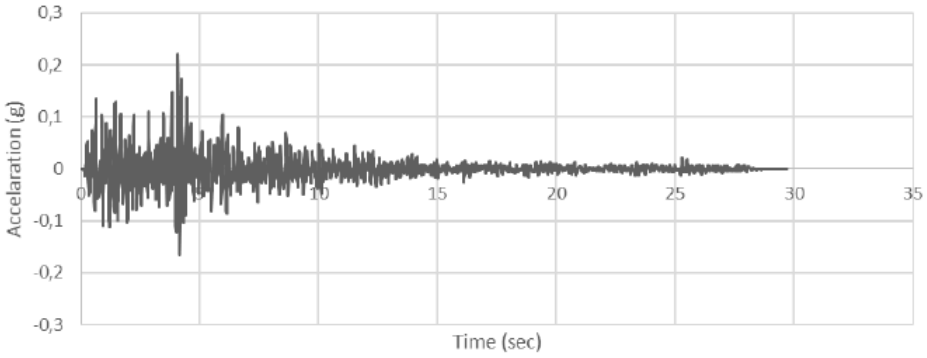

Figure 3.34 San Fernando-02 EQ2

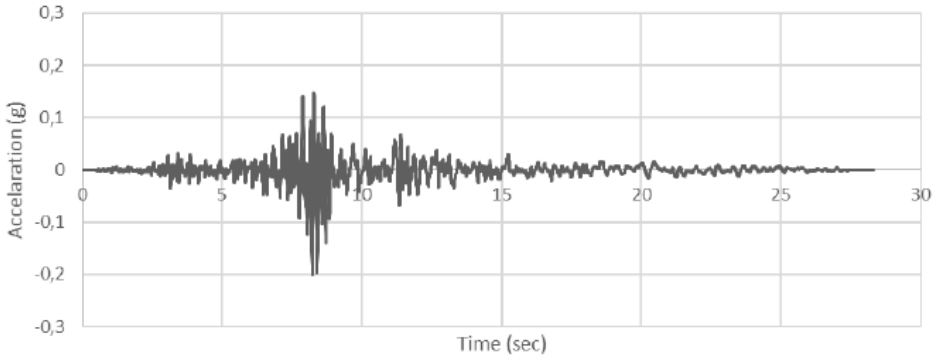

Figure 3.35 Imperial Valley EQ3

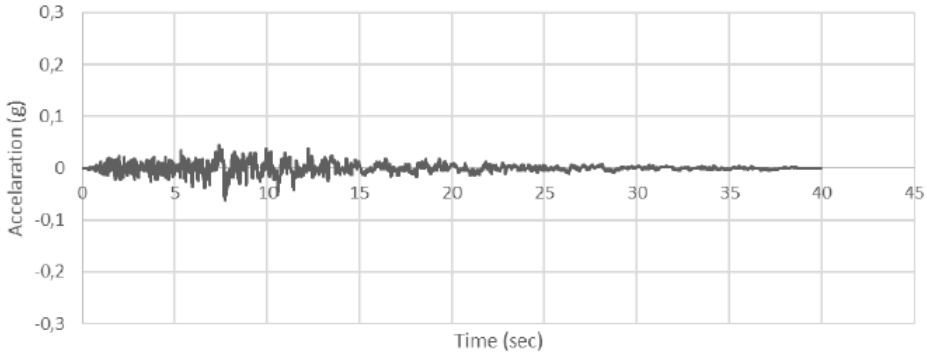

Figure 3.36 Loma Prieta-01 EQ4

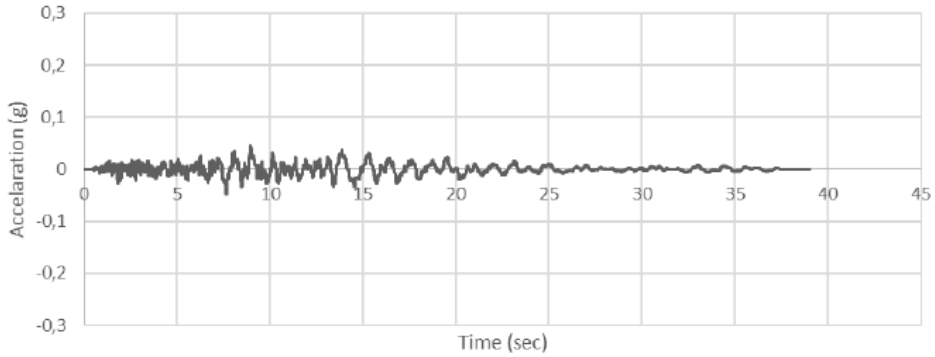

Figure 3.37 Loma Prieta-02 EQ5

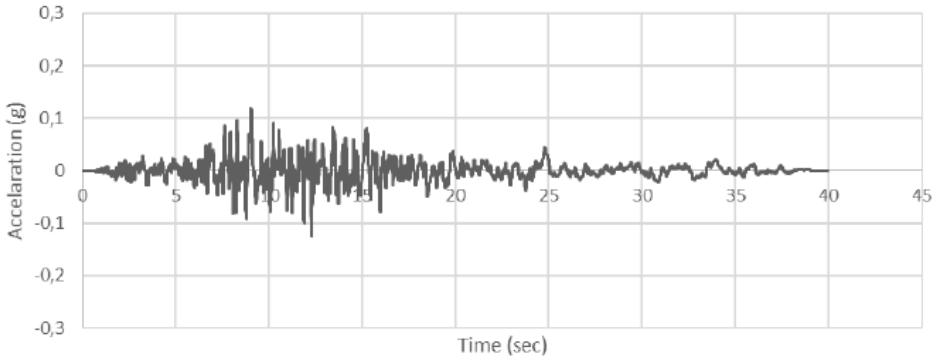

Figure 3.38 Loma Prieta-03 EQ6

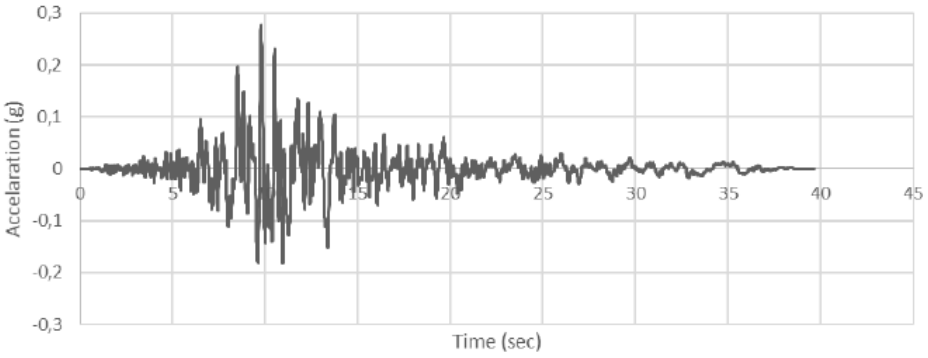

Figure 3.39 Loma Prieta-04 EQ7

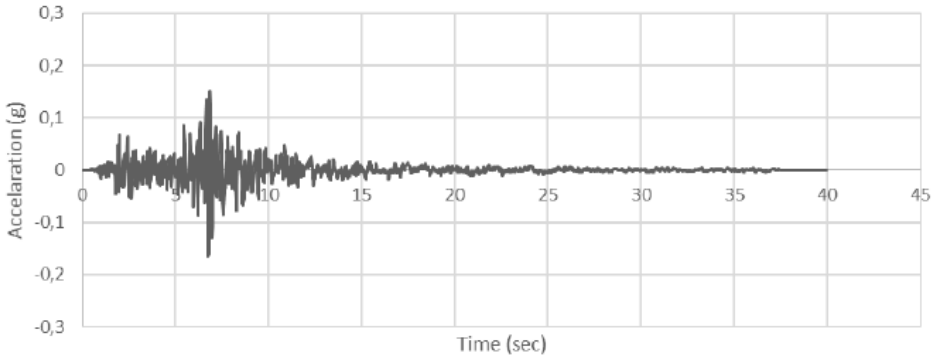

Figure 3.40 Northridge-01 EQ8

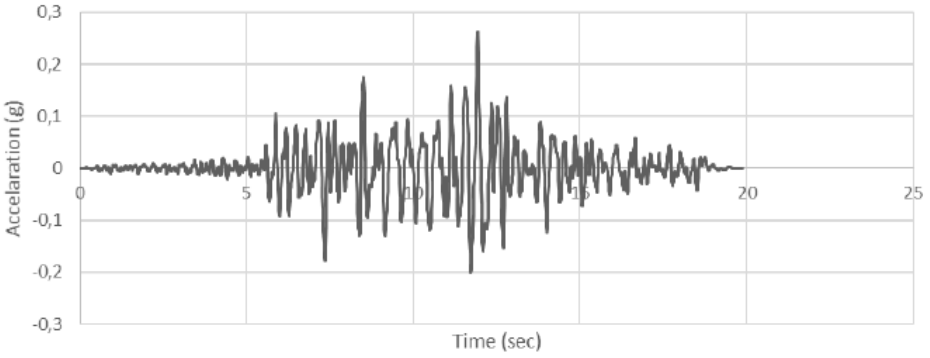

Figure 3.41 Northridge-02 EQ9

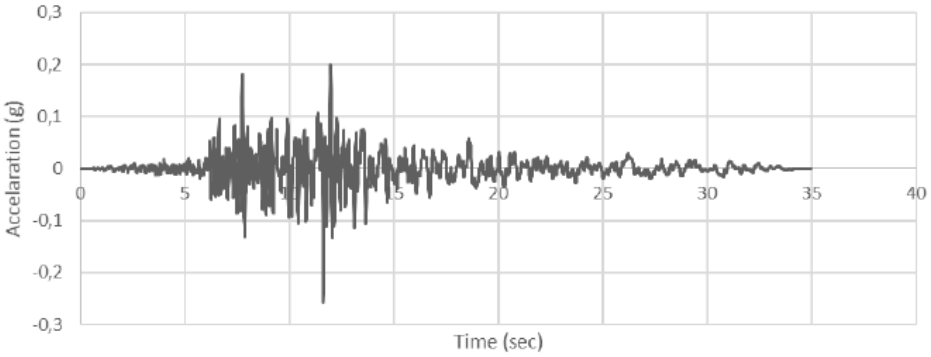

Figure 3.42 Northridge-03 EQ10

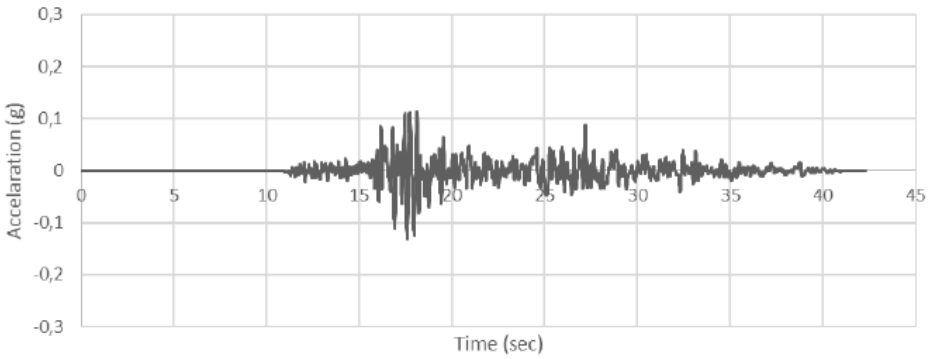

Figure 3.43 Düzce EQ11

As stated earlier, the raw earthquake ground motion records were scaled to match the earthquake demand of used in this study. Therefore, the maximum acceleration of the horizontal elastic response spectrum shown in Figure 3.11 was used to modify amplitude of the accelerations of the raw earthquake ground motion records. There are various methods to perform the scaling of the ground motion records. In this study, the scaling procedure defined in SAP2000 V22 Analysis Software [24] was used. The screenshots of the scaling method and the scaled earthquake ground motion record of EQ1 using SAP2000 Structural Software [24] are shown in Figure 3.44 and Figure 3.45. The scaled earthquake ground motion records used in this study is shown in figures from Figure 3.46 to Figure 3.56.

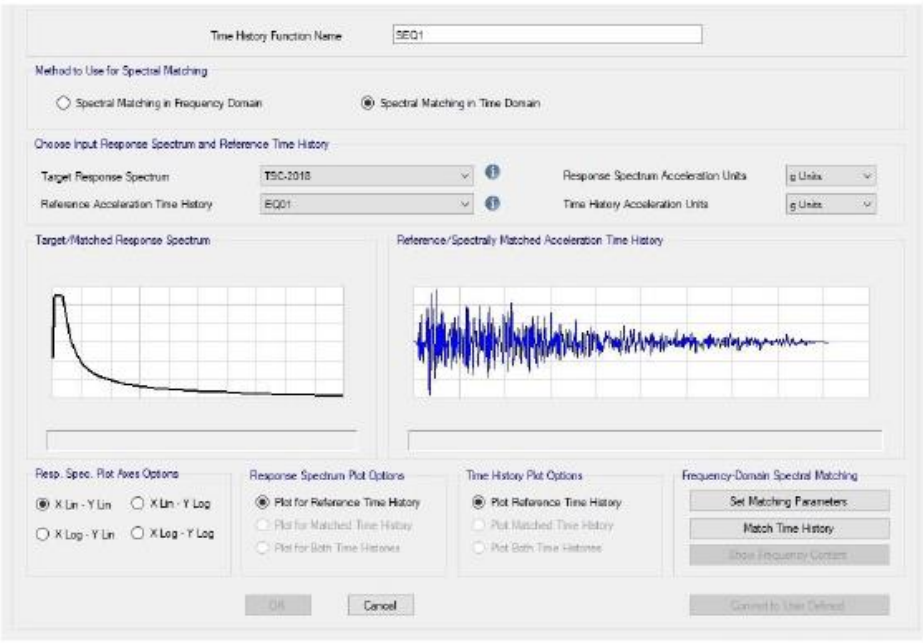

Figure 3.44 Scaling Method in SAP2000 Structural Software [24]

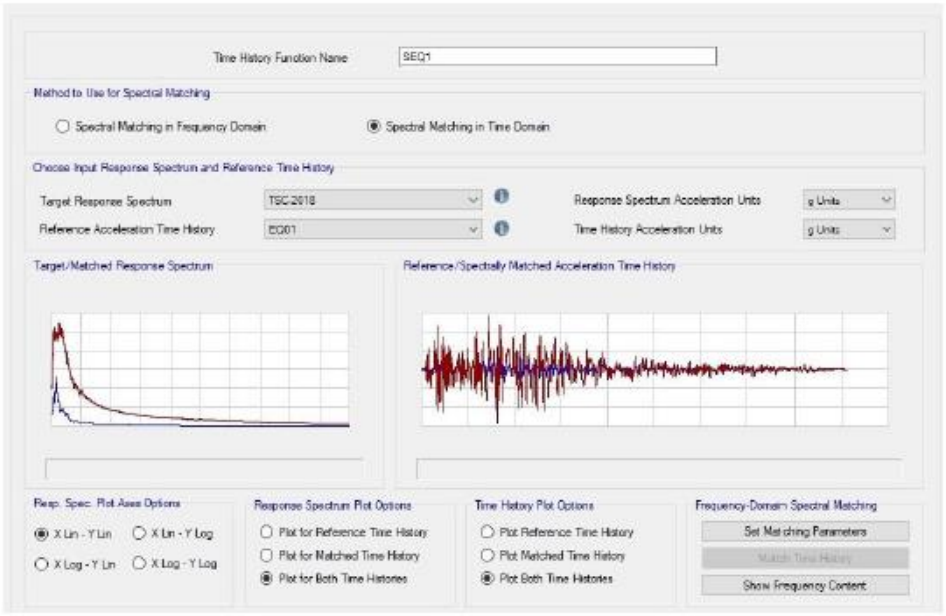

Figure 3.45 Results of Scaling for EQ1

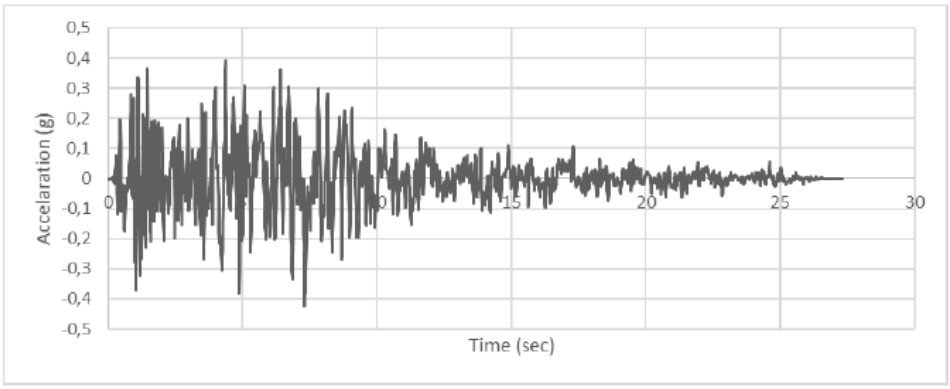

Figure 3.46 San Fernando-01 EQ1 (Scaled)

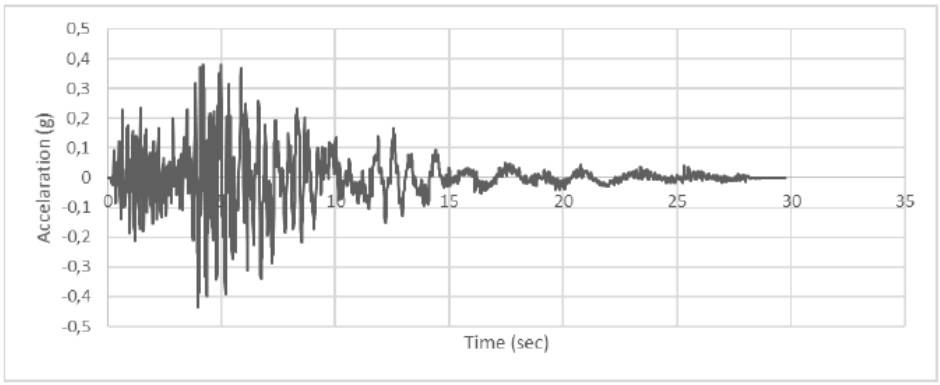

Figure 3.47 San Fernando-02 EQ2 (Scaled)

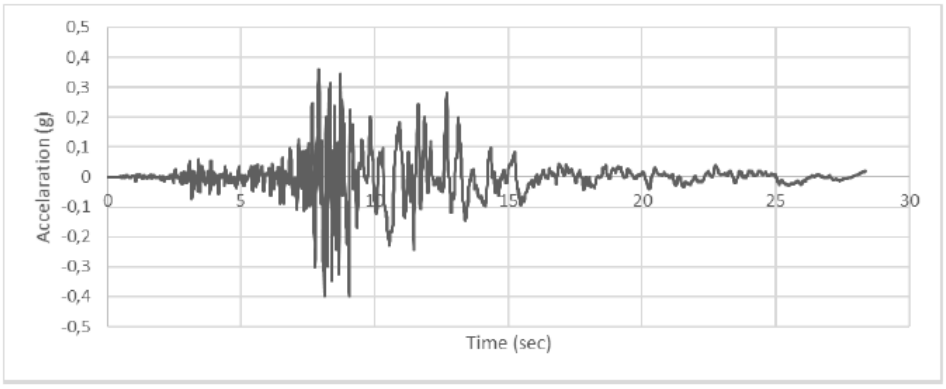

Figure 3.48 Imperial Valley EQ3 (Scaled)

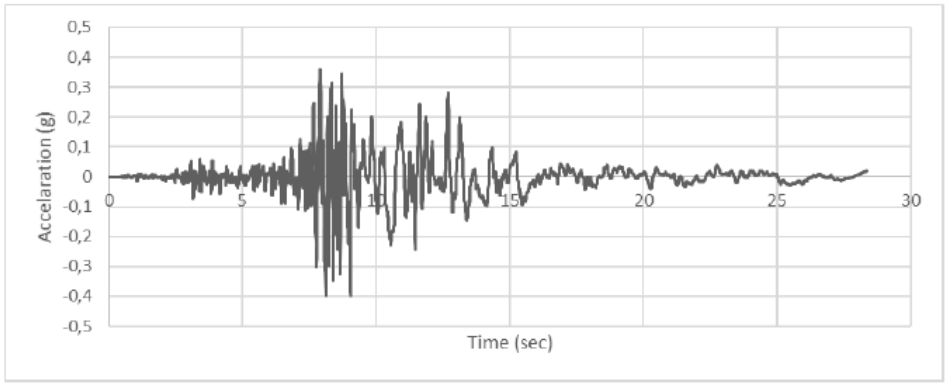

Figure 3.49 Loma Prieta-01 EQ4 (Scaled)

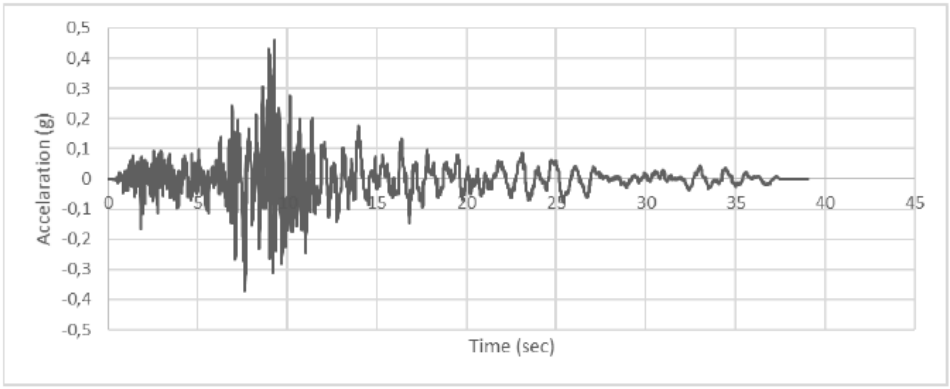

Figure 3.50 Loma Prieta-02 EQ5 (Scaled)

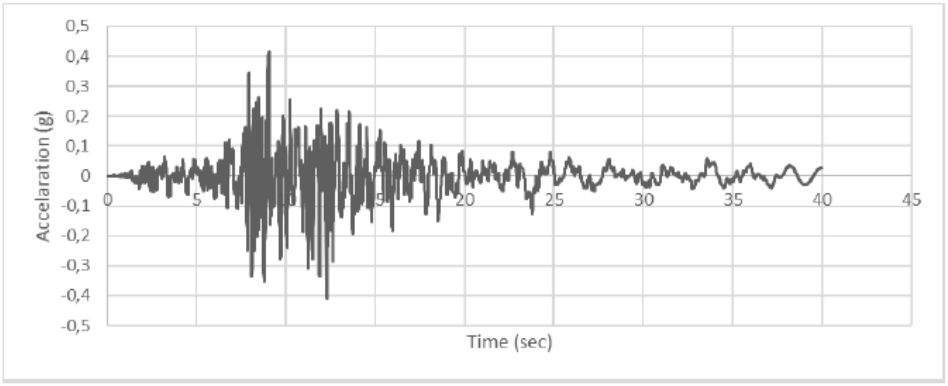

Figure 3.51 Loma Prieta-03 EQ6 (Scaled)

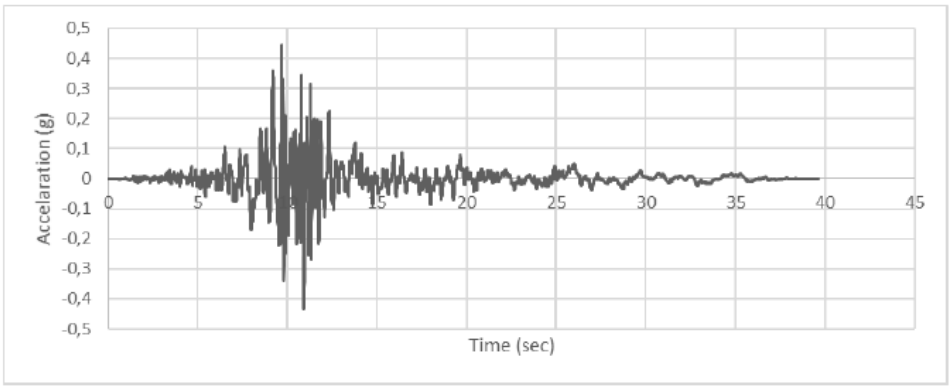

Figure 3.52 Loma Prieta-04 EQ7 (Scaled)

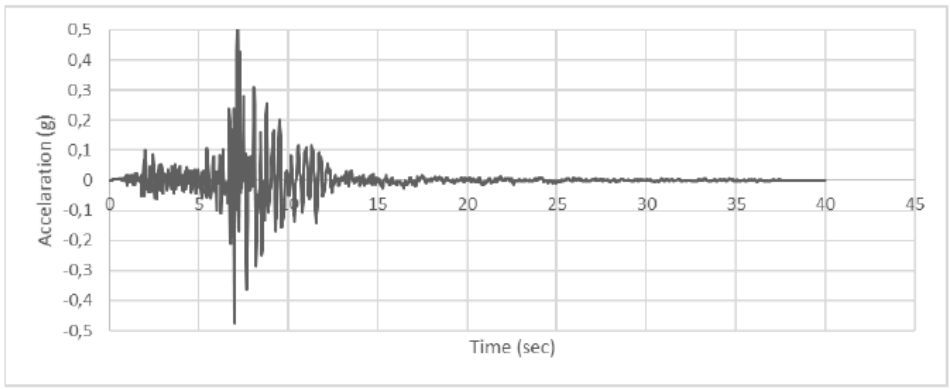

Figure 3.53 Northridge-01 EQ8 (Scaled)

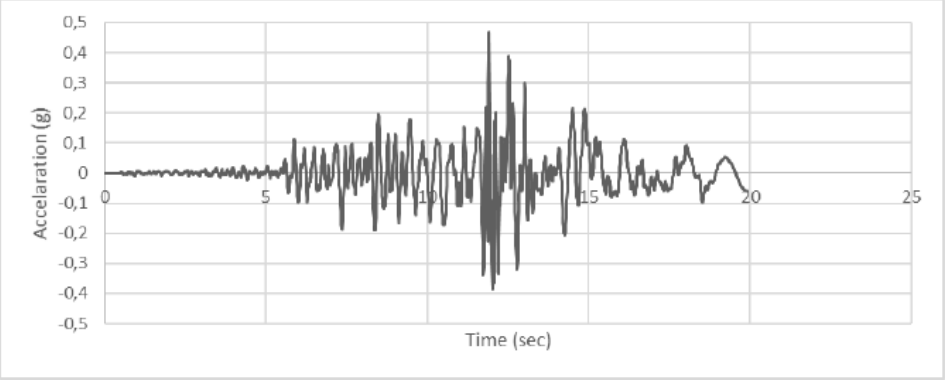

Figure 3.54 Northridge-02 EQ9 (Scaled)

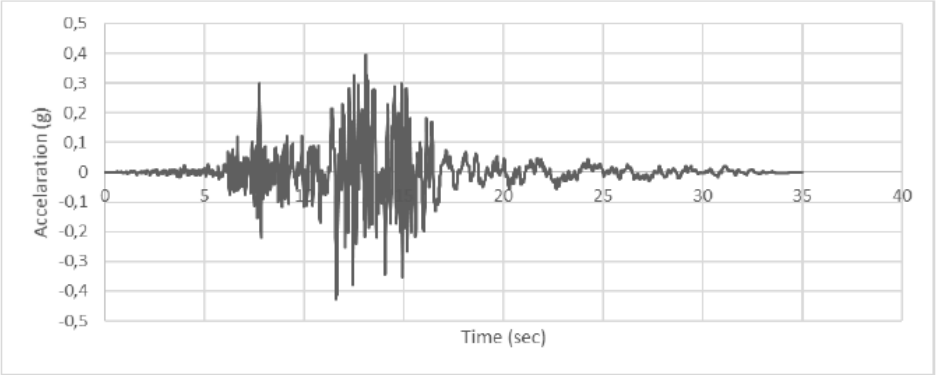

Figure 3.55 Northridge-03 EQ10 (Scaled)

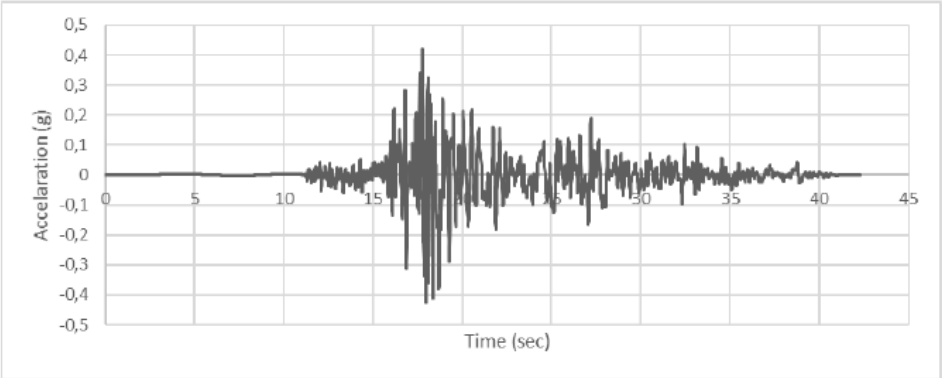

Figure 3.56 Düzce EQ11 (Scaled)

3.5.5.3.1 Definitions for Time-History Analysis in SAP2000 Structural Software

For all the earthquake records, initially load cases were defined. All the time-history analyses started from the gravity load analysis state at the end of nonlinear case. This

option was selected in SAP2000 Structural Software [23] as shown in Figure 3.57. Nonlinear analysis type option, direct integration solution type, and P-delta option for geometric nonlinearity parameter were selected. The scale factors for acceleration were defined for both x- and y-directions. Damping value was selected as 5% and Newmark method was used to calculate the time integration (Figure 3.57).

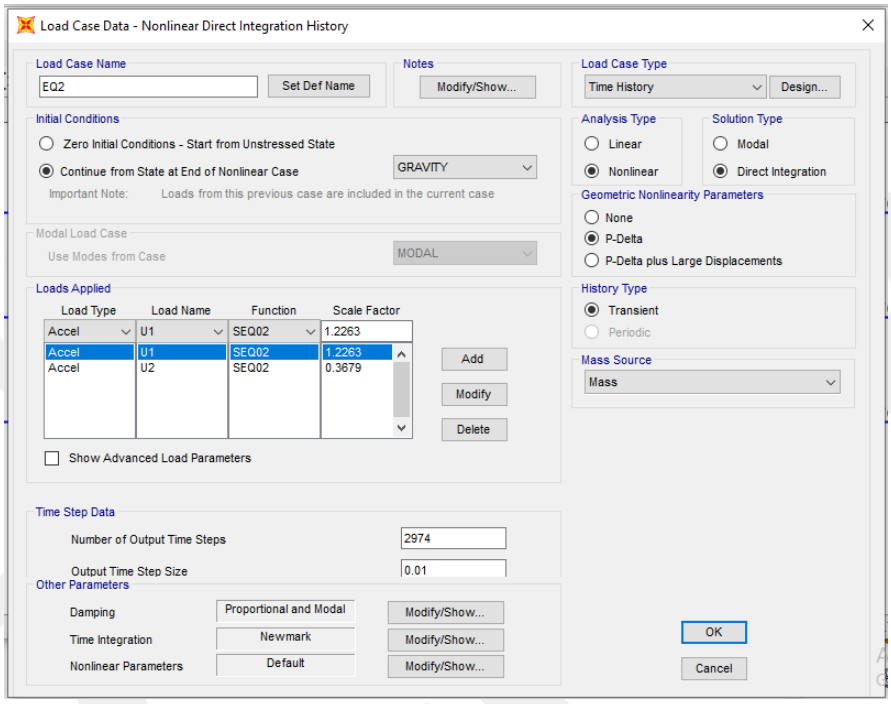

Figure 3.57 Load Case Data Definition for Time-History Analysis of EQ2

The number of output time steps and output step sizes shall match the scaled earthquake ground motion records. Therefore, step sizes were adjusted for this purpose as shown in Table 3.16.

Table 3.16 Adjustment of Number of Output Time Steps and Output Step Sizes

Case	Input Steps	Output Steps	Step Size	Damping
EQ1	2734	2734	0.01	0.05
EQ2	2974	2974	0.01	
EQ3	5669	5669	0.005	
EQ4	7998	7998	0.005	
EQ5	7811	7811	0.005	
EQ6	7998	7998	0.005	
EQ7	7930	7930	0.005	
EQ8	2000	2000	0.02	
EQ9	1991	1991	0.01	
EQ10	3499	3499	0.01	
EQ11	4233	4233	0.01	

3.5.6 Combinations

The load combinations for dead, live, snow, wind, and earthquake loads specified in TS500 [14] and TBEC [15] were used in the analysis. The basic load combinations defined in TS500 [14] are listed below:

$$F_d = 1.4 \times G + 1.6 \times Q \quad \text{Equation 3-16}$$

$$F_d = 1.0 \times G + 1.3 \times Q + 1.3 \times W \quad \text{Equation 3-17}$$

$$F_d = 0.9 \times G + 1.3 \times W \quad \text{Equation 3-18}$$

$$F_d = 1.0 \times G + 1.0 \times Q + 1.0 \times E \quad \text{Equation 3-19}$$

$$F_d = 0.9 \times G + 1.0 \times E \quad \text{Equation 3-20}$$

where F_d is the design load effect, G is the dead load, Q is the live load, W is the wind load, and E is the earthquake load.

The earthquake load was calculated using the load combination specified in TBEC [15]. This load combination in x-direction consisted of full earthquake load in x-direction combined with 30% of the earthquake load y-direction. Similarly, the load combination in y-direction consisted of full earthquake load in y-direction combined with 30% of the earthquake load x-direction. The two basic equations of the load combinations are shown below:

$$E_x = \mp E_d^{(X)} \mp 0.3 \times E_d^{(Y)} + 0.3 \times E_d^{(Z)} \quad \text{Equation 3-21}$$

$$E_y = \mp 0.3 \times E_d^{(X)} \mp E_d^{(Y)} + 0.3 \times E_d^{(Z)} \quad \text{Equation 3-22}$$

where E_x and E_y are the total earthquake load in x- and y-directions, $E_d^{(X)}$ and $E_d^{(Y)}$ are the horizontal earthquake load in x- and y-directions, and $E_d^{(Z)}$ is the vertical earthquake load.

Using the basic combinations explained above, the combinations listed in Table 3.17 were used in the analysis of the models.

Table 3.17 Load Combinations

1.4DL+1.6LL	0.9DL+1.3WINDY	1.0DL+1.3LL-1.3WINDY
1.0DL+1.0LL+1.0EQX -E+0.3EQY+0.3EQZ	0.9DL-1.3WINDY	0.9DL+1.3WINDX
1.0DL+1.0LL+1.0EQY +E+0.3EQX+0.3EQZ	0.9DL+1.0EQX +0.3EQY-0.3EQZ	0.9DL-1.3WINDX
1.0DL+1.0LL+1.0EQY -E+0.3EQX+0.3EQZ	0.9DL-1.0EQX +0.3EQY-0.3EQZ	1.0DL+1.0LL+0.2SL +1.0EQX+0.3EQY+0.3EQZ
1.0DL+1.0LL-1.0EQX +E+0.3EQY+0.3EQZ	0.9DL+1.0EQX+E +0.3EQY-0.3EQZ	0.9DL-1.0EQY+E +0.3EQX-0.3EQZ
1.0DL+1.0LL-1.0EQX -E+0.3EQY+0.3EQZ	0.9DL-1.0EQX+E +0.3EQY-0.3EQZ	0.9DL+1.0EQY +0.3EQX-0.3EQZ
1.0DL+1.0LL-1.0EQY +E+0.3EQX+0.3EQZ	0.9DL+1.0EQX-E +0.3EQY-0.3EQZ	0.9DL-1.0EQY-E +0.3EQX-0.3EQZ
1.0DL+1.0LL-1.0EQY -E+0.3EQX+0.3EQZ	0.9DL-1.0EQX-E +0.3EQY-0.3EQZ	1.0DL+1.0LL+0.2SL +1.0EQY+0.3EQX+0.3EQZ
1.0DL+1.3LL +1.3WINDX	0.9DL+1.0EQY +0.3EQX-0.3EQZ	
1.0DL+1.3LL -1.3WINDX	0.9DL-1.0EQY +0.3EQX-0.3EQZ	
1.0DL+1.3LL +1.3WINDY	0.9DL+1.0EQY+E +0.3EQX-0.3EQZ	

CHAPTER 4

DISCUSSION OF RESULTS

This section includes the analysis and design of building models with proper design based on TS500 [14] and TBEC [15]. SAP2000 Structural Software [23]-[24] was used during analysis and design. The properly designed buildings were converted to a deficient design by removing two exterior columns at each face. The deficient building models were strengthened using external steel braces at each side. The strengthened buildings were analyzed using three different analysis method, namely equivalent earthquake load, pushover analysis and time-history analysis method. The details, results, and discussion of the results related to each design and analysis are presented in this chapter.

The building models were named using their number of stories (3, 6, 9, and 12), their condition (ND: non-deficient, D: deficient, SV: strengthened using v-braces, and SX: strengthened using x-braces), and their analysis method (EE: equivalent earthquake, PA: pushover analysis, and TH: time-history analysis). As an example, 9-SV-EE shows the equivalent earthquake analysis results of 9-story building model strengthened using v-braces.

The values the results in y-direction were not shown in this study since the building models were fully symmetric. The values of the results in y-direction were similar to those of x-direction. This was also valid for both the deficient and strengthened buildings since removal of columns and placement of strengthening configuration were also symmetric.

4.1 Analysis and Design of Non-Deficient Building Models

The building models were properly designed according to specifications valid in Turkey, namely TS500 [14] and TBEC [15] as shown in Figure 4.1. These non-deficient buildings were fully functional buildings, designed to effectively resist all the loads and their combinations. A review of the dynamic properties related to non-

deficient building models are presented in Table 4.1. These values were used to compare the results of deficient and strengthened building models. The design results of building models for various number of stories are shown in figures from Figure 4.2 to Figure 4.5. These design results indicated that the non-deficient buildings were properly designed according to TS500 [14] and TBEC [15].

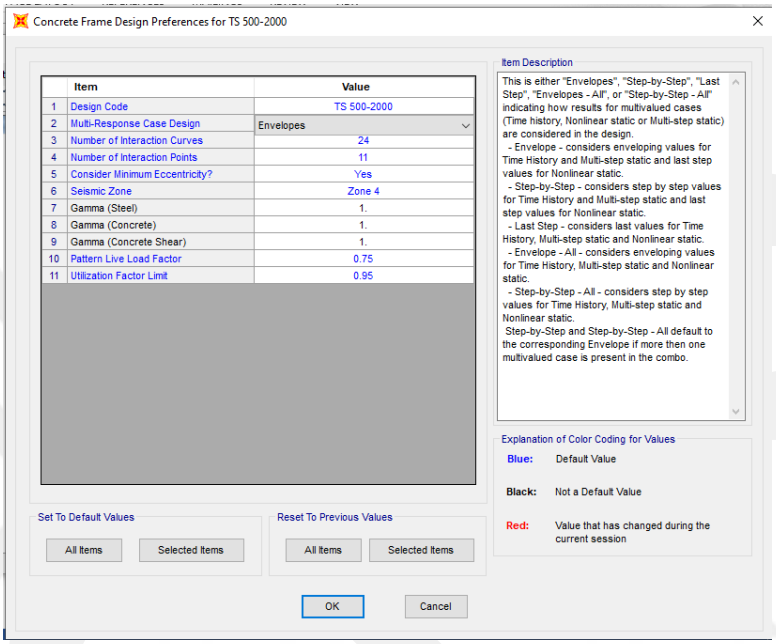

Figure 4.1 Design Preferences in SAP2000 Structural Software [23]

Table 4.1 Dynamic Properties of Non-Deficient Building Models

Model Name	Seismic Weight (kN)	T_x (s)
3-ND	31461	0.62
6-ND	72547	0.82
9-ND	103998	1.23
12-ND	169807	1.38

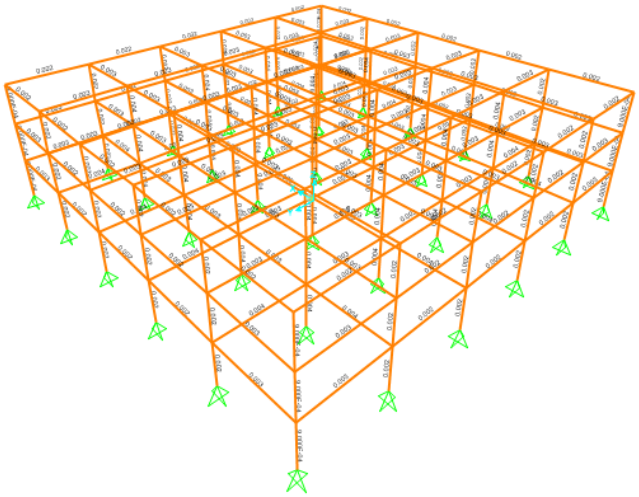

Figure 4.2 Design Results of 3-Story Non-Deficient Building Model

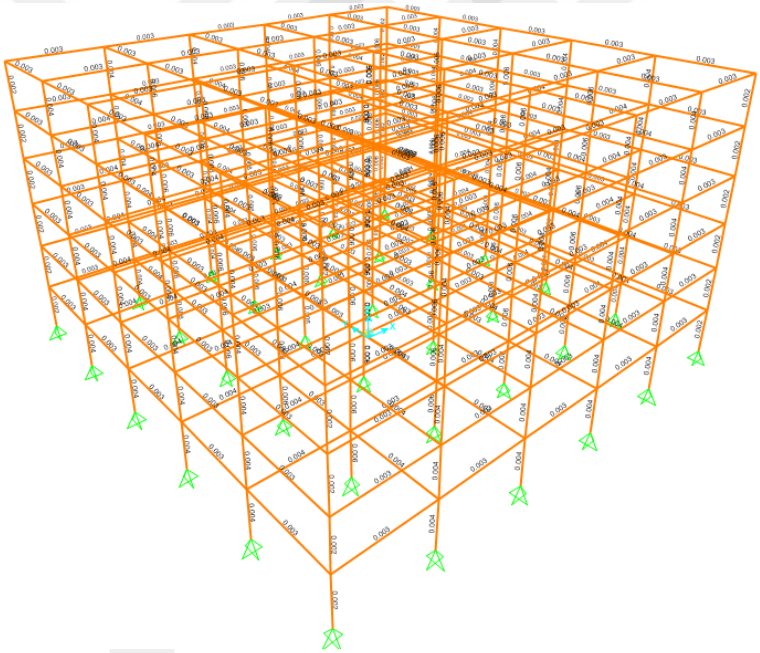

Figure 4.3 Design Results of 6-Story Non-Deficient Building Model

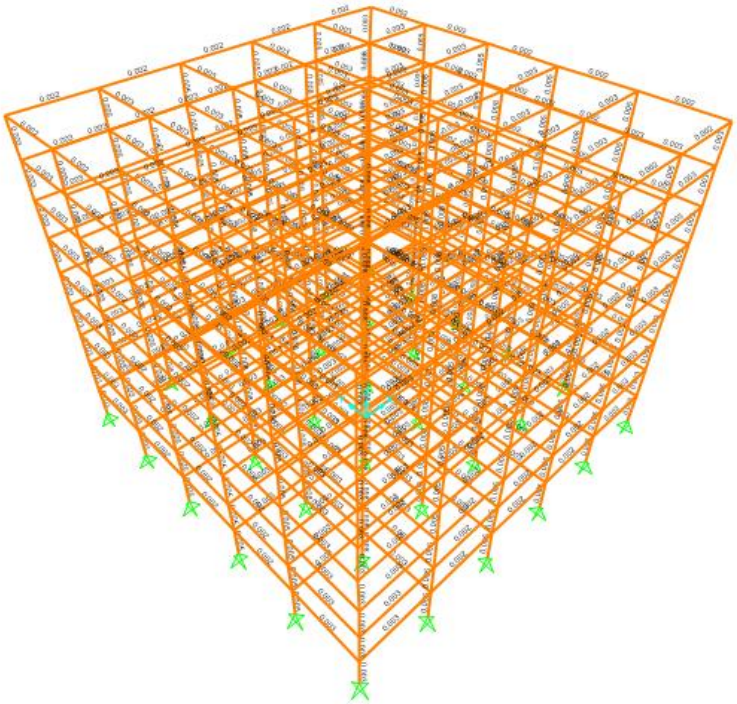

Figure 4.4 Design Results of 9-Story Non-Deficient Building Model

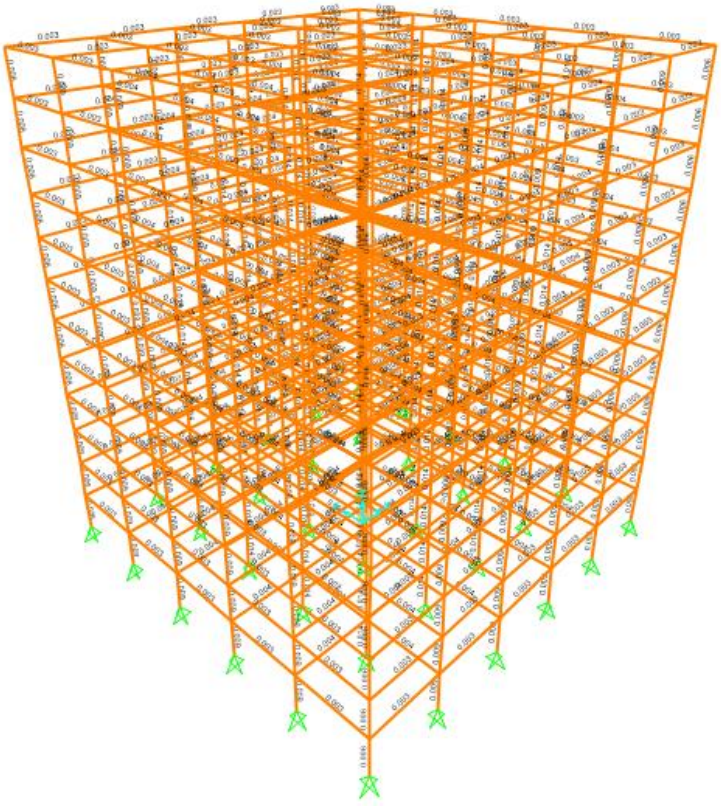

Figure 4.5 Design Results of 12-Story Non-Deficient Building Model

4.2 Analysis and Design of Deficient Building Models

To simulate a deficient building model experienced column loss due to any reason, two exterior columns at each face of the building model were removed. When each outer face of the building model is considered, the two middle columns were removed from the model throughout the height of the building. A total of 8-outer-middle columns were removed per story. One of the outer faces of the building model before and after column removal are shown in Figure 4.6 and Figure 4.7. Note that the removal of these columns still resulted in a symmetric building.

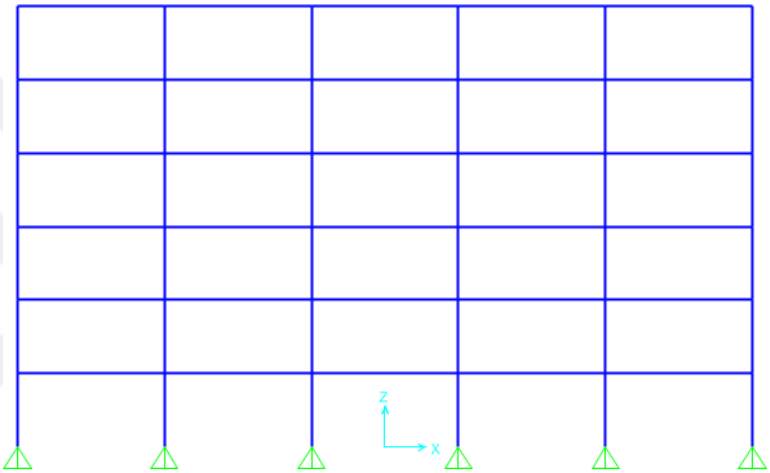

Figure 4.6 Outer Face of Non-Deficient Building Model (Before Column Removal)

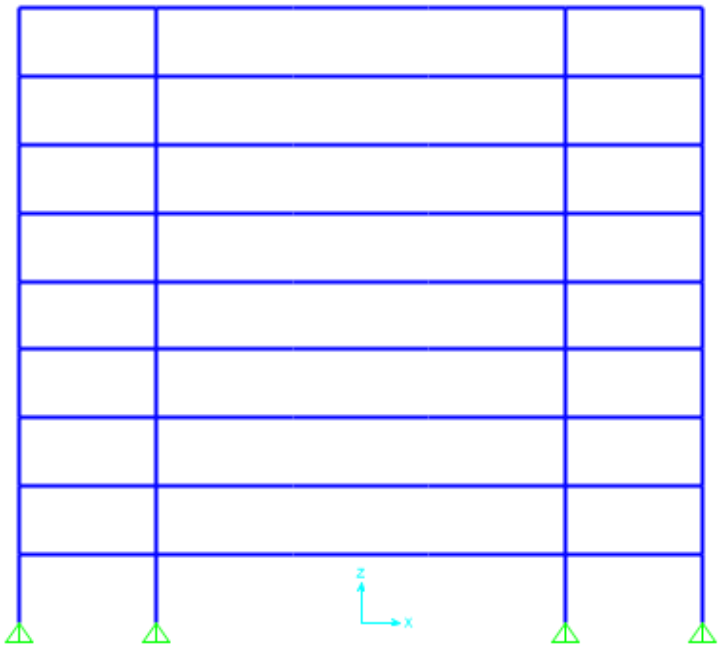

Figure 4.7 Outer Face of Non-Deficient Building Model (After Column Removal)

After the columns were removed and the building models became deficient buildings, the buildings were checked using SAP2000 Structural Software [23]. A summary of dynamic properties of deficient building models are presented in Table 4.2. The design results of deficient building models for various number of stories are shown in figures from Figure 4.8 and Figure 4.11. These design results indicated that the deficient buildings were not complying with the regulations specified by TS500 [14] and TBEC [15].

Table 4.2 Dynamic Properties of Deficient Building Models

Modal Name	**Seismic Weight (kN)**	**Period T_x (s)**
3-D	30806	0.68
6-D	71152	0.94
9-D	115832	1.23
12-D	163580	1.47

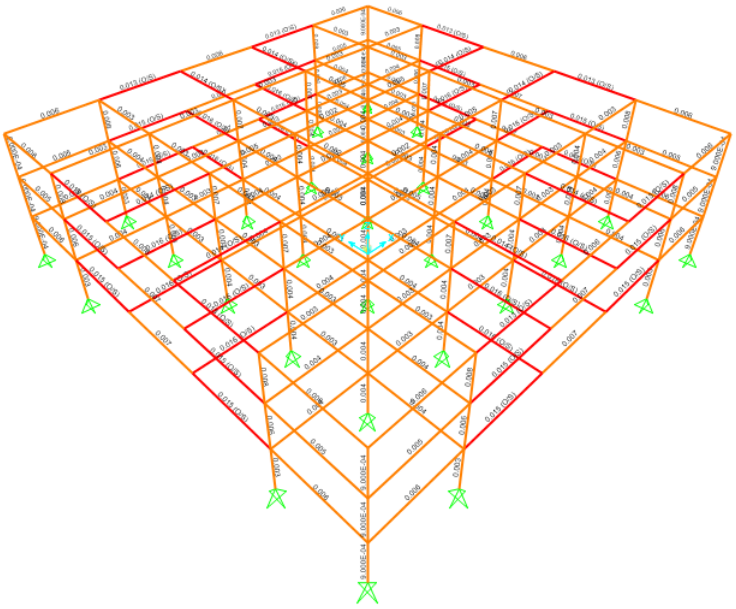

Figure 4.8 Design Results of 3-Story Deficient Building Model

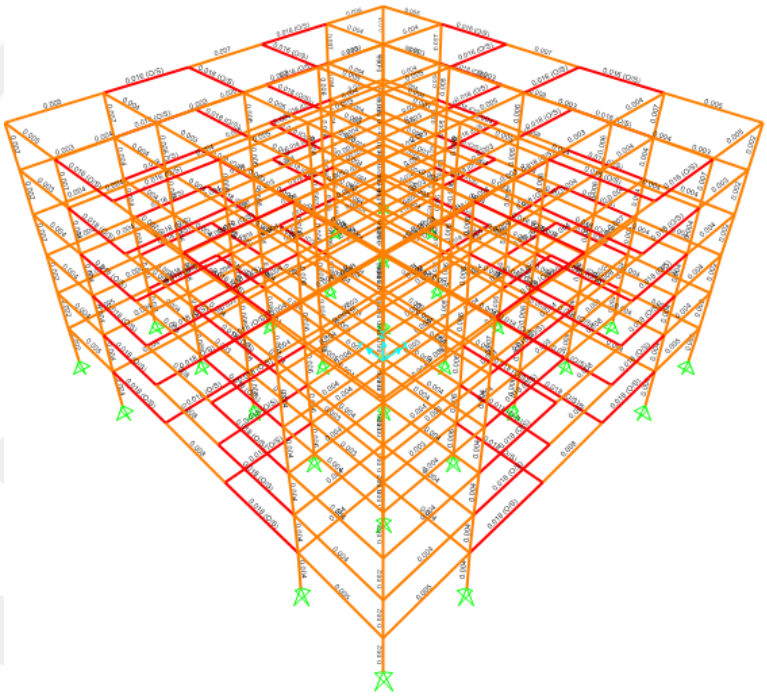

Figure 4.9 Design Results of 6-Story Deficient Building Model

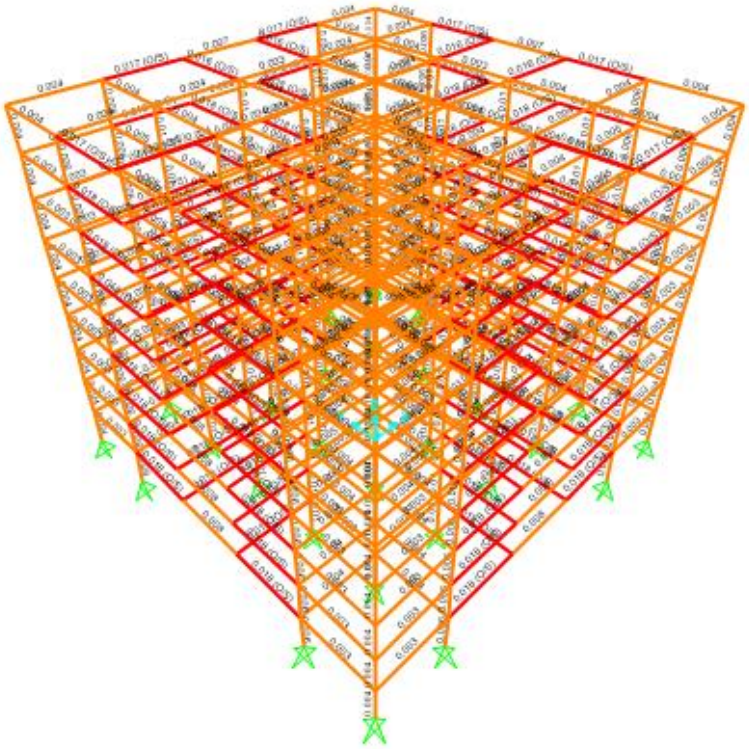

Figure 4.10 Design Results of 9-Story Deficient Building Model

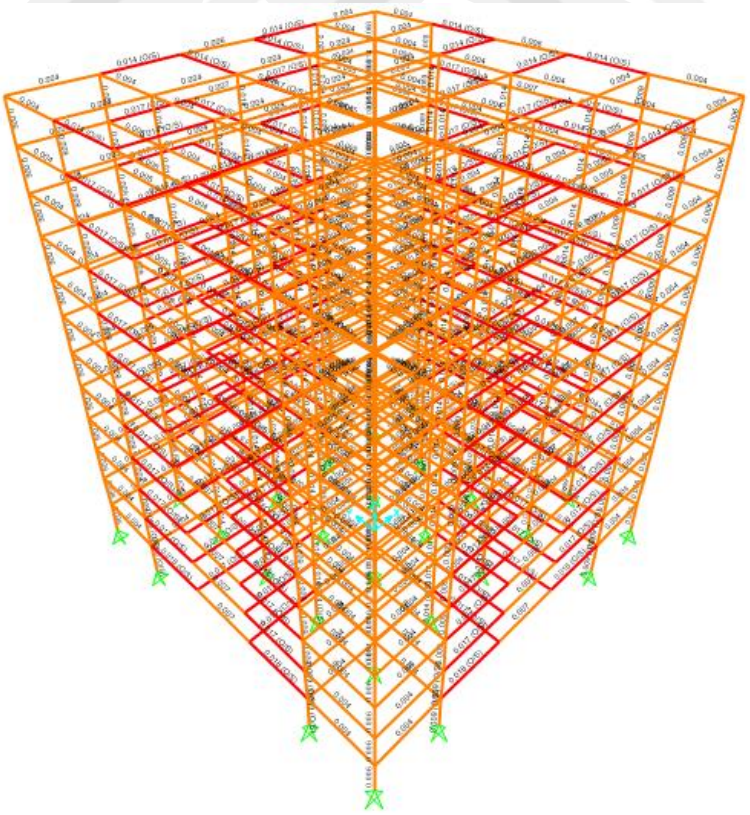

Figure 4.11 Design Results of 12-Story Deficient Building Model

4.3 Analysis and Design of Strengthened Building Models

The deficient building models were strengthened using two different configurations of external steel bracing systems, namely inverted v- and x-type as shown in Figure 4.12. These steel braces were selected based on the previous research performed by Erpek [11]. Either inverted v- or x-type bracing system was used in the same building model. The horizontal length of each bracing system was selected as 6 m which was equal to the span length of each bay of the building models. The vertical height of the bracing system was selected as 3 m which was the story height of building models. Figure 4.13 to Figure 4.16 show the configuration of inverted v- and x-type steel bracing systems around the deficient building models used in this study. A summary of dynamic properties of strengthened building models are presented in Table 4.3. The design results of building models and bracing systems for various number of stories are shown in figures from Figure 4.17 to Figure 4.32. These design results indicated that the strengthened building models and bracing systems could be properly designed according to TS500 [14], TBEC [15], and AISC 360-10 [6].

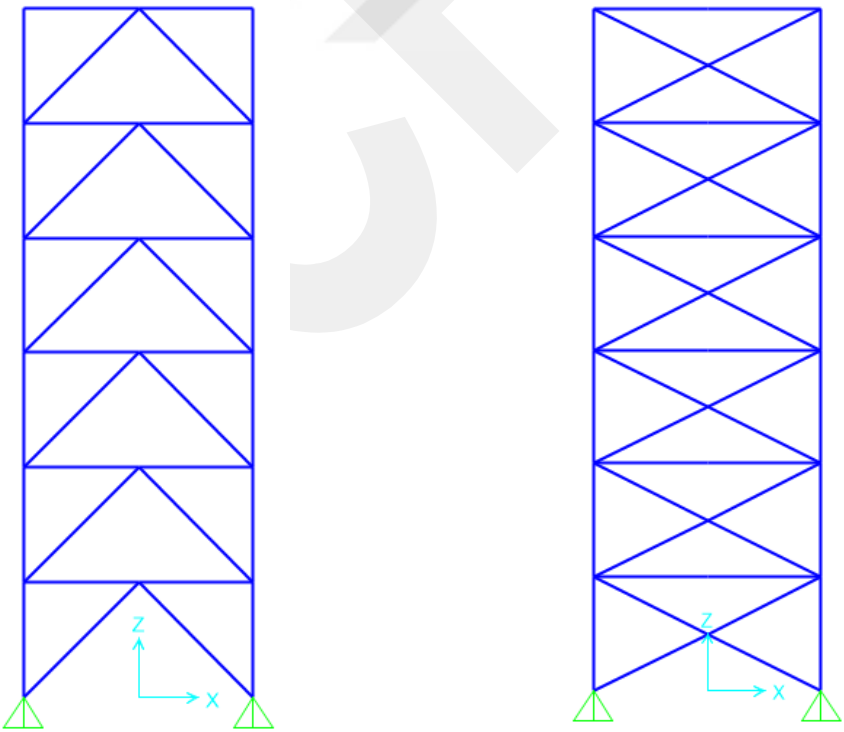

Figure 4.12 Inverted V- and X-Type Steel Bracing Systems

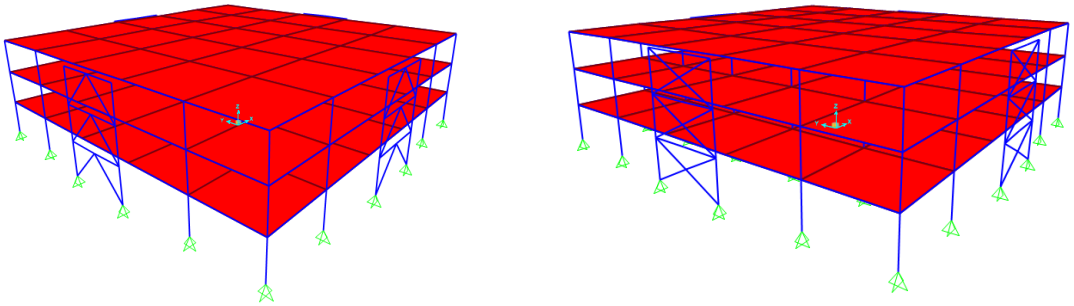

Figure 4.13 3-Story Strenthened Building Model with Inverted V- and X-Type External Steel Braces

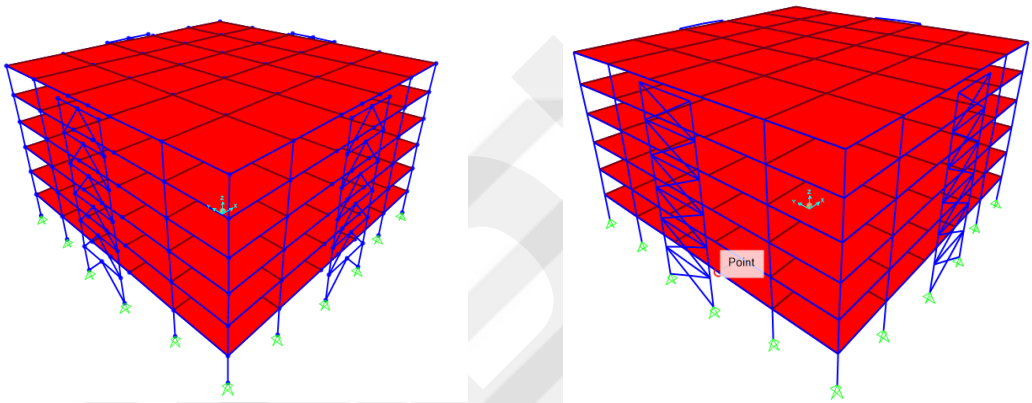

Figure 4.14 6-Story Strenthened Building Model with Inverted V- and X-Type External Steel Braces

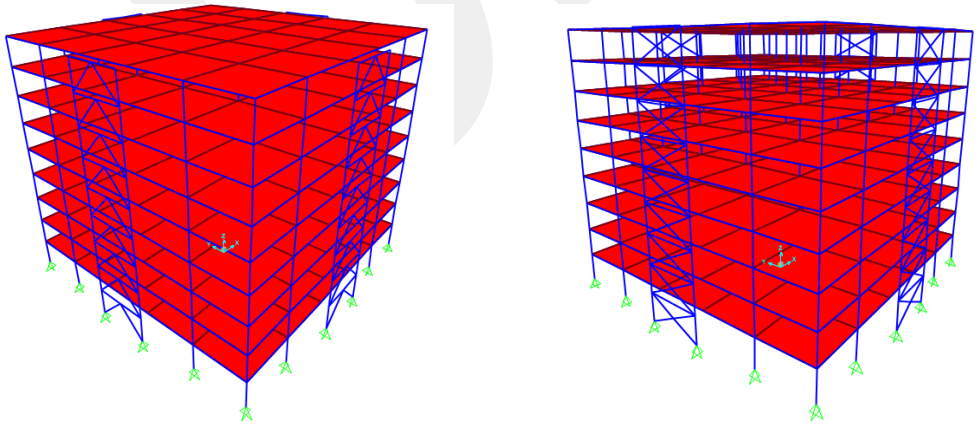

Figure 4.15 9-Story Strenthened Building Model with Inverted V- and X-Type External Steel Braces

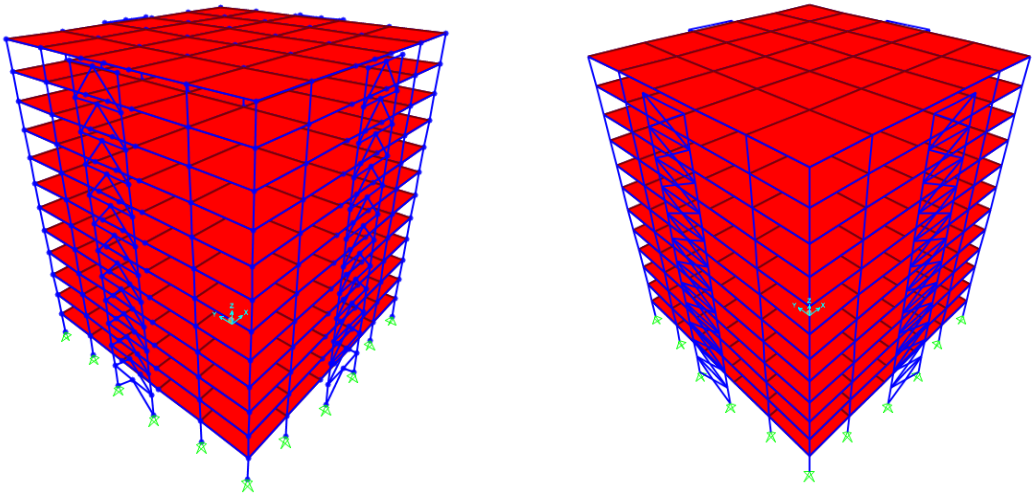

Figure 4.16 12-Story Strenthened Building Model with Inverted V- and X-Type External Steel Braces

Table 4.3 Dynamic Properties of Strengthened Building Models

Modal Name	Seismic Weight (kN)	Period T_x (s)
3-SV	31201	0.5
6-SV	71985	0.76
9-SV	117051	1.05
12-SV	165213	1.36
3-SX	31165	0.54
6-SX	72528	0.75
9-SX	117481	1.03
12-SX	164983	1.39

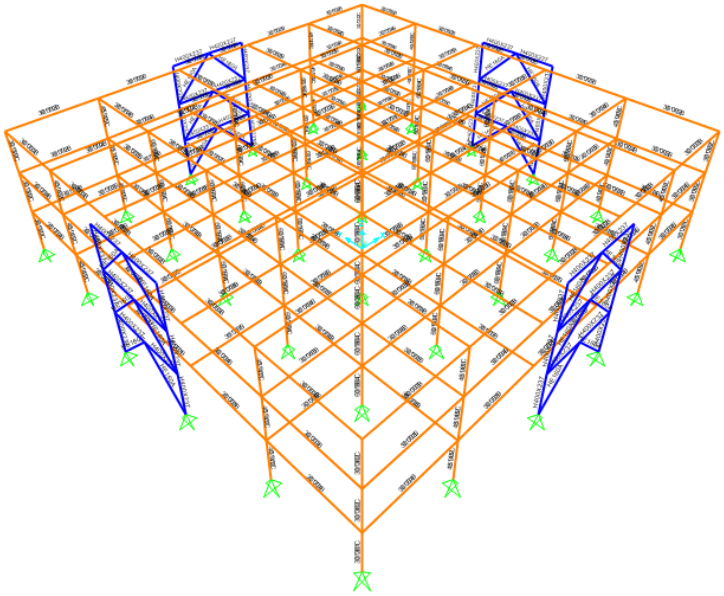

Figure 4.17 Design Results of 3-Story Strengthened Building Model using Inverted V-Type Bracing System

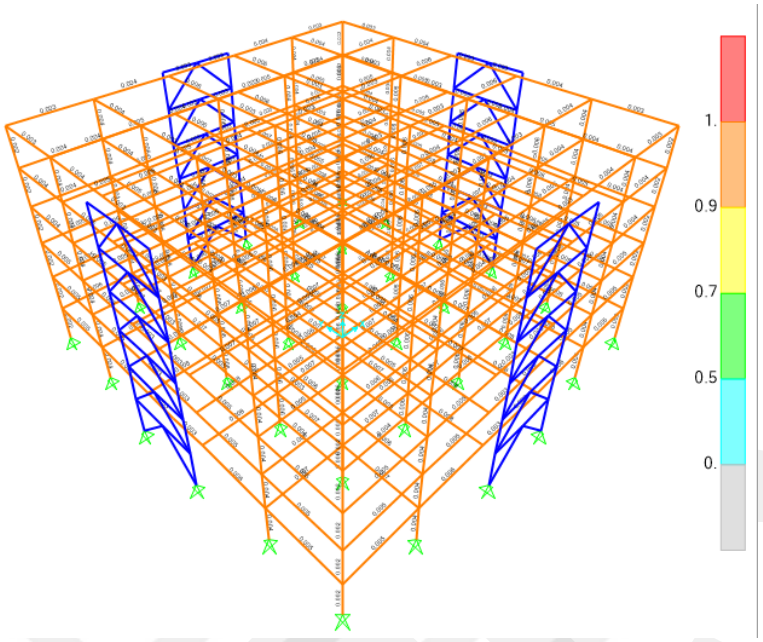

Figure 4.18 Design Results of 6-Story Strengthened Building Model using Inverted V-Type Bracing System

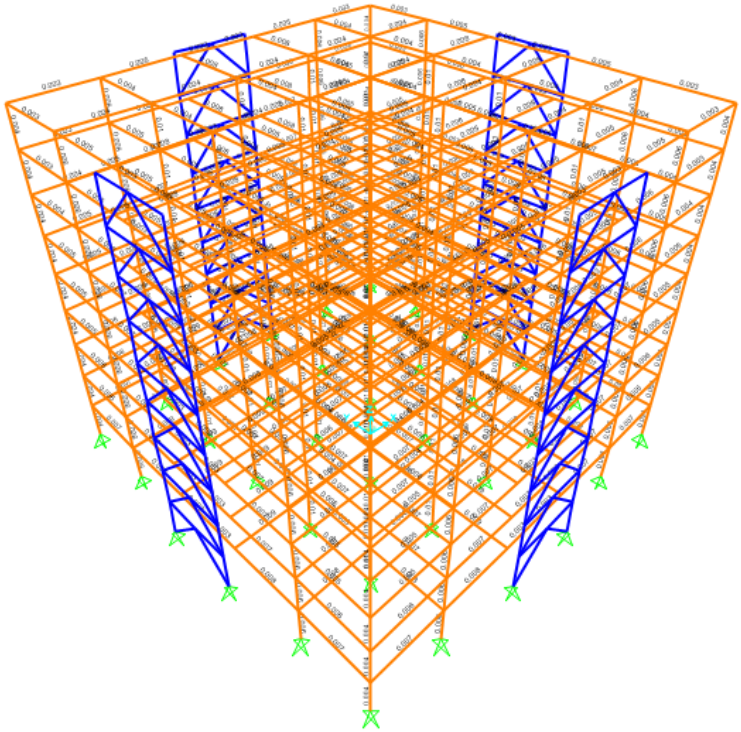

Figure 4.19 Design Results of 9-Story Strengthened Building Model using Inverted V-Type Bracing System

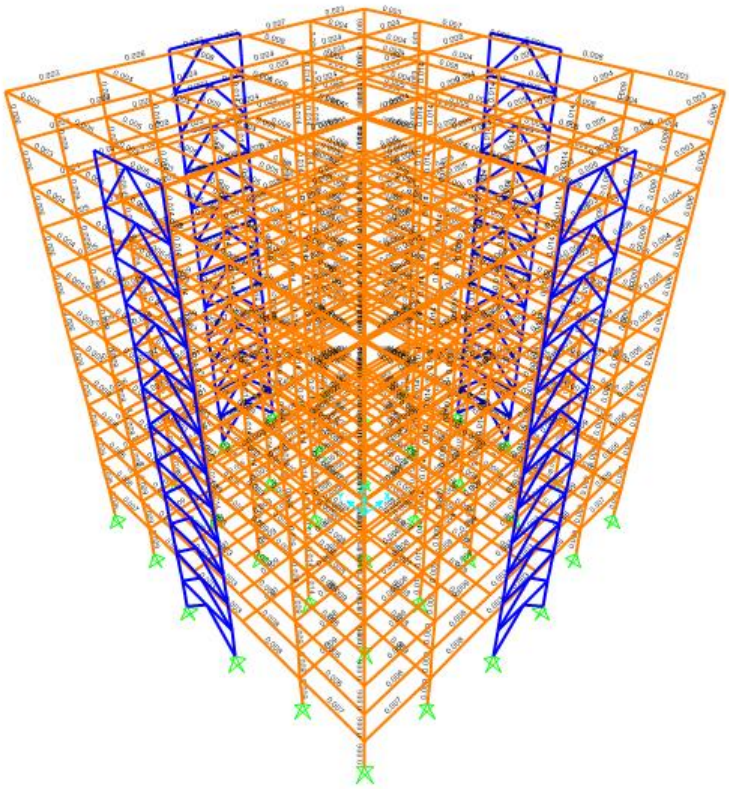

Figure 4.20 Design Results of 12-Story Strengthened Building Model using Inverted V-Type Bracing System

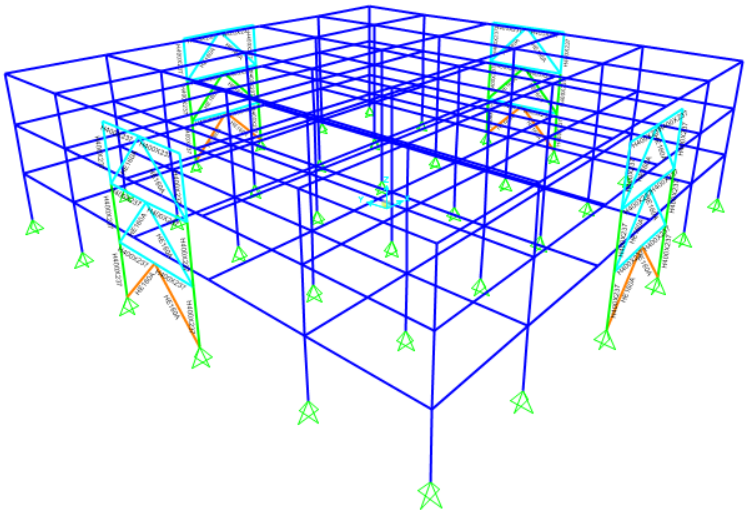

Figure 4.21 Design Results of Inverted V-Type Bracing System for 3-Story Strengthened Building Model

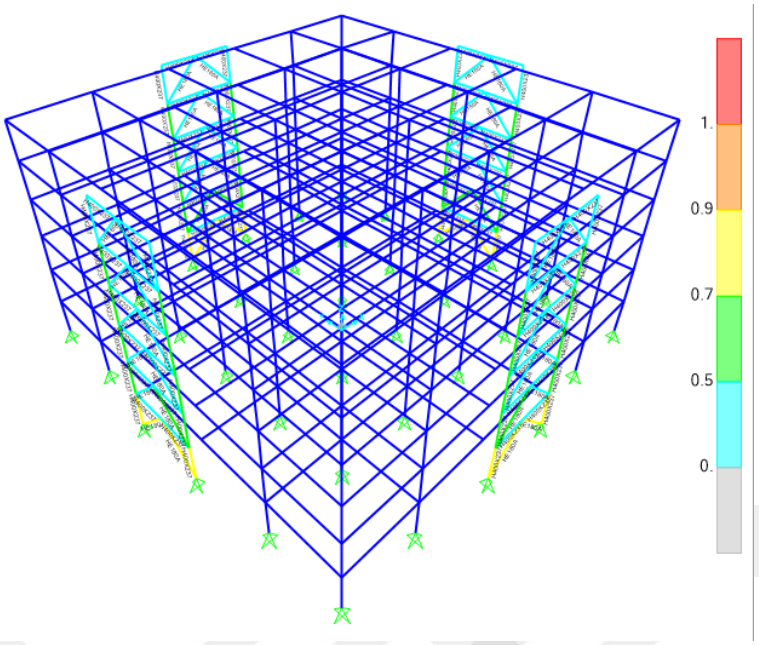

Figure 4.22 Design Results of Inverted V-Type Bracing System for 6-Story Strengthened Building Model

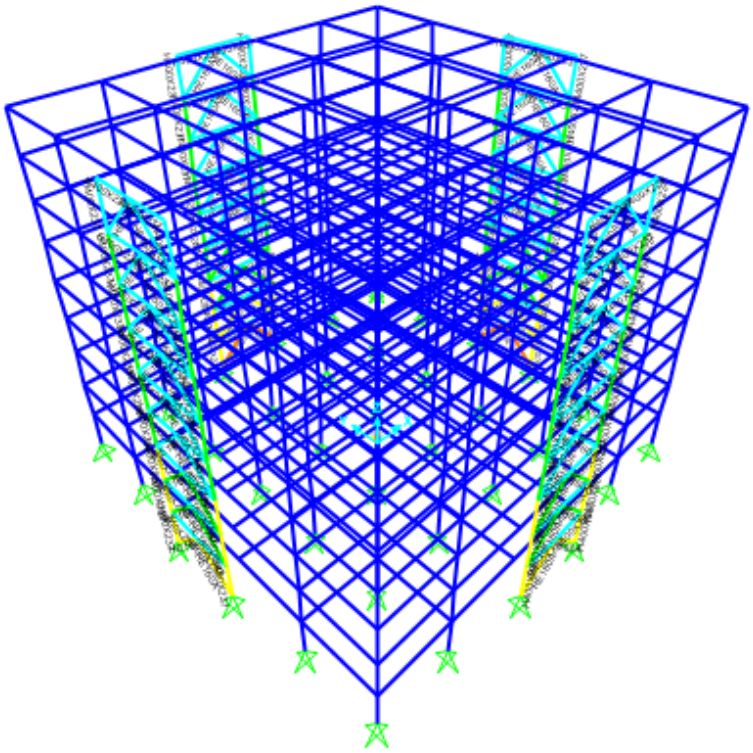

Figure 4.23 Design Results of Inverted V-Type Bracing System for 9-Story Strengthened Building Model

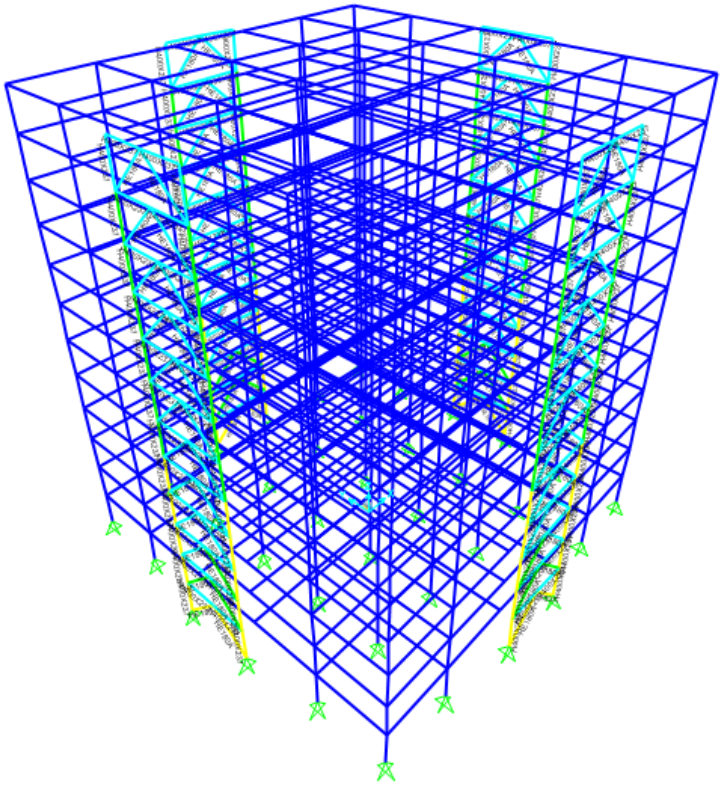

Figure 4.24 Design Results of Inverted V-Type Bracing System for 12-Story Strengthened Building Model

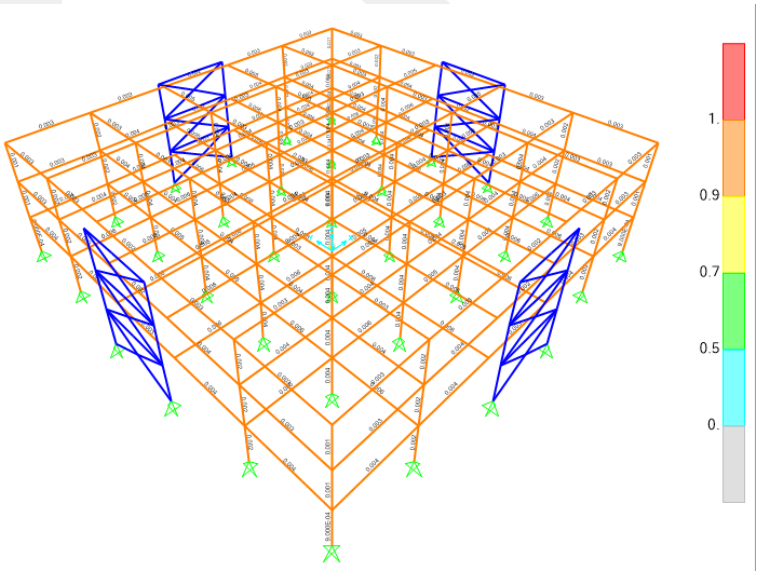

Figure 4.25 Design Results of 3-Story Strengthened Building Model using X-Type Bracing System

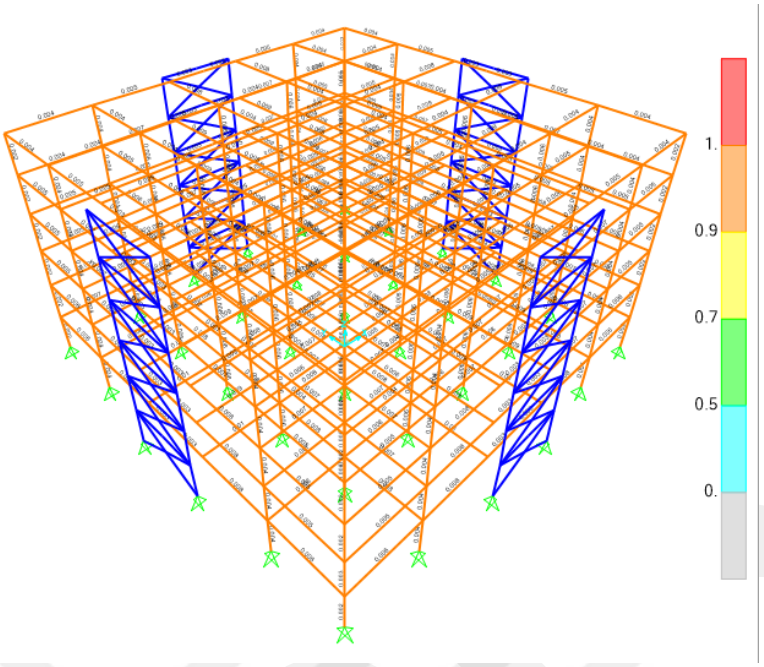

Figure 4.26 Design Results of 6-Story Strengthened Building Model using X-Type Bracing System

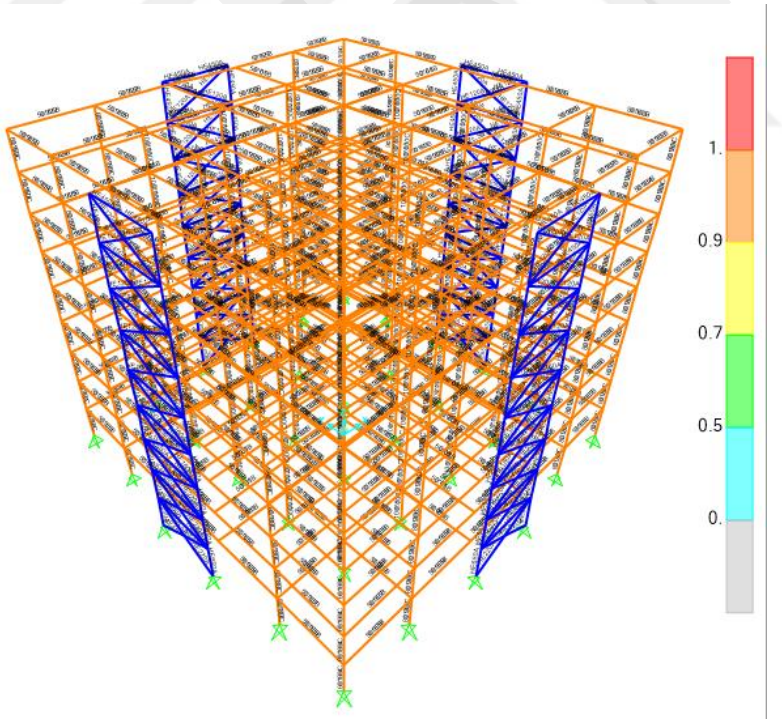

Figure 4.27 Design Results of 9-Story Strengthened Building Model using X-Type Bracing System

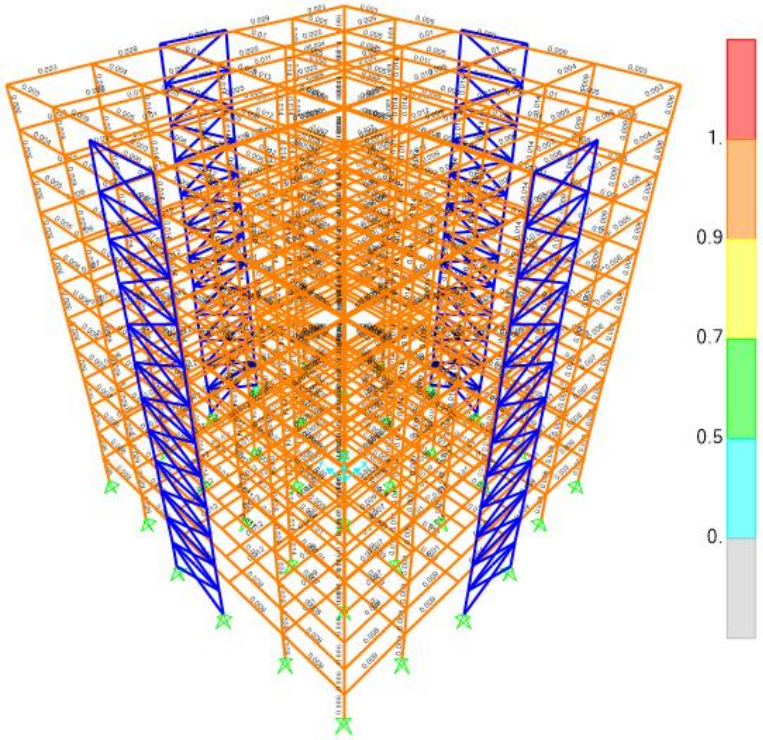

Figure 4.28 Design Results of 12-Story Strengthened Building Model using X-Type Bracing System

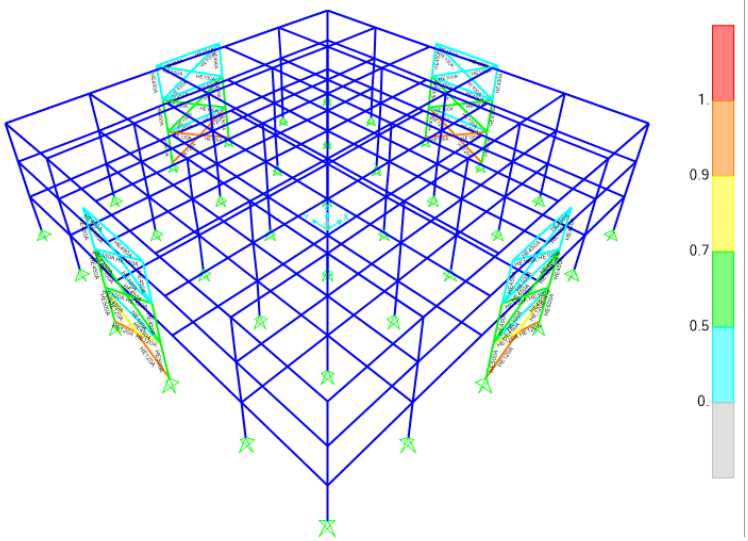

Figure 4.29 Design Results of X-Type Bracing System for 3-Story Strengthened Building Model

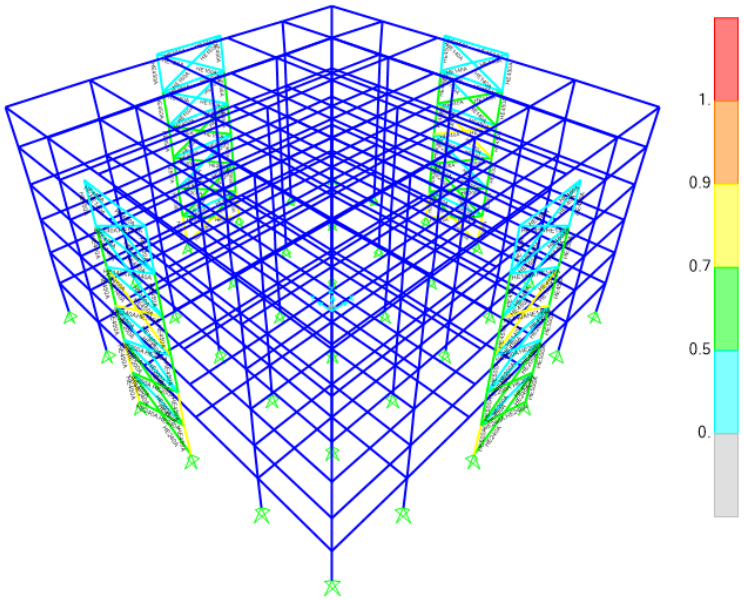

Figure 4.30 Design Results of X-Type Bracing System for 6-Story Strengthened Building Model

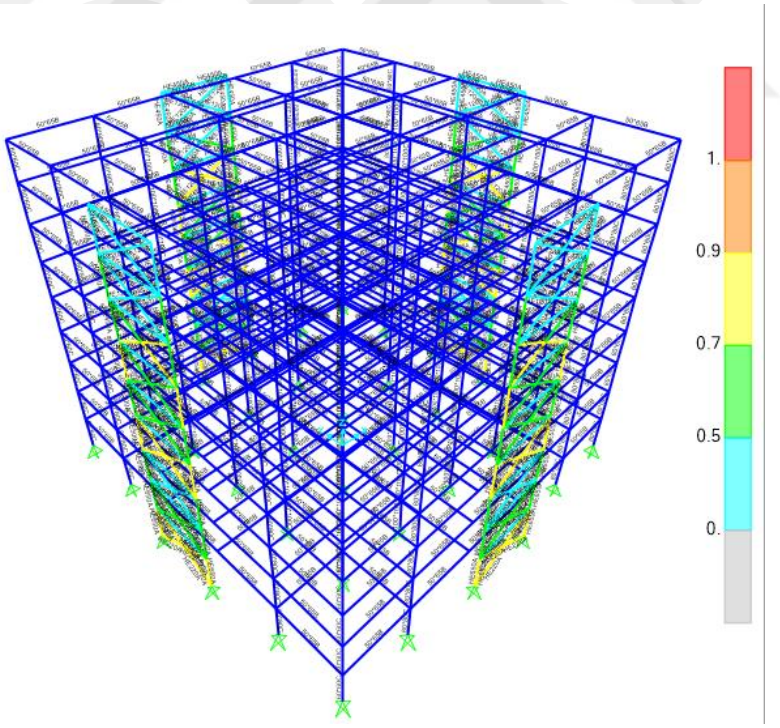

Figure 4.31 Design Results of X-Type Bracing System for 9-Story Strengthened Building Model

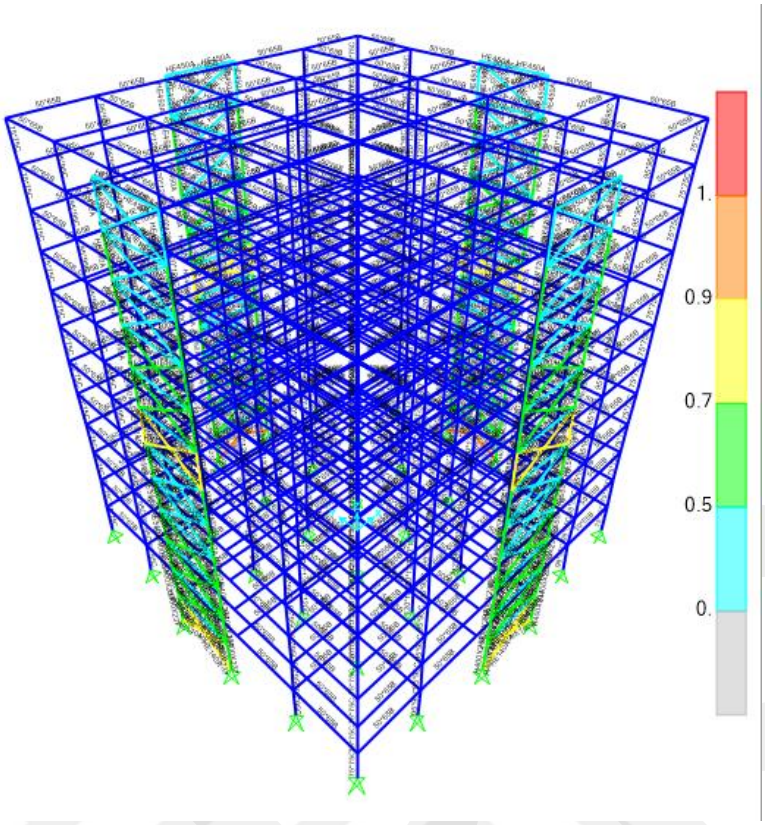

Figure 4.32 Design Results of X-Type Bracing System for 12-Story Strengthened Building Model

4.4 Results of Analysis and Design

4.4.1 Deficient Building Models

4.4.1.1 Equivalent Earthquake Load Method

The deficient building models were analyzed using equivalent earthquake load method specified by TBEC [15]. Results of the analysis are tabulated in Table 4.4.

Table 4.4 Total Base Shear, Maximum Displacement, and Drift Ratio Results of Equivalent Earthquake Load Method for Deficient Building Models

Model Name	V_{tx} (kN)	Δ_{maxx} (mm)	Combination for X	Drift Ratios X-Dir.
3-D-EE	4179	22	1.0DL+1.0LL+1.0EQX+E	2.43E-03
6-D-EE	6983	32	1.0DL+1.0LL+1.0EQX+E	1.75E-03
9-D-EE	8687	42	1.0DL+1.0LL+1.0EQX+E	1.54E-03
12-D-EE	10265	56	1.0DL+1.0LL+1.0EQX+E	1.55E-03

Where V_{tx} are the total base shear in x- direction, Δ_{maxx} are the maximum displacement values in x-direction.

4.4.1.2 Pushover Analysis Method

The deficient building models were analyzed using the pushover analysis method using SAP2000 Structural Software [23]. Results of the analysis are tabulated in Table 4.5. The calculated performance points by intersecting the performance and demand curves for all the deficient building models are shown in figures from Figure 4.33 to Figure 4.40.

Table 4.5 Pushover Analysis Results for Deficient Model Buildings

Model Names	Performance Point X-Dir.		Performance Point Y-Dir.	
	Base Shear (kN)	Δ (mm)	Base Shear (kN)	Δ (mm)
3-D-PA	5408	66	5443	66
6-D-PA	5559	89	5539	88
9-D-PA	16226	117	16301	117
12-D-PA	21708	139	21708	139

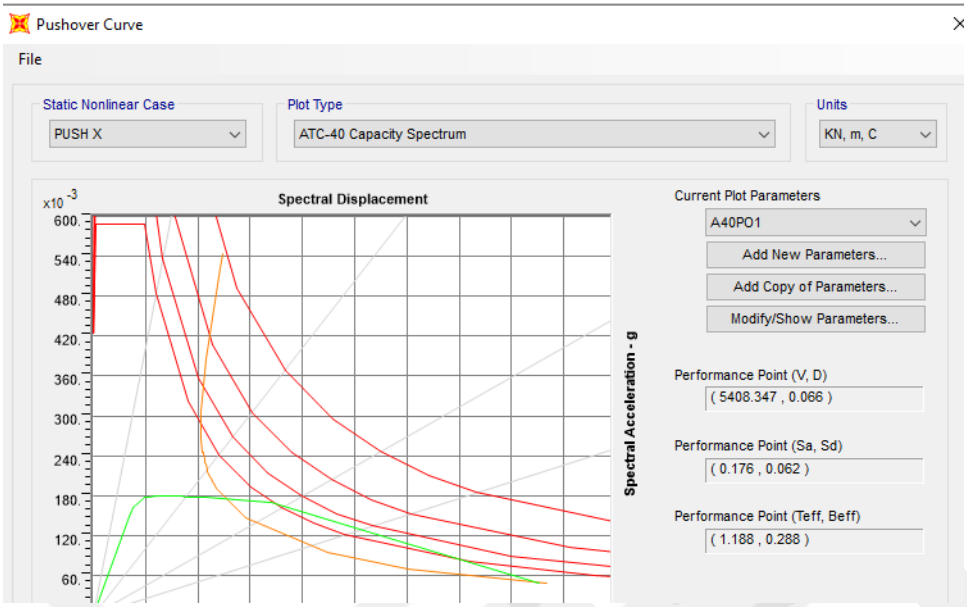

Figure 4.33 Performance Point in X-Direction for 3-D-PA Building Model

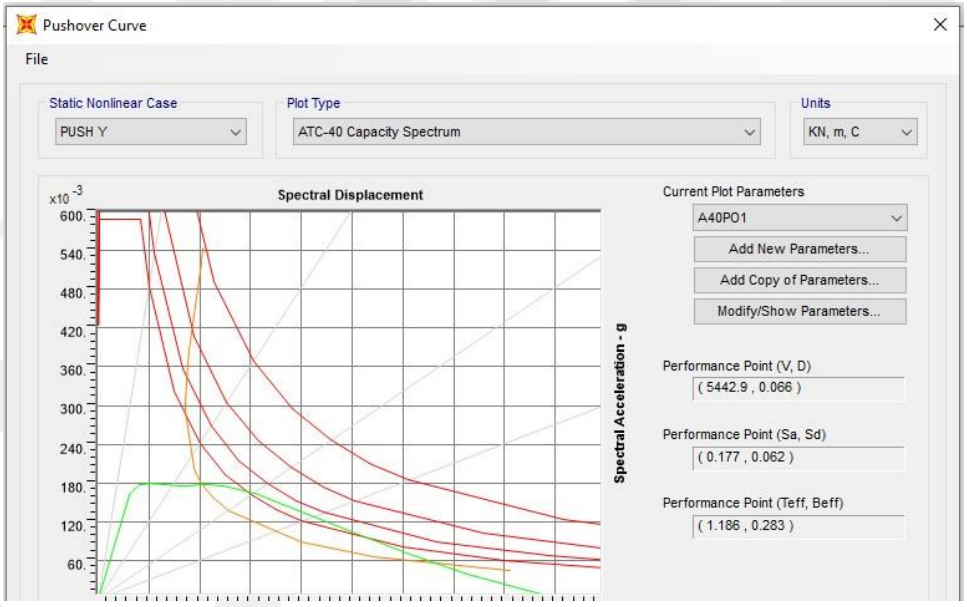

Figure 4.34 Performance Point in Y-Direction for 3-D-PA Building Model

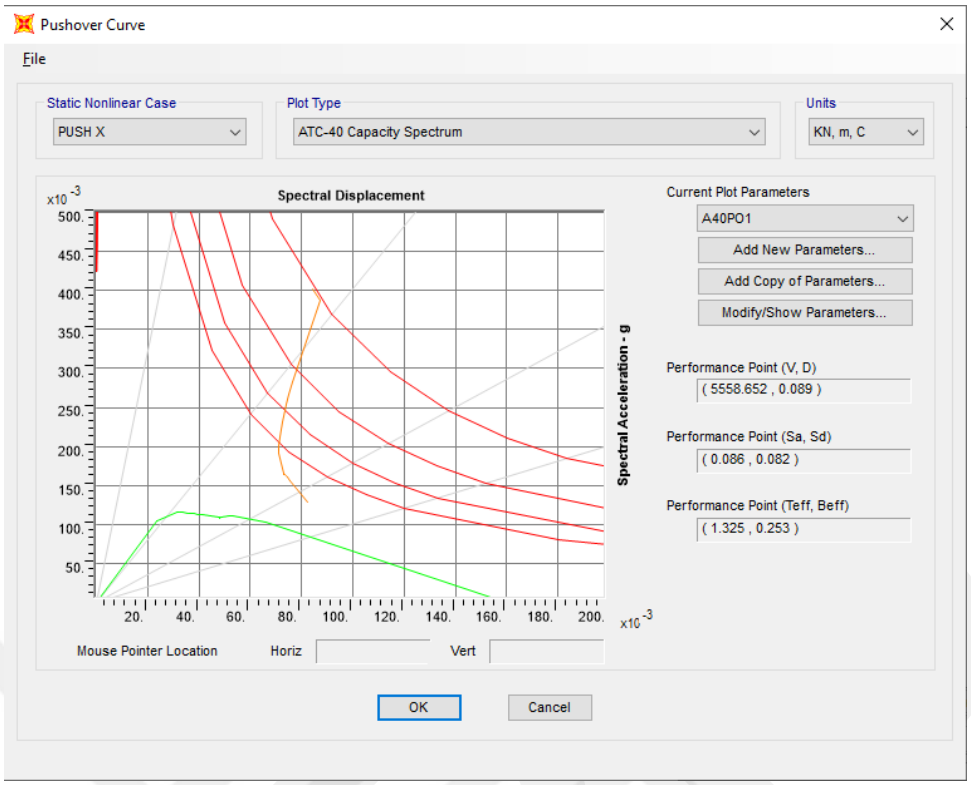

Figure 4.35 Performance Point in X-Direction for 6-D-PA Building Model

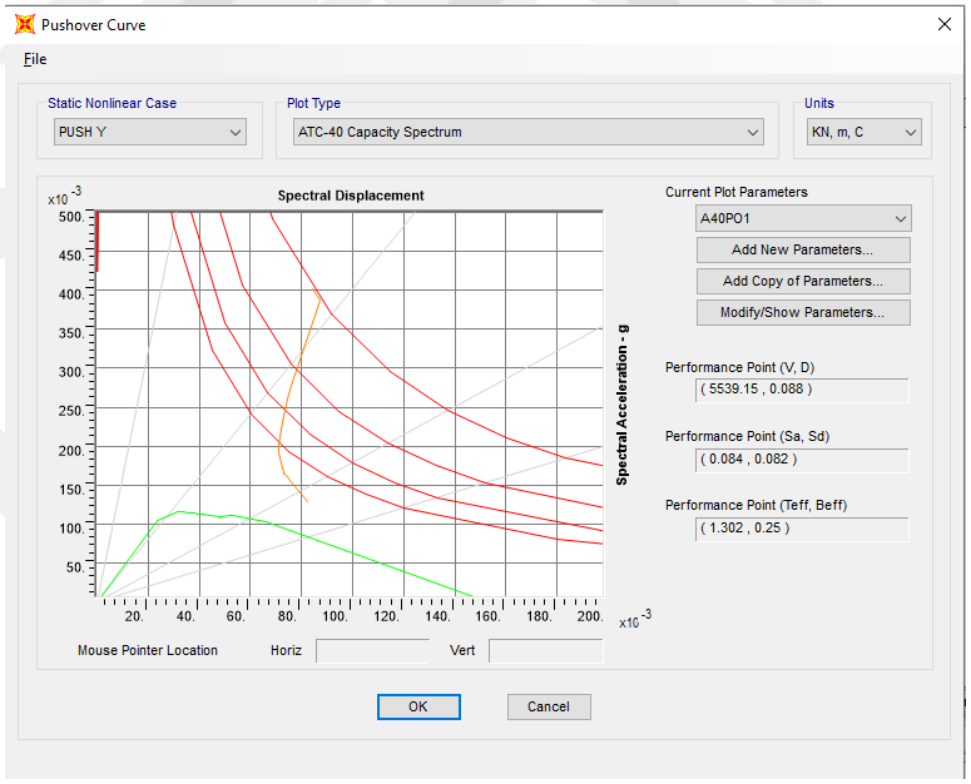

Figure 4.36 Performance Point in Y-Direction for 6-D-PA Building Model

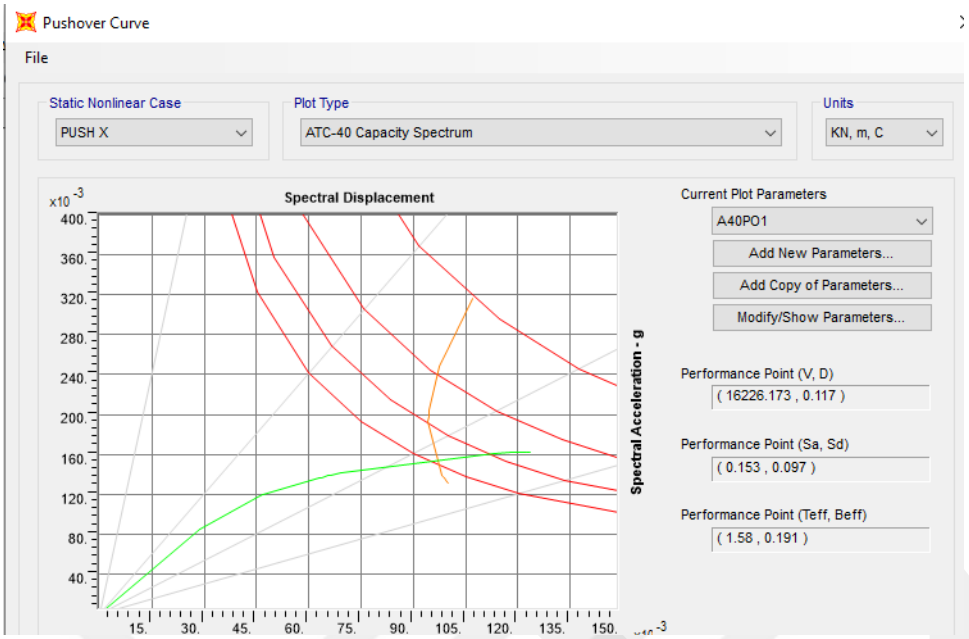

Figure 4.37 Performance Point in X-Direction for 9-D-PA Building Model

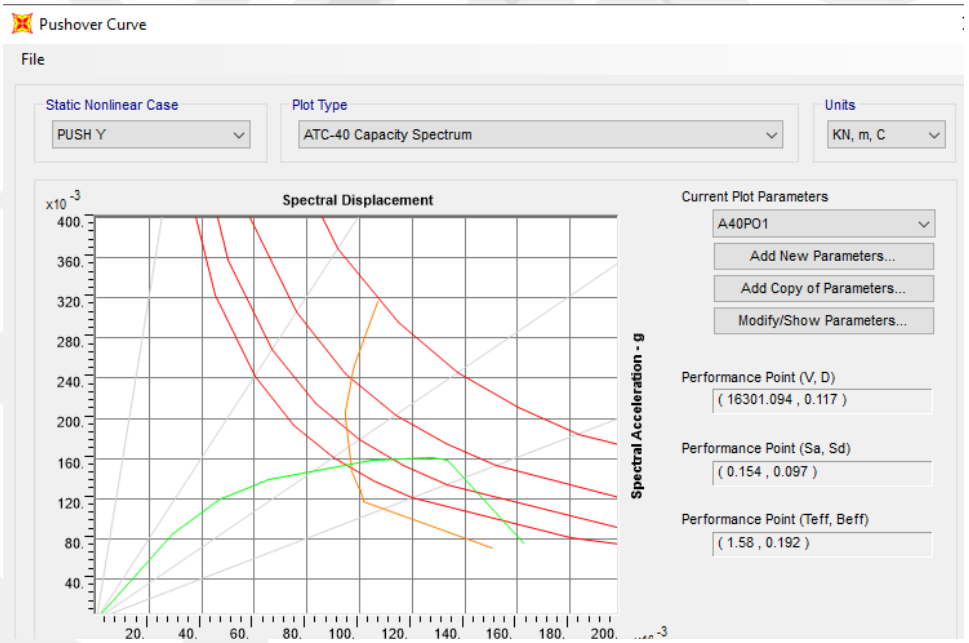

Figure 4.38 Performance Point in Y-Direction for 9-D-PA Building Model

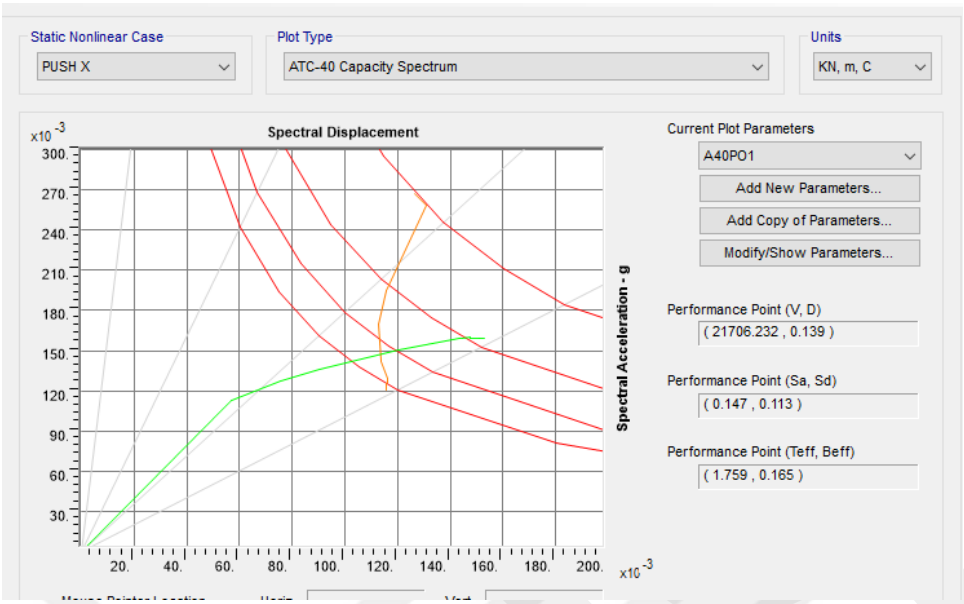

Figure 4.39 Performance Point in X-Direction for 12-D-PA Building Model

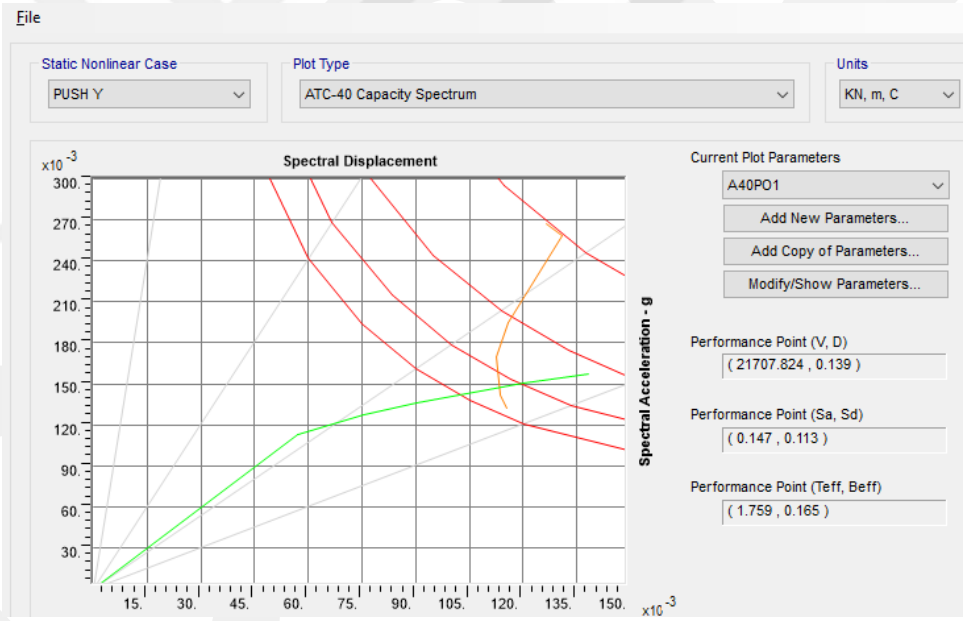

Figure 4.40 Performance Point in Y-Direction for 12-D-PA Building Model

4.4.1.3 Time-History Analysis Method

Time-history analysis was performed on deficient building models using 11 scaled earthquake ground motion records. The results of the analysis are tabulated in Table 4.6 and Table 4.7.

Table 4.6 Time-History Analysis Results of Deficient Building Models for Maximum Base Shear

Model Name	Dir.	EQ1	EQ2	EQ3	EQ4	EQ5	EQ6	EQ7	EQ8	EQ9	EQ10	EQ11
		(kN)										
3-D-TH	X	2661	2941	3425	2832	2870	3112	3000	3361	2927	3152	3325
	Y	799	881	1022	855	864	928	898	1006	878	948	994
6-D-TH	X	4987	5894	6336	4940	4514	5401	5814	6381	6269	4773	6227
	Y	1496	1768	1901	1482	1354	1620	1744	1915	1881	1432	1868
9-D-TH	X	5421	6047	5519	5340	4607	5098	5641	7568	5718	5913	5526
	Y	1632	1815	1665	1605	1381	1530	1700	2408	1718	1785	1656
12-D-TH	X	5261	4823	4153	6501	5460	5803	6979	6291	6066	5295	6343
	Y	1579	1509	1297	1971	1639	1741	2117	2049	1823	1603	1971

Table 4.7 Time-History Analysis Results of Deficient Building Models for Maximum Deflection

Model Name	Dir.	EQ1	EQ2	EQ3	EQ4	EQ5	EQ6	EQ7	EQ8	EQ9	EQ10	EQ11
		(mm)										
3-D-TH	X	15	14	17	18	14	15	16	16	15	16	15
	Y	5	4	5	5	4	4	5	5	5	5	5
6-D-TH	X	18	18	19	21	17	17	19	20	20	17	21
	Y	5	6	6	6	5	5	6	6	6	5	6
9-D-TH	X	29	28	30	28	23	24	26	33	24	30	26
	Y	9	9	9	8	7	7	8	10	7	9	8
12-D-TH	X	33	34	43	33	32	34	36	46	30	39	38
	Y	10	10	13	10	10	10	11	14	9	12	12

4.4.2 Strengthened Building Models

4.4.2.1 Equivalent Earthquake Load Method

The strengthened building models were analyzed using equivalent earthquake load method specified by TBEC [15]. Results of the analysis are tabulated in Table 4.8.

Table 4.8 Total Base Shear, Maximum Displacement, and Drift Ratio Results of Equivalent Earthquake Load Method for Strengthened Building Models

Model Name	V_{tx} (kN)	Δ_{maxx} (mm)	Combination for X	Drift Ratios X-Dir.
3-SV-EE	5757	9	1.0DL+1.0LL+1.0EQX+E	9.51-E04
6-SV-EE	8738	14	1.0DL+1.0LL+1.0EQX+E	7.55E-04
9-SV-EE	10284	20	1.0DL+1.0LL+1.0EQX+E	7.33E-04
12-SV-EE	11207	28	1.0DL+1.0LL+1.0EQX+E	7.77E-04
3-SX-EE	5324	13	1.0DL+1.0LL+1.0EQX+E	2.56E-03
6-SX-EE	8921	24	1.0DL+1.0LL-1.0EQX+E	1.33E-03
9-SX-EE	10522	28	1.0DL+1.0LL+1.0EQX+E	1.56E-03
12-SX-EE	10949	37	1.0DL+1.0LL+1.0EQX+E	1.03E-03

Where V_{tx} are the total base shear in x-directions, Δ_{maxx} are the maximum displacement values in x-directions.

4.4.2.2 Pushover Analysis Method

The strengthened building models were analyzed using the pushover analysis method using SAP2000 Structural Software [23]. Results of the analysis are tabulated in Table 4.9. The calculated performance points by intersecting the performance and demand curves for all the strengthened building models are shown in figures from Figure 4.41 to Figure 4.56.

Table 4.9 Pushover Analysis Results for Strengthened Model Buildings

Model Names	Performance Point X-Dir.		Performance Point Y-Dir.	
	Base Shear (kN)	Δ (mm)	Base Shear (kN)	Δ (mm)
3-SV-PA	7798	52	7814	52
6-SV-PA	12940	76	12972	76
9-SV-PA	18392	113	18392	113
12-SV-PA	19690	146	19690	146
3-SX-PA	6809	59	6777	59
6-SX-PA	14816	85	14904	82.3
9-SX-PA	19127	117	19127	117
12-SX-PA	19019	175	19019	175

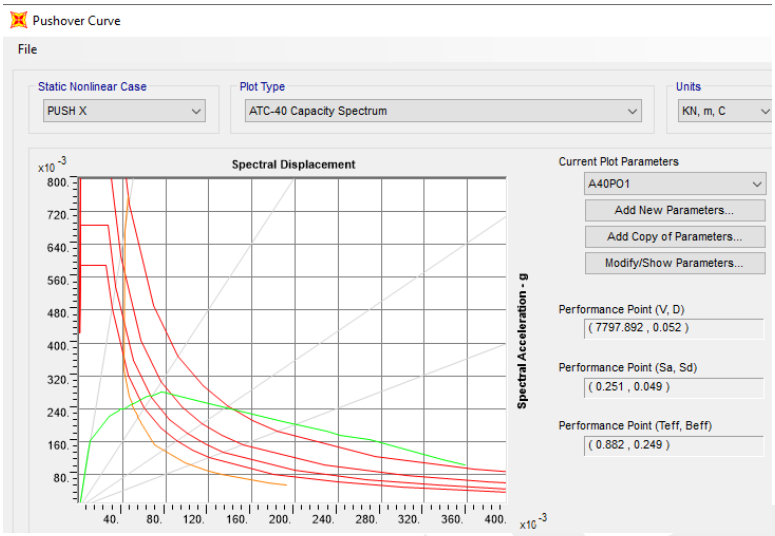

Figure 4.41 Performance Point in X-Direction for 3-SV-PA Building Model

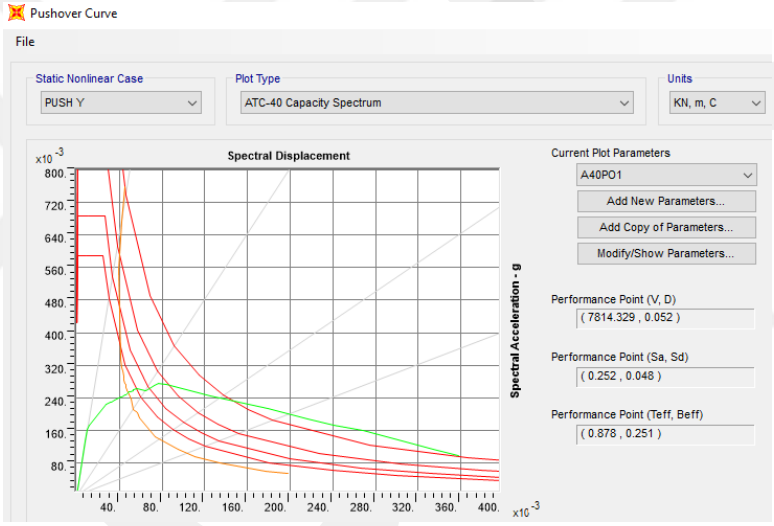

Figure 4.42 Performance Point in Y-Direction for 3-SV-PA Building Model

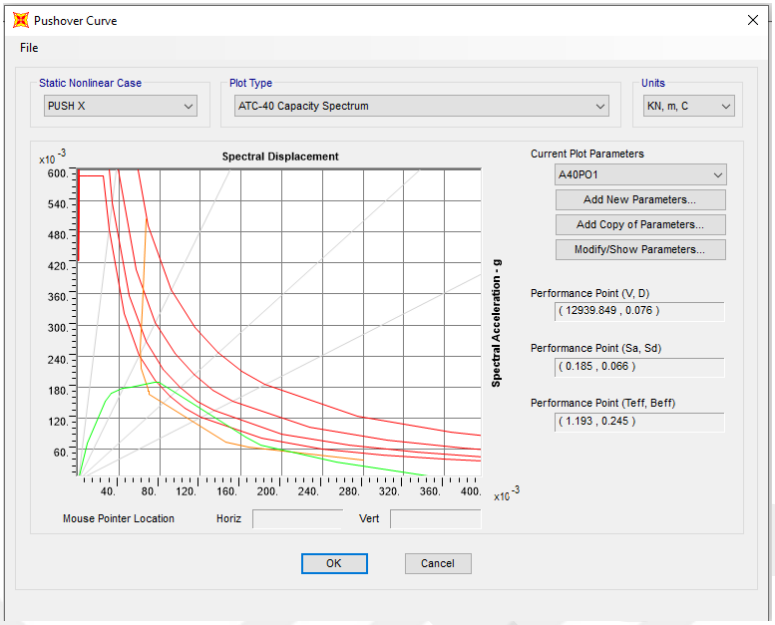

Figure 4.43 Performance Point in X-Direction for 6-SV-PA Building Model

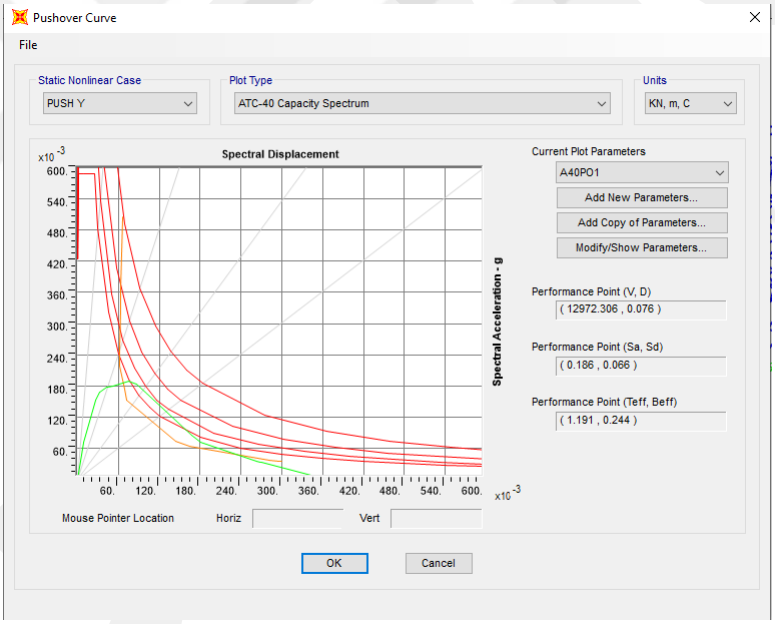

Figure 4.44 Performance Point in Y-Direction for 6-SV-PA Building Model

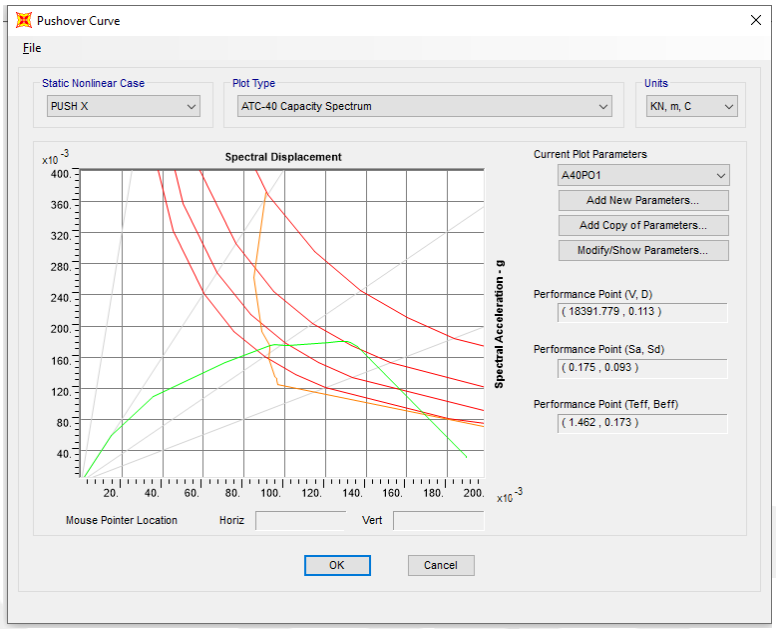

Figure 4.45 Performance Point in X-Direction for 9-SV-PA Building Model

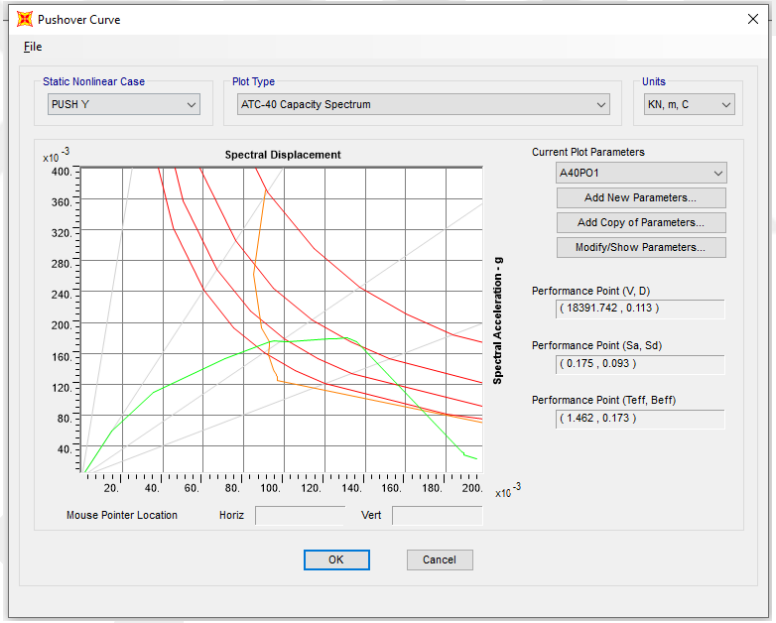

Figure 4.46 Performance Point in Y-Direction for 9-SV-PA Building Model

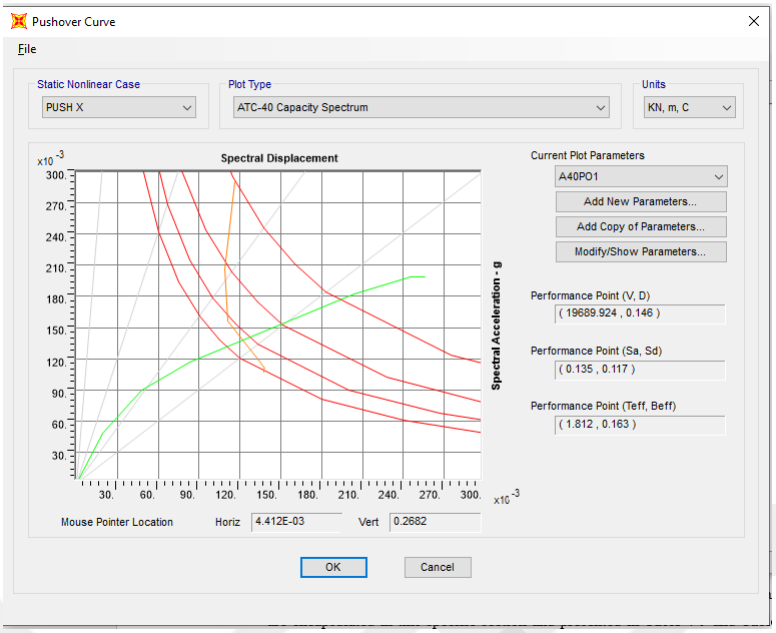

Figure 4.47 Performance Point in X-Direction for 12-SV-PA Building Model

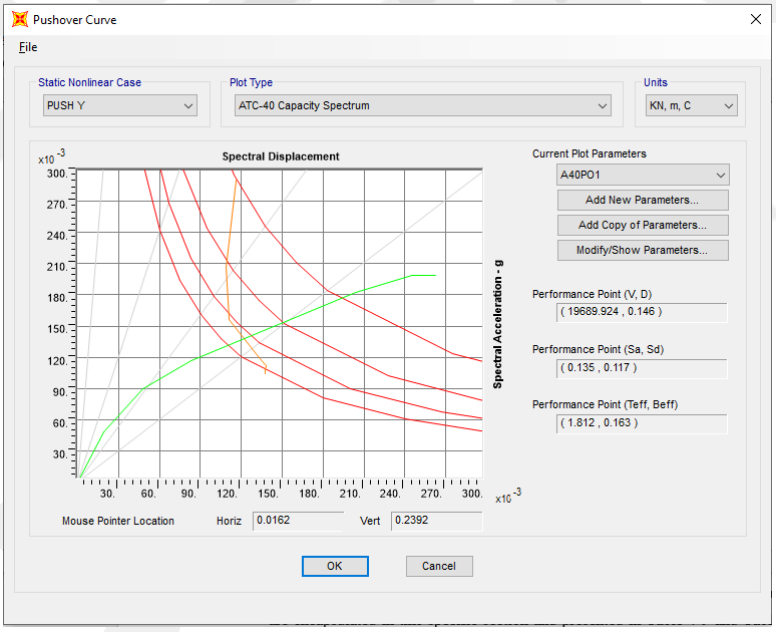

Figure 4.48 Performance Point in Y-Direction for 12-SV-PA Building Model

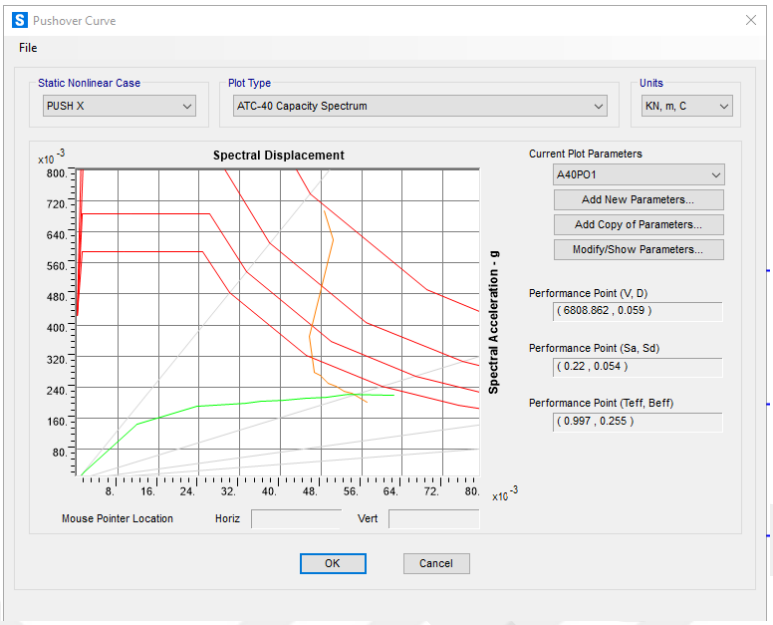

Figure 4.49 Performance Point in X-Direction for 3-SX-PA Building Model

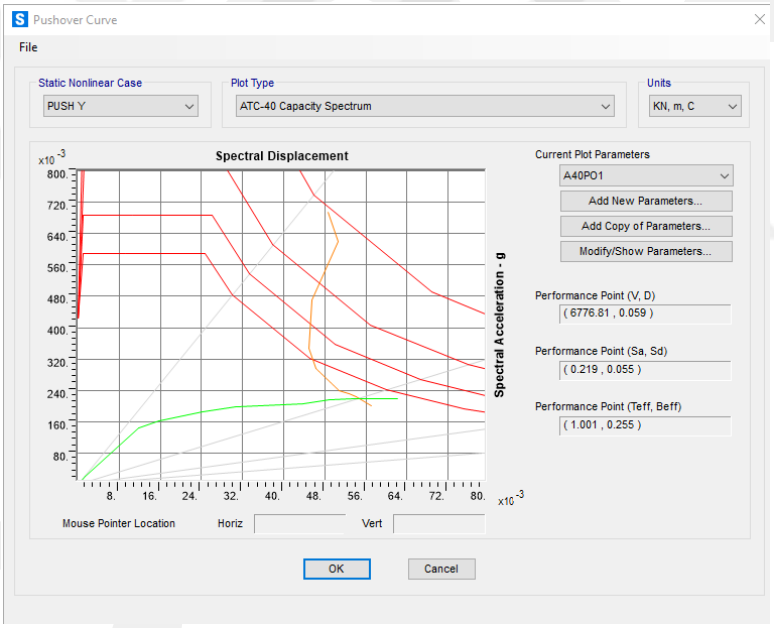

Figure 4.50 Performance Point in Y-Direction for 3-SX-PA Building Model

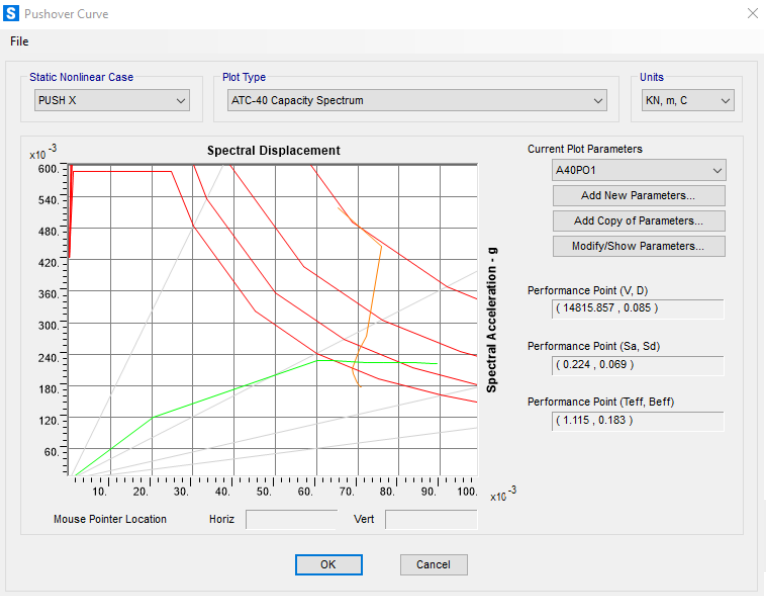

Figure 4.51 Performance Point in X-Direction for 6-SX-PA Building Model

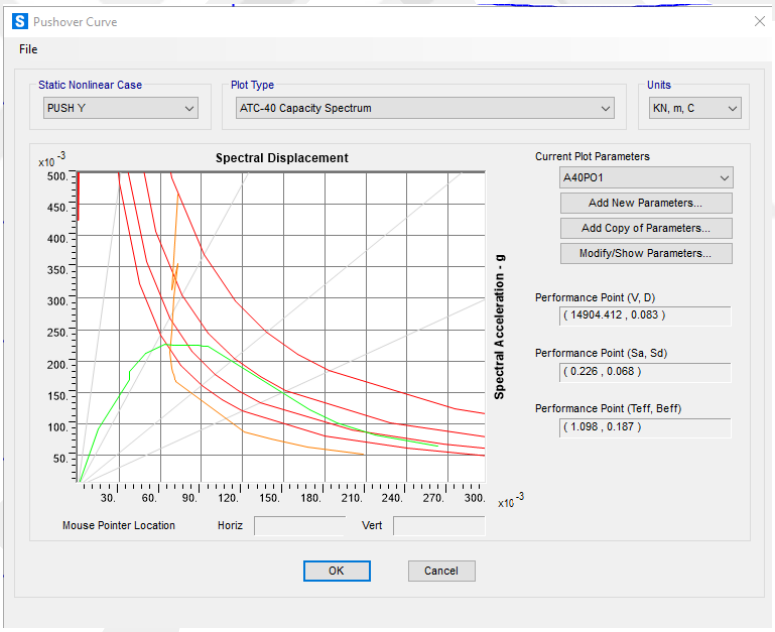

Figure 4.52 Performance Point in Y-Direction for 6-SX-PA Building Model

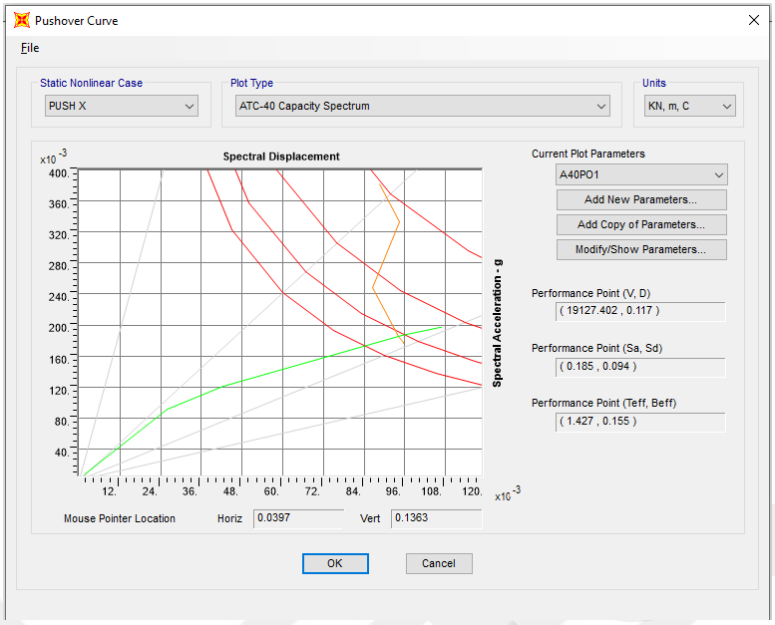

Figure 4.53 Performance Point in X-Direction for 9-SX-PA Building Model

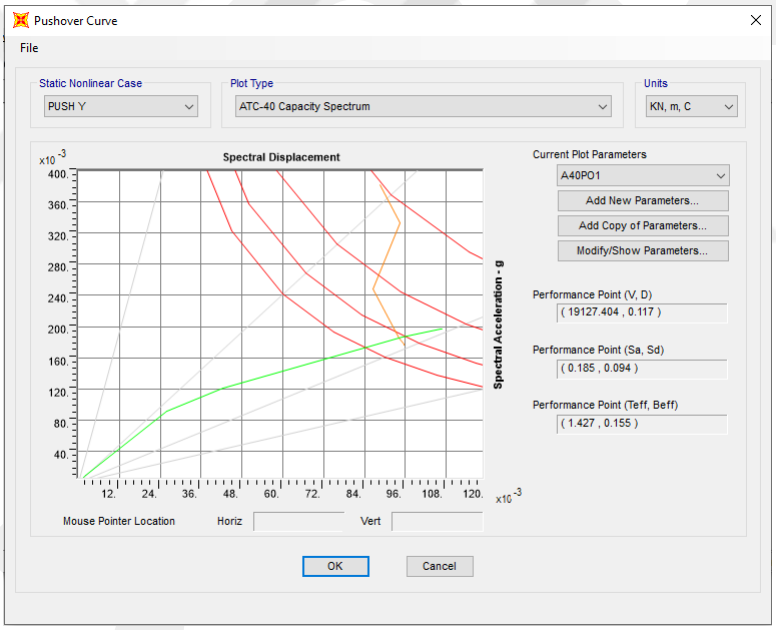

Figure 4.54 Performance Point in Y-Direction for 9-SX-PA Building Model

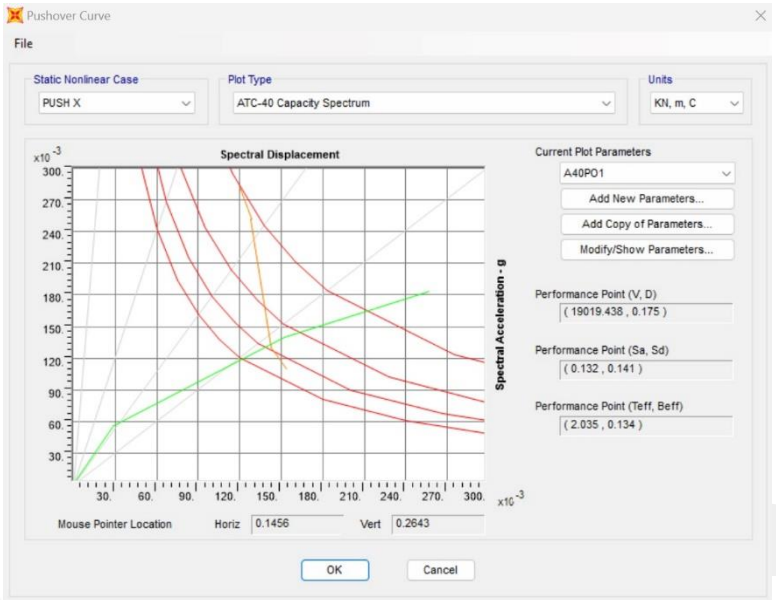

Figure 4.55 Performance Point in X-Direction for 12-SX-PA Building Model

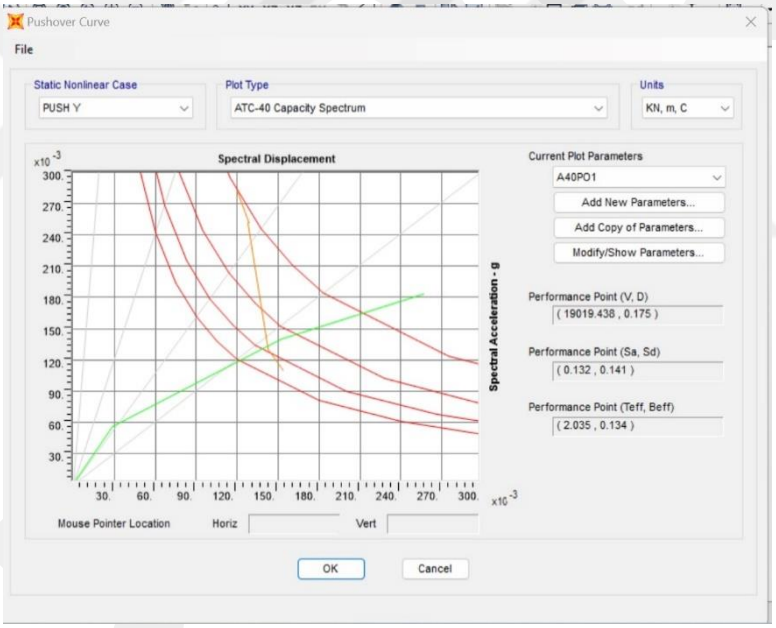

Figure 4.56 Performance Point in Y-Direction for 12-SX-PA Building Model

4.4.2.3 Time-History Analysis Method

Time-history analysis was performed on strengthened building models using 11 scaled earthquake ground motion records. The results of the analysis are tabulated in Table 4.10.

Table 4.10 Time-History Analysis Results of Strengthened Building Models for Maximum Base Shear

Model Name	Dir.	EQ1	EQ2	EQ3	EQ4	EQ5	EQ6	EQ7	EQ8	EQ9	EQ10	EQ11
		(kN)										
3-SV-TH	X	2464	2712	2088	2508	2394	2435	2671	2762	2265	2357	2130
	Y	739	814	626	753	718	731	801	829	680	707	639
6-SV-TH	X	2766	2765	3403	3021	2723	2445	3075	3339	3244	2714	3632
	Y	830	829	1021	906	817	734	923	1002	973	814	1090
9-SV-TH	X	4278	4147	3592	3934	3319	2818	4124	4776	3811	3515	3234
	Y	1283	1244	1078	1180	996	845	1237	1433	1143	1054	971
12-SV-TH	X	3178	3999	3398	3199	2528	3579	3718	4870	3217	4013	3671
	Y	953	1204	1029	966	760	1078	1119	1492	966	1219	1105
3-SX-TH	X	1806	2191	2240	2309	2170	2194	1907	2470	2104	2309	2021
	Y	542	657	672	693	651	658	572	741	631	693	606
6-SX-TH	X	2881	2840	3355	3046	2748	2457	3013	3337	3232	2785	3668
	Y	859	845	1007	910	822	730	903	997	973	833	1096
9-SX-TH	X	3349	3370	2970	3083	2849	2691	3630	4100	3105	3264	3286
	Y	1054	1095	957	946	886	818	1156	1352	950	1059	1017
12-SX-TH	X	3022	1086	2758	2912	2401	3129	3482	3696	2822	3061	3418
	Y	940	1370	944	909	722	1002	1114	1338	897	1070	1130

Table 4.11 Time-History Analysis Results of Strengthened Building Models for Maximum Deflection

Model Name	Dir.	EQ1	EQ2	EQ3	EQ4	EQ5	EQ6	EQ7	EQ8	EQ9	EQ10	EQ11
		(mm)										
3-SV-TH	X	6	6	5	7	6	6	6	6	5	6	5
	Y	2	2	2	2	2	2	2	2	2	2	2
6-SV-TH	X	8	8	10	10	8	8	9	10	9	9	10
	Y	3	3	3	3	2	2	3	3	3	3	3
9-SV-TH	X	9	13	11	12	12	10	11	13	13	11	11
	Y	3	4	4	4	4	3	3	4	4	3	3
12-SV-TH	X	15	15	18	15	13	15	14	19	14	16	13
	Y	5	5	6	5	4	5	4	6	4	5	4
3-SX-TH	X	6	6	6	7	6	7	7	7	6	7	6
	Y	2	2	2	2	2	2	2	2	2	2	2
6-SX-TH	X	8	8	10	11	8	8	9	10	9	9	10
	Y	3	3	3	3	2	2	3	3	3	3	3
9-SX-TH	X	11	13	12	13	14	15	13	20	14	15	13
	Y	3	4	4	4	4	5	4	6	4	5	4
12-SX-TH	X	15	13	19	15	14	15	14	20	14	15	13
	Y	5	4	6	5	4	5	4	6	4	5	4

4.5 Discussions

The dynamic properties of the building models are shown in tables from Table 4.1 to Table 4.3. When the seismic weights of the building models were compared, the deficient buildings had less seismic weights than those of non-deficient buildings, since the columns were removed in deficient buildings. This difference was small for

low-story buildings. The difference increased as the number of stories of the buildings increased. When the periods both in x- and y-directions of the building models were compared, the deficient buildings had higher periods than those of non-deficient buildings, since the building models became more flexible by removing columns. When strengthened buildings were considered, the seismic weights of the strengthened buildings were greater than those of deficient buildings due to the addition of external steel braces. The periods of strengthened building models both in x- and y-directions were less than those of the deficient building models as the external steel braces produced stiffer building models.

Table 4.12 Comparison of Dynamic Properties of the Building Models

Modal Name	**Seismic Weight (kN)**	**Period T_x (s)**
3-ND	31461	0.62
3-D	30806	0.68
3-SV	31201	0.5
3-SX	31165	0.54
6-ND	72547	0.82
6-D	71152	0.94
6-SV	71985	0.76
6-SX	72528	0.75
9-ND	119096	1.23
9-D	115832	1.23
9-SV	117051	1.05
9-SX	117481	1.03
12-ND	169807	1.38
12-D	163580	1.47
12-SV	165213	1.36
12-SX	164983	1.39

The equivalent earthquake load method results of the deficient and strengthened buildings using inverted V- and X-type external steel bracing systems are shown in Table 4.4 and Table 4.8. When the total base shear both in x- and y-directions of the building models were compared, the deficient buildings had less total base shear than those of strengthened building models, since the addition of the strengthening system increased the seismic weight of the building. This addition also increased the stiffness of the building resulting in a reduction in the period and an increase in the demand acceleration. When the two steel strengthening configurations were compared, there was no distinct pattern on the superiority of any bracing system related to total base shear. When the maximum displacements both in x- and y-directions of the building models were compared, the deficient buildings had more displacements than those of

strengthened building models. Comparison of maximum displacement values of deficient, strengthened using inverted V-type and X-type bracing systems are shown in Table 4.13 and Table 4.14. This table indicates that the inverted V-type external steel bracing system resulted in lower displacement values compared to X-type bracing system for all the models used in this study. These results were also valid for drift ratios.

Table 4.13 Comparison of Total Base Shear, Maximum Displacement, and Drift Ratio Results of Equivalent Earthquake Load Method for Strengthened Building Models

Model Name	V_{tx} (kN)	Δ_{maxx} (mm)	Combination for X	Drift Ratios X-Dir.
3-D-EE	4179	22	1.0DL+1.0LL+1.0EQX+E	2.43E-03
3-SV-EE	5757	9	1.0DL+1.0LL+1.0EQX+E	9.51-E04
3-SX-EE	5324	13	1.0DL+1.0LL+1.0EQX+E	2.56E-03
6-D-EE	6983	32	1.0DL+1.0LL+1.0EQX+E	1.75E-03
6-SV-EE	8738	14	1.0DL+1.0LL+1.0EQX+E	7.55E-04
6-SX-EE	8921	24	1.0DL+1.0LL-1.0EQX+E	1.33E-03
9-D-EE	8687	42	1.0DL+1.0LL+1.0EQX+E	1.54E-03
9-SV-EE	10284	20	1.0DL+1.0LL+1.0EQX+E	7.33E-04
9-SX-EE	10522	28	1.0DL+1.0LL+1.0EQX+E	1.56E-03
12-D-EE	10265	56	1.0DL+1.0LL+1.0EQX+E	1.55E-03
12-SV-EE	11207	28	1.0DL+1.0LL+1.0EQX+E	7.77E-04
12-SX-EE	10949	37	1.0DL+1.0LL+1.0EQX+E	1.03E-03

Table 4.14 Comparison of Maximum Displacements of Equivalent Earthquake Load Method Analysis

Story Number of Models	Δ_{maxx} (mm)			% Decrease in Displacement	
	Deficient	Strengthening Bracing Type		Deficient vs. Inverted V	Deficient vs. X
		Inverted V	X		
3	22	9	19	59	14
6	32	14	24	56	25
9	42	20	28	52	33
12	56	28	37	50	34

The pushover analysis of the deficient and strengthened buildings using inverted V- and X-type external steel bracing systems are shown in Table 4.5 and Table 4.9. When the total base shear both in x- and y-directions of the building models were compared, the deficient buildings had less total base shear than those of strengthened building models for the models up to 9 stories. The analysis resulted in conflicting values for building models having 12 stories. When the two steel strengthening configurations

were compared, there was no distinct pattern on the superiority of any bracing system related to total base shear. When the maximum displacements both in x- and y-directions of the building models were compared, the deficient buildings had more or equal displacements than those of strengthened building models. Comparison of maximum displacement values of deficient, strengthened using inverted V-type and X-type bracing systems are shown in Table 4.15 and Table 4.16. This table indicates that the inverted V-type external steel bracing system resulted in lower displacement values compared to X-type bracing system for the models having a story number up to 9 stories. The analysis resulted in conflicting values for building models having 12 stories. These results were also valid for drift ratios.

Table 4.15 Pushover Analysis Results for Strengthened Model Buildings

Model Names	**Performance Point X-Dir.**		**Performance Point Y-Dir.**	
	Base Shear (kN)	**Δ (mm)**	**Base Shear (kN)**	**Δ (mm)**
3-D-PA	5408	66	5443	66
3-SV-PA	7798	52	7814	52
6-SV-PA	12940	76	12972	76
9-SV-PA	18392	113	18392	113
12-SV-PA	19690	146	19690	146
3-SX-PA	6809	59	6777	59
6-SX-PA	14816	85	14904	82.3
9-SX-PA	19127	117	19127	117
12-SX-PA	19019	175	19019	175

Table 4.16 Comparison of Maximum Displacements of Pushover Analysis

Model Story Number	**Δ_{maxx} (mm)**			**% Decrease in Displacement**	
	Deficient	**Strengthening Bracing Type**		**Deficient vs. Inverted V**	**Deficient vs. X**
		Inverted V	**X**		
3	66	52	59	21	11
6	89	76	85	15	4
9	117	113	117	3	0
12	139	146	175	-5	-26

Comparison of time -history analysis of the deficient and strengthened buildings using inverted V- and X-type external steel bracing systems are shown in Table 4.17 and Table 4.18. When the total base shear both in x- and y-directions of the building models were compared, the deficient buildings had less total base shear than those of strengthened building models. When the two steel strengthening configurations were compared, there was no distinct pattern on the superiority of any bracing system related to total base shear. When the maximum displacements both in x- and y-directions of

the building models were compared, the deficient buildings had more displacements than those of strengthened building models. When the two steel strengthening configurations were compared, there was no distinct pattern on the superiority of any bracing system related to maximum deflections.

Table 4.17 Comparison of Time-History Analysis Results for Maximum Base Shear

Model Name	Dir.	EQ1	EQ2	EQ3	EQ4	EQ5	EQ6	EQ7	EQ8	EQ9	EQ10	EQ11
		(kN)										
3-D-TH	X	2661	2941	3425	2832	2870	3112	3000	3361	2927	3152	3325
	Y	799	881	1022	855	864	928	898	1006	878	948	994
3-SV-TH	X	2464	2712	2088	2508	2394	2435	2671	2762	2265	2357	2130
	Y	739	814	626	753	718	731	801	829	680	707	639
3-SX-TH	X	1806	2191	2240	2309	2170	2194	1907	2470	2104	2309	2021
	Y	542	657	672	693	651	658	572	741	631	693	606
6-D-TH	X	4987	5894	6336	4940	4514	5401	5814	6381	6269	4773	6227
	Y	1496	1768	1901	1482	1354	1620	1744	1915	1881	1432	1868
6-SV-TH	X	2766	2765	3403	3021	2723	2445	3075	3339	3244	2714	3632
	Y	830	829	1021	906	817	734	923	1002	973	814	1090
6-SX-TH	X	2881	2840	3355	3046	2748	2457	3013	3337	3232	2785	3668
	Y	859	845	1007	910	822	730	903	997	973	833	1096
9-D-TH	X	5421	6047	5519	5340	4607	5098	5641	7568	5718	5913	5526
	Y	1632	1815	1665	1605	1381	1530	1700	2408	1718	1785	1656
9-SV-TH	X	4278	4147	3592	3934	3319	2818	4124	4776	3811	3515	3234
	Y	1283	1244	1078	1180	996	845	1237	1433	1143	1054	971
9-SX-TH	X	3349	3370	2970	3083	2849	2691	3630	4100	3105	3264	3286
	Y	1054	1095	957	946	886	818	1156	1352	950	1059	1017
12-D-TH	X	5261	4823	4153	6501	5460	5803	6979	6291	6066	5295	6343
	Y	1579	1509	1297	1971	1639	1741	2117	2049	1823	1603	1971
12-SV-TH	X	3178	3999	3398	3199	2528	3579	3718	4870	3217	4013	3671
	Y	953	1204	1029	966	760	1078	1119	1492	966	1219	1105
12-SX-TH	X	3022	1086	2758	2912	2401	3129	3482	3696	2822	3061	3418
	Y	940	1370	944	909	722	1002	1114	1338	897	1070	1130

Table 4.18 Comparison of Time-History Analysis Results for Maximum Deflection

Model Name	Dir.	EQ1	EQ2	EQ3	EQ4	EQ5	EQ6	EQ7	EQ8	EQ9	EQ10	EQ11
		(mm)										
3-D-TH	X	15	14	17	18	14	15	16	16	15	16	15
	Y	5	4	5	5	4	4	5	5	5	5	5
3-SV-TH	X	6	6	5	7	6	6	6	6	5	6	5
	Y	2	2	2	2	2	2	2	2	2	2	2
3-SX-TH	X	6	6	6	7	6	7	7	7	6	7	6
	Y	2	2	2	2	2	2	2	2	2	2	2
6-D-TH	X	18	18	19	21	17	17	19	20	20	17	21
	Y	5	6	6	6	5	5	6	6	6	5	6
6-SV-TH	X	8	8	10	10	8	8	9	10	9	9	10
	Y	3	3	3	3	2	2	3	3	3	3	3
6-SX-TH	X	8	8	10	11	8	8	9	10	9	9	10
	Y	3	3	3	3	2	2	3	3	3	3	3
9-D-TH	X	29	28	30	28	23	24	26	33	24	30	26
	Y	9	9	9	8	7	7	8	10	7	9	8
9-SV-TH	X	9	13	11	12	12	10	11	13	13	11	11
	Y	3	4	4	4	4	3	3	4	4	3	3
9-SX-TH	X	11	13	12	13	14	15	13	20	14	15	13
	Y	3	4	4	4	4	5	4	6	4	5	4
12-D-TH	X	33	34	43	33	32	34	36	46	30	39	38
	Y	10	10	13	10	10	10	11	14	9	12	12
12-SV-TH	X	15	15	18	15	13	15	14	19	14	16	13
	Y	5	5	6	5	4	5	4	6	4	5	4
12-SX-TH	X	15	13	19	15	14	15	14	20	14	15	13
	Y	5	4	6	5	4	5	4	6	4	5	4

CHAPTER 5

SUMMARY, CONCLUSIONS AND RECOMMENDATIONS

5.1 Summary and Conclusions

The primary focus of this study was to investigate the effectiveness of external steel braces to strengthen RC buildings when some of the columns of the buildings were lost due to any reason. For this purpose, models of RC buildings having square plan area of 900 m^2 and varying story numbers, specifically 3, 6, 9, and 12 were produced using SAP2000 Structural Software [23]. The building models were first properly designed based on the Turkish Specifications, TS500 [14] and TBEC [15]. The properly designed buildings were converted to a deficient design by removing two exterior columns at each face. The deficient building models were strengthened using two different configurations of external steel braces at each side, inverted V- and X-type. The strengthened buildings were analyzed using three different analysis method, namely equivalent earthquake load, pushover analysis and time-history analysis method. The following conclusion were made on the results of the analyses.

- The seismic weights of the deficient building models were less than those of non-deficient building models due to the removal of columns in deficient building models.
- The seismic weights of the strengthened building models were higher than those of deficient building models due to the addition of external steel bracing system on deficient building models.
- When the periods of the building models compared, the strengthened buildings had less period values than the deficient buildings. Addition of external steel bracing systems increased the stiffness of the strengthened buildings which resulted in lower periods.

- For equivalent earthquake load method analysis:
    - The deficient building models had less total base shear than those of strengthened building models.
    - There was no distinct pattern on the superiority of any bracing system related to total base shear.
    - The deficient building models had more displacements than those of strengthened building models.
    - The inverted V-type external steel bracing system resulted in lower displacement values compared to X-type bracing system for all the models used in this study. These results were also valid for drift ratios.
- For pushover analysis method:
    - The deficient building models had less total base shear than those of strengthened building models for the models up to 9 stories. The analysis resulted in conflicting values for building models having 12 stories.
    - There was no distinct pattern on the superiority of any bracing system related to total base shear.
    - The deficient building models had more or equal displacements than those of strengthened building models.
    - The inverted V-type external steel bracing system resulted in lower displacement values compared to X-type bracing system for the models having a story number up to 9 stories. The analysis resulted in conflicting values for building models having 12 stories. These results were also valid for drift ratios.
- For time-history analysis method:
    - The deficient building models had less total base shear than those of strengthened building models.
    - There was no distinct pattern on the superiority of any bracing system related to total base shear.
    - The deficient building models had more displacements than those of strengthened building models.
    - There was no distinct pattern on the superiority of any bracing system related to maximum deflections.

5.2 Recommendations for Future Studies

On the basis of this research, the following the suggestions were made for future studies:

- While the scope of this study focused on regular RC buildings, the scope may be expanded to include irregular RC buildings.
- The columns in this study were removed in such a way to preserve the regular structural layout of the building. Considering all columns in a building are susceptible to failures, a future study may investigate various arrangements of column removal.
- In this study, two configurations of external steel braces were used. Future studies may increase the number of configurations of external steel bracing systems.
- Laboratory or field tests may be performed to validate the results of this numerical study.
- The connection problems between the RC beam-column connections and steel bracing systems were ignored in this study. Semi-rigid connections may be studied as future research.

REFERENCES

[1] C. Pearson, and N. Delatte, "Ronan Point Apartment Tower Collapse and its Effect on Building Codes," *Journal of Performance of Constructed Facilities*. Vol. 19(2), pp. 172-177, 2005

[2] J.X. Lu, and H. Wu, "Progressive collapse of Murrah Federal Building: Revisited," *Journal of Building Engineering*, Vol. 57, 2022.

[3] Disaster and Emergency Management Presidency AFAD "Kahramanmaras and Hatay Earthquake Report 2023," Internet: https://www.sbb.gov.tr/wp-content/uploads/2023/03/2023-Kahramanmaras-and-Hatay-Earthquakes-Report.pdf, [Sep. 22, 2023].

[4] TRTHABER, "The Building with Reinforced Columns in Adana Survived the Kahramanmaraş Earthquake," Internet: https://www.trthaber.com/foto-galeri/adanada-kolonu-guclendirilen-bina-kahramanmaras-depreminde-ayakta-kaldi/54422/sayfa-1.html, Feb. 28, 2023 [Sep. 22, 2023].

[5] H. Esmaeili, A. Kheyroddin, M. A. Kafi, and H. Nikbakht, "Comparison of nonlinear behavior of steel moment frames accompanied with RC shear walls or steel bracings," Structural Design of Tall and Special Buildings, Vol. 22(14), pp. 1062–1074, 2013.

[6] American Institute of Steel Construction, "AISC 360-10, Specification for Structural Steel Buildings," Chicago, Illinois, 2010.

[7] M. R. Maheri and A. Sahebi "Use of steel bracing in reinforced concrete frames," *Engineering Structures*, Vol. 19(2), pp. 1018-1024, 1997.

[8] Gunderao, V. Nandi. And G. Hiremath, "Seismic Behavior of Reinforced Concrete Frame with Eccentric Bracing," *SSRG International Journal of Civil Engineering*, Vol. 2(6), pp. 41-46, 2015.

[9] J. Yu, Y. P. Gan, and J. Ji, "Behavior and Design of Reinforced Concrete Frames Retrofitted with Steel Bracing against Progressive Collapse," *Structural Design of Tall and Special Buildings*, Volume. 29(12), pp. 1-19, 2020.

[10] E. Boru, and E. Aydin, “The Effect of Different Steel Brace Types on Reinforced Concrete Frame System Retrofit,” *Turkish Journal of Nature and Science,* Vol. 11(10), pp. 118-124, 2022.

[11] B. Erpek, “Strengthening Deficient RC Buildings Using External Steel Braces” MSc. thesis, Civil Engineering Department, Atilim University, Ankara, Turkey, 2022.

[12] Turkish statistical institute, “Survey on Building and Dwelling Characteristics,” Internet: https://data.tuik.gov.tr/Bulten/Index?p=Survey-on-Building-and-Dwelling-Characteristics-2021-45870&dil=2, [Aug. 10, 2023]

[13] American Society for Testing and Materials, “American Society for Testing and Materials ASTM A992,” West Conshohocken, PA, 2009.

[14] Turkish Standards Institute, “TS500: Requirements for design and construction of reinforced concrete structures.” Ankara, 2000.

[15] Disaster and Emergency Management Presidency (AFAD), “TBDY 2018: Turkish Building Earthquake Code,” Ankara, 2018.

[16] Turkish Standards Institute, “TS498: Design Loads for Buildings” Ankara, 1987.

[17] Turkish Standards Institute, “TS ISO9194: Bases for Design of Structures; Actions due to the Self-Weight of Structures, Non-Structural Elements and Stored Materials; Density” Ankara, 1997.

[18] Disaster and Emergency Management Presidency (AFAD), “Earthquake Map of Turkey” Internet: https://deprem.afad.gov.tr/deprem-tehlike-haritasi, [Sep. 22.2023]

[19] Applied Technology Council “Seismic Evaluation and Retrofit of Concrete Buildings,” Vol. 1, 1996.

[20] M.G. Kalibhat, and Y.M Kumar, K. Kamath, and S.K Prasad, “Seismic performance of RC frames with vertical stiffness irregularity from pushover analysis,” *IOSR Journal of Mechanical and Civil Engineering*, pp. 61-66, 2014.

[21] S. Lee, “Nonlinear Dynamic Earthquake Analysis of Skyscrapers,” *CTBUH 8th World Congress*, 2008, pp. 1-9.

[22] K. Qian, and B. Li, “Dynamic performance of RC beam-column substructures under the scenario of the loss of a corner column-Experimental results.” *Engineering Structures*, Vol. 44, pp. 154–167, 2006.

[23] CSI America, “SAP2000 v19 | STRUCTURAL ANALYSIS AND DESIGN.” Internet: https://www.csiamerica.com/products/sap2000. [Aug. 20, 2023]

[24] CSI America, “SAP2000 v22 | STRUCTURAL ANALYSIS AND DESIGN.” Internet: https://www.csiamerica.com/products/sap2000 [Aug. 20, 2023]

[25] Pacific Earthquake Engineering Research Center, “*PEER Ground Motion Database*.” Internet: https://ngawest2.berkeley.edu/ [Aug. 11, 2023]

APPENDIX

A - Seismic Load Calculation based on Equivalent Earthquake Load Method

Table App.1 Seismic Load Calculations of Model 3-ND

EQX				
Story No	**H_i (m)**	**w_i (kN)**	**$H_i \times w_i$ (kN.m)**	**F_i (kN)**
1	3	11165	33496.176	814.5729
2	6	11165	66992.424	1629.148
3	9	8778.9	79010.1	1921.398
Total=		31110	179498.7	4365.119
EQY				
Story No	**H_i (m)**	**w_i (kN)**	**$H_i \times w_i$ (kN.m)**	**F_i (kN)**
1	3	11165	33496.176	814.5729
2	6	11165	66992.424	1629.148
3	9	8778.9	79010.1	1921.398
Total=		31110	179498.7	4365.119

Table App.2 Seismic Load Calculations of Model 3-D-EE

EQX				
Story No	**H_i (m)**	**w_i (kN)**	**$H_i \times w_i$ (kN.m)**	**F_i (kN)**
1	3	11044	33131.7	725.9228
2	6	11044	66263.376	1451.845
3	9	8718.152	78463.368	1719.15
Total=		30805.9	177858	3896.918
EQY				
Story No	**H_i (m)**	**w_i (kN)**	**$H_i \times w_i$ (kN.m)**	**F_i (kN)**
1	3	11044	33131.7	725.9228
2	6	11044	66263.376	1451.845
3	9	8718.152	78463.368	1719.15
Total=		30805.9	177858	3896.918

Table App.3 Seismic Load Calculations of Model 3-SV-EE

EQX				
Story No	**H_i (m)**	**w_i (kN)**	**$H_i \times w_i$ (kN.m)**	**F_i (kN)**
1	3	11184	33552.624	999.3687
2	6	11182	67089.408	1998.266
3	9	8843.972	79595.748	2370.768
Total=		31209.7	180238	5368.403
Story No				
Story No	**H_i (m)**	**w_i (kN)**	**$H_i \times w_i$ (kN.m)**	**F_i (kN)**
1	3	11184	33552.624	999.3687
2	6	11182	67089.408	1998.266
3	9	8843.972	79595.748	2370.768
Total=		31209.7	180238	5368.403

Table App.4 Seismic Load Calculations of Model 3-SX-EE

EQX				
Story No	**H_i (m)**	**w_i (kN)**	**$H_i \times w_i$ (kN.m)**	**F_i (kN)**
1	3	11188	33564.888	1001.806
2	6	11164	66985.104	1999.293
3	9	8812.784	79315.056	2367.303
Total=		31165.3	179865	5368.403
EQY				
Story No	**H_i (m)**	**w_i (kN)**	**$H_i \times w_i$ (kN.m)**	**F_i (kN)**
1	3	11188	33564.888	1001.806
2	6	11164	66985.104	1999.293
3	9	8812.784	79315.056	2367.303
Total=		31165.3	179865	5368.403

Table App.5 Seismic Load Calculations of Model 6-ND

EQX				
Story No	**H_i (m)**	**w_i (kN)**	**$H_i \times w_i$ (kN.m)**	**F_i (kN)**
1	3	12542	37624.956	272.4153
2	6	12542	75249.888	544.8304
3	9	12541.65	112874.832	817.2456
4	12	12541.7	150499.872	1089.662
5	15	12541.64	188124.66	1362.076
6	18	9838.276	177088.968	1282.174
Total=		72547	741463.176	5368.403
EQY				
Story No	**H_i (m)**	**w_i (kN)**	**$H_i \times w_i$ (kN.m)**	**F_i (kN)**
1	3	12542	37624.956	272.4153
2	6	12542	75249.888	544.8304
3	9	12541.65	112874.832	817.2456
4	12	12541.7	150499.872	1089.662
5	15	12541.64	188124.66	1362.076
6	18	9838.276	177088.968	1282.174
Total=		72547	741463.176	5368.403

Table App.6 Seismic Load Calculations of Model 6-D-EE

EQX				
Story No	**H_i (m)**	**w_i (kN)**	**$H_i \times w_i$ (kN.m)**	**F_i (kN)**
1	3	12288	36864.468	329.8392
2	6	12288	73728.864	659.6777
3	9	12288.14	110593.296	989.5165
4	12	12288.2	147457.872	1319.357
5	15	12288.15	184322.22	1649.195
6	18	9711.524	174807.432	1564.063
Total=		71152	727774.152	6511.648
EQY				
Story No	**H_i (m)**	**w_i (kN)**	**$H_i \times w_i$ (kN.m)**	**F_i (kN)**
1	3	12288	36864.468	329.8392
2	6	12288	73728.864	659.6777
3	9	12288.14	110593.296	989.5165
4	12	12288.2	147457.872	1319.357
5	15	12288.15	184322.22	1649.195
6	18	9711.524	174807.432	1564.063
Total=		71152	727774.152	6511.648

Table App.7 Seismic Load Calculations of Model 6-SV-EE

EQX				
Story No	**H_i (m)**	**w_i (kN)**	**$H_i \times w_i$ (kN.m)**	**F_i (kN)**
1	3	12427	37281.9	412.438
2	6	12426	74553.12	824.7578
3	9	12425.76	111831.876	1237.161
4	12	12426.5	149117.856	1649.644
5	15	12425.27	186379.02	2061.853
6	18	9854.608	177382.944	1962.332
Total=		71985	736546.716	8148.185
EQY				
Story No	**H_i (m)**	**w_i (kN)**	**$H_i \times w_i$ (kN.m)**	**F_i (kN)**
1	3	12427	37281.9	412.438
2	6	12426	74553.12	824.7578
3	9	12425.76	111831.876	1237.161
4	12	12426.5	149117.856	1649.644
5	15	12425.27	186379.02	2061.853
6	18	9854.608	177382.944	1962.332
Total=		71985	736546.716	8148.185

Table App.8 Seismic Load Calculations of Model 6-SX-EE

EQX				
Story No	**H_i (m)**	**w_i (kN)**	**$H_i \times w_i$ (kN.m)**	**F_i (kN)**
1	3	12814	38440.74	432.8074
2	6	12460	74761.746	841.7486
3	9	12556.96	113012.622	1272.418
4	12	12437.8	149254.02	1680.463
5	15	12429.33	186439.89	2099.142
6	18	9830.35	176946.3	1992.253
Total=		72528	738855.318	8318.833
EQY				
Story No	**H_i (m)**	**w_i (kN)**	**$H_i \times w_i$ (kN.m)**	**F_i (kN)**
1	3	12814	38440.74	432.8074
2	6	12460	74761.746	841.7486
3	9	12556.96	113012.622	1272.418
4	12	12437.8	149254.02	1680.463
5	15	12429.33	186439.89	2099.142
6	18	9830.35	176946.3	1992.253
Total=		72528	738855.318	8318.833

Table App.9 Seismic Load Calculations of Model 9-ND

EQX				
Story No	**H_i (m)**	**w_i (kN)**	**$H_i \times w_i$ (kN.m)**	**F_i (kN)**
1	3	13190	39571.2	385.7441
2	6	13190	79142.4	771.4883
3	9	13190.4	118713.564	1157.232
4	12	13190.4	158284.752	1542.976
5	15	13190.41	197856.12	1928.722
6	18	13190.4	237427.2	2314.465
7	21	13190	276998.484	2700.21
8	24	13190	316569.6	3085.953
9	27	10308.9	278340.192	2713.289
Total=		115832	830995.236	8100.628
EQY				
Story No	**H_i (m)**	**w_i (kN)**	**$H_i \times w_i$ (kN.m)**	**F_i (kN)**
1	3	13190	39571.2	385.7441
2	6	13190	79142.4	771.4883
3	9	13190.4	118713.564	1157.232
4	12	13190.4	158284.752	1542.976
5	15	13190.41	197856.12	1928.722
6	18	13190.4	237427.2	2314.465
7	21	13190	276998.484	2700.21
8	24	13190	316569.6	3085.953
9	27	10308.9	278340.192	2713.289
Total=		115832	830995.236	8100.628

Table App.10 Seismic Load Calculations of Model 9-D-EE

EQX				
Story No	**H_i (m)**	**w_i (kN)**	**$H_i \times w_i$ (kN.m)**	**F_i (kN)**
1	3	11875	35624.904	346.3507
2	6	11875	71249.712	692.7005
3	9	11874.96	106874.64	1039.052
4	12	11875.0	142499.568	1385.402
5	15	11874.96	178124.4	1731.753
6	18	11874.96	213749.208	2078.102
7	21	11875	249374.16	2424.454
8	24	11875	284998.944	2770.803
9	27	8998.684	242964.468	2362.138
Total=		103998	748122.432	7273.36
EQY				
Story No	**H_i (m)**	**w_i (kN)**	**$H_i \times w_i$ (kN.m)**	**F_i (kN)**
1	3	11875	35624.904	346.3507
2	6	11875	71249.712	692.7005
3	9	11874.96	106874.64	1039.052
4	12	11875.0	142499.568	1385.402
5	15	11874.96	178124.4	1731.753
6	18	11874.96	213749.208	2078.102
7	21	11875	249374.16	2424.454
8	24	11875	284998.944	2770.803
9	27	8998.684	242964.468	2362.138
Total=		103998	748122.432	7273.36

Table App.11 Seismic Load Calculations of Model 9-SV-EE

EQX				
Story No	**H_i (m)**	**w_i (kN)**	**$H_i \times w_i$ (kN.m)**	**F_i (kN)**
1	3	13698	41094.528	456.5369
2	6	13702	82209.528	913.3012
3	9	13702.04	123318.36	1369.997
4	12	13702.0	164424.576	1826.664
5	15	13702.03	205530.48	2283.327
6	18	13702.09	246637.656	2740.004
7	21	13702	287750.736	3196.747
8	24	13708	328999.776	3655.001
9	27	10605.15	286339.104	3181.065
Total=		120224	863215.128	9589.83
EQY				
Story No	**H_i (m)**	**w_i (kN)**	**$H_i \times w_i$ (kN.m)**	**F_i (kN)**
1	3	13698	41094.528	456.5369
2	6	13702	82209.528	913.3012
3	9	13702.04	123318.36	1369.997
4	12	13702.0	164424.576	1826.664
5	15	13702.03	205530.48	2283.327
6	18	13702.09	246637.656	2740.004
7	21	13702	287750.736	3196.747
8	24	13708	328999.776	3655.001
9	27	10605.15	286339.104	3181.065
Total=		120224	863215.128	9589.83

Table App.12 Seismic Load Calculations of Model 9-SX-EE

EQX				
Story No	**H_i (m)**	**w_i (kN)**	**$H_i \times w_i$ (kN.m)**	**F_i (kN)**
1	3	13496	40487.376	470.9402
2	6	13380	80278.68	933.7839
3	9	13490.85	121417.632	1412.303
4	12	13352.2	160225.824	1863.712
5	15	13343.66	200154.96	2328.158
6	18	13387.02	240966.36	2802.868
7	21	13317	279661.032	3252.956
8	24	13304	319303.968	3714.073
9	27	10410.05	281071.404	3269.361
Total=		117481	843530.832	9811.765
EQY				
Story No	**H_i (m)**	**w_i (kN)**	**$H_i \times w_i$ (kN.m)**	**F_i (kN)**
1	3	13496	40487.376	470.9402
2	6	13380	80278.68	933.7839
3	9	13490.85	121417.632	1412.303
4	12	13352.2	160225.824	1863.712
5	15	13343.66	200154.96	2328.158
6	18	13387.02	240966.36	2802.868
7	21	13317	279661.032	3252.956
8	24	13304	319303.968	3714.073
9	27	10410.05	281071.404	3269.361
Total=		117481	843530.832	9811.765

Table App.13 Seismic Load Calculations of Model 12-ND

EQX				
Story No	**H_i (m)**	**w_i (kN)**	**$H_i \times w_i$ (kN.m)**	**F_i (kN)**
1	3	14478	43434.4	504.0
2	6	14478	86868.9	1008.1
3	9	14478.15	130303.3	1512.1
4	12	14478.2	173737.9	2016.2
5	15	14478.15	217172.3	2520.2
6	18	14478.14	260606.5	3024.3
7	21	14478	304041.2	3528.3
8	24	14478	347475.6	4032.4
9	27	14478.15	390910.1	4536.4
10	30	14478.15	434344.4	5040.5
11	33	14478.16	477779.1	5544.6
12	36	10547.77	379719.6	4406.6
Total=		130303	912123.4	10585.0
EQY				
Story No	**H_i (m)**	**w_i (kN)**	**$H_i \times w_i$ (kN.m)**	**F_i (kN)**
1	3	14478	43434.4	504.0
2	6	14478	86868.9	1008.1
3	9	14478.15	130303.3	1512.1
4	12	14478.2	173737.9	2016.2
5	15	14478.15	217172.3	2520.2
6	18	14478.14	260606.5	3024.3
7	21	14478	304041.2	3528.3
8	24	14478	347475.6	4032.4
9	27	14478.15	390910.1	4536.4
10	30	14478.15	434344.4	5040.5
11	33	14478.16	477779.1	5544.6
12	36	10547.77	379719.6	4406.6
Total=		130303	912123.4	10585.0

Table App.14 Seismic Load Calculations of Model 12-D-EE

EQX				
Story No	**H_i (m)**	**w_i (kN)**	**$H_i \times w_i$ (kN.m)**	**F_i (kN)**
1	3	13937	41810.0	455.8
2	6	13937	83619.9	911.6
3	9	13936.64	125429.8	1367.4
4	12	13936.6	167239.8	1823.3
5	15	13936.66	209049.8	2279.1
6	18	13936.64	250859.6	2734.9
7	21	13937	292669.9	3190.7
8	24	13937	334479.4	3646.5
9	27	13936.66	376289.8	4102.3
10	30	13936.64	418099.3	4558.1
11	33	13936.65	459909.4	5014.0
12	36	10277.03	369973.0	4033.5
Total=		125430	878008.9	9572.1
EQY				
Story No	**H_i (m)**	**w_i (kN)**	**$H_i \times w_i$ (kN.m)**	**F_i (kN)**
1	3	13937	41810.0	455.8
2	6	13937	83619.9	911.6
3	9	13936.64	125429.8	1367.4
4	12	13936.6	167239.8	1823.3
5	15	13936.66	209049.8	2279.1
6	18	13936.64	250859.6	2734.9
7	21	13937	292669.9	3190.7
8	24	13937	334479.4	3646.5
9	27	13936.66	376289.8	4102.3
10	30	13936.64	418099.3	4558.1
11	33	13936.65	459909.4	5014.0
12	36	10277.03	369973.0	4033.5
Total=		125430	878008.9	9572.1

Table App.15 Seismic Load Calculations of Model 12-SV-EE

EQX				
Story No	**H_i (m)**	**w_i (kN)**	**$H_i \times w_i$ (kN.m)**	**F_i (kN)**
1	3	14071.6	42214.8	497.7
2	6	14069.1	84414.4	995.3
3	9	14069.0	126620.8	1492.9
4	12	14069.1	168829.0	1990.5
5	15	14069.2	211037.6	2488.2
6	18	14069.3	253247.8	2985.9
7	21	14069.5	295460.3	3483.6
8	24	14069.8	337674.2	3981.3
9	27	14070.1	379891.5	4479.0
10	30	14070.7	422119.8	4976.9
11	33	14064.0	464112.8	5472.0
12	36	10451.3	376246.9	4436.1
Total=		126626.6	886364.4	10450.5
EQY				
Story No	**H_i (m)**	**w_i (kN)**	**$H_i \times w_i$ (kN.m)**	**F_i (kN)**
1	3	14071.6	42214.8	497.7
2	6	14069.1	84414.4	995.3
3	9	14069.0	126620.8	1492.9
4	12	14069.1	168829.0	1990.5
5	15	14069.2	211037.6	2488.2
6	18	14069.3	253247.8	2985.9
7	21	14069.5	295460.3	3483.6
8	24	14069.8	337674.2	3981.3
9	27	14070.1	379891.5	4479.0
10	30	14070.7	422119.8	4976.9
11	33	14064.0	464112.8	5472.0
12	36	10451.3	376246.9	4436.1
Total=		126626.6	886364.4	10450.5

Table App.16 Seismic Load Calculations of Model 12-SX-EE

EQX				
Story No	**H_i (m)**	**w_i (kN)**	**$H_i \times w_i$ (kN.m)**	**F_i (kN)**
1	3	14112.1	42336.3	487.8
2	6	14084.6	84507.8	973.6
3	9	13948.7	125538.6	1446.3
4	12	14078.3	168939.3	1946.4
5	15	14065.7	210985.3	2430.8
6	18	14105.3	253895.2	2925.1
7	21	14050.9	295067.9	3399.5
8	24	14046.8	337122.4	3884.0
9	27	14045.9	379239.7	4369.2
10	30	14046.4	421391.2	4854.8
11	33	14031.9	463054.0	5334.8
12	36	10366.1	373180.3	4299.4
Total=		126538.2	886202.4	10209.9
EQY				
Story No	**H_i (m)**	**w_i (kN)**	**$H_i \times w_i$ (kN.m)**	**F_i (kN)**
1	3	14112.1	42336.3	487.8
2	6	14084.6	84507.8	973.6
3	9	13948.7	125538.6	1446.3
4	12	14078.3	168939.3	1946.4
5	15	14065.7	210985.3	2430.8
6	18	14105.3	253895.2	2925.1
7	21	14050.9	295067.9	3399.5
8	24	14046.8	337122.4	3884.0
9	27	14045.9	379239.7	4369.2
10	30	14046.4	421391.2	4854.8
11	33	14031.9	463054.0	5334.8
12	36	10366.1	373180.3	4299.4
Total=		126538.2	886202.4	10209.9

B - Plastic Hinge Formation based on Pushover Analysis

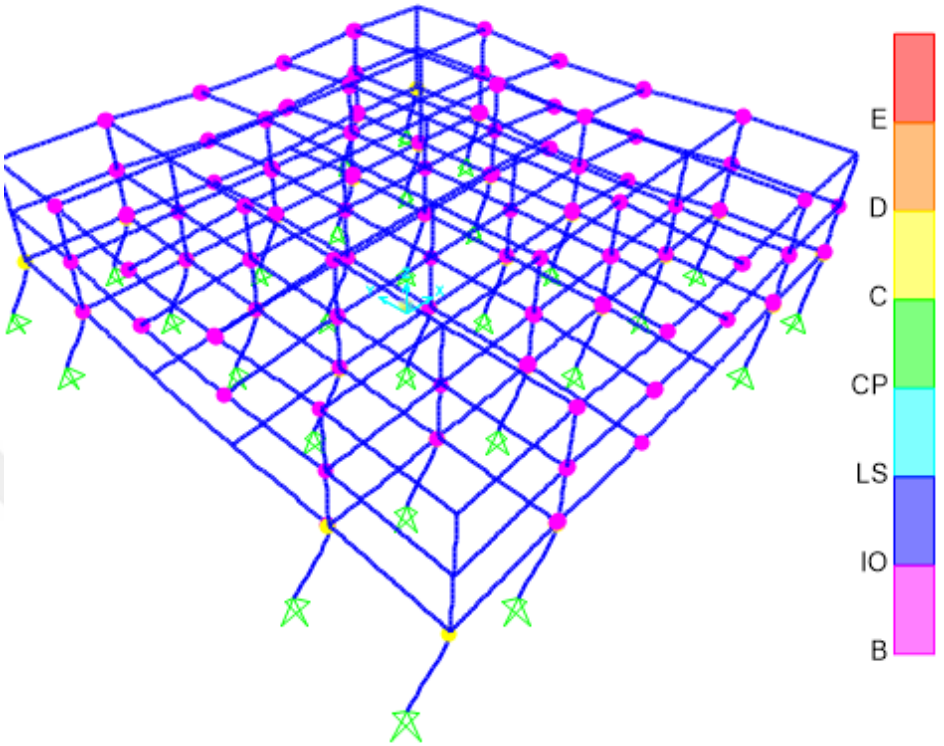

Figure App.1 Plastic Hinge Formation of Push-X Load Case for Model 3-D-PA

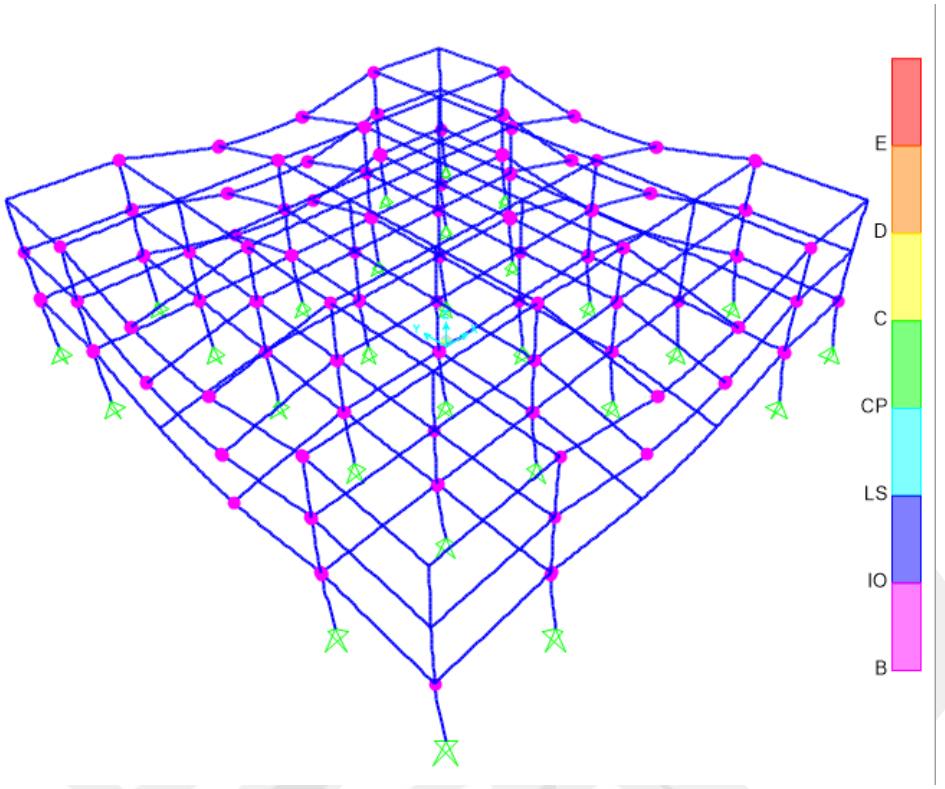

Figure App.2 Plastic Hinge Formation of Push-Y Load Case for Model 3-D-PA

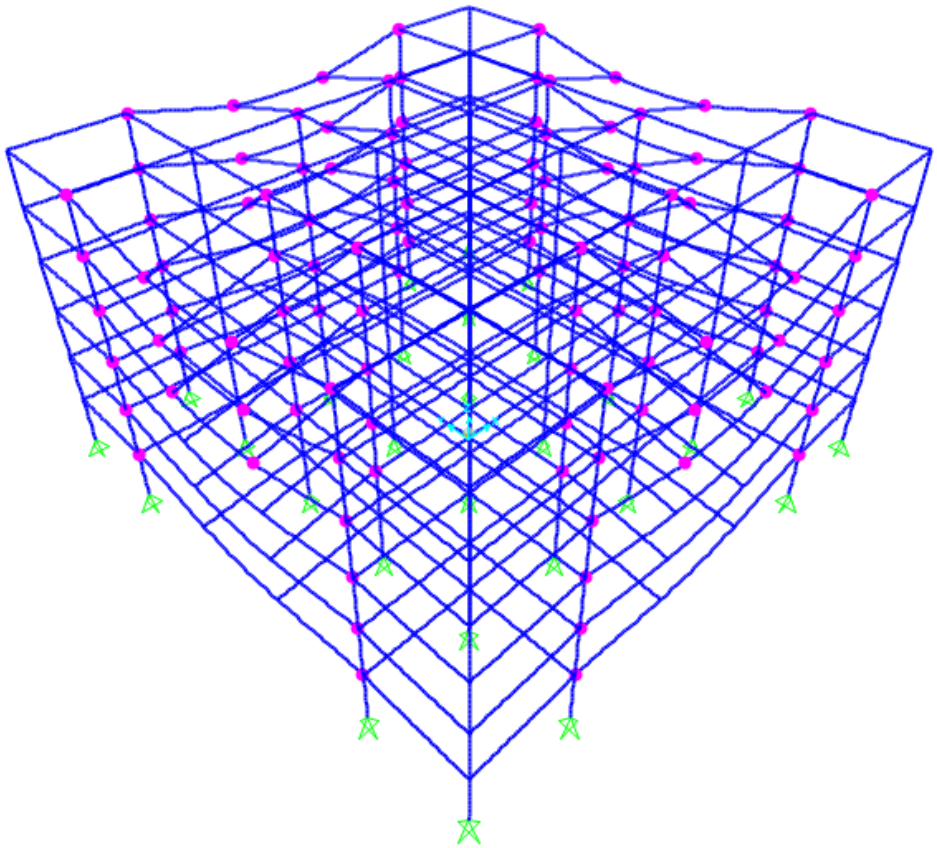

Figure App.3 Plastic Hinge Formation of Push-X Load Case for Model 6-D-PA

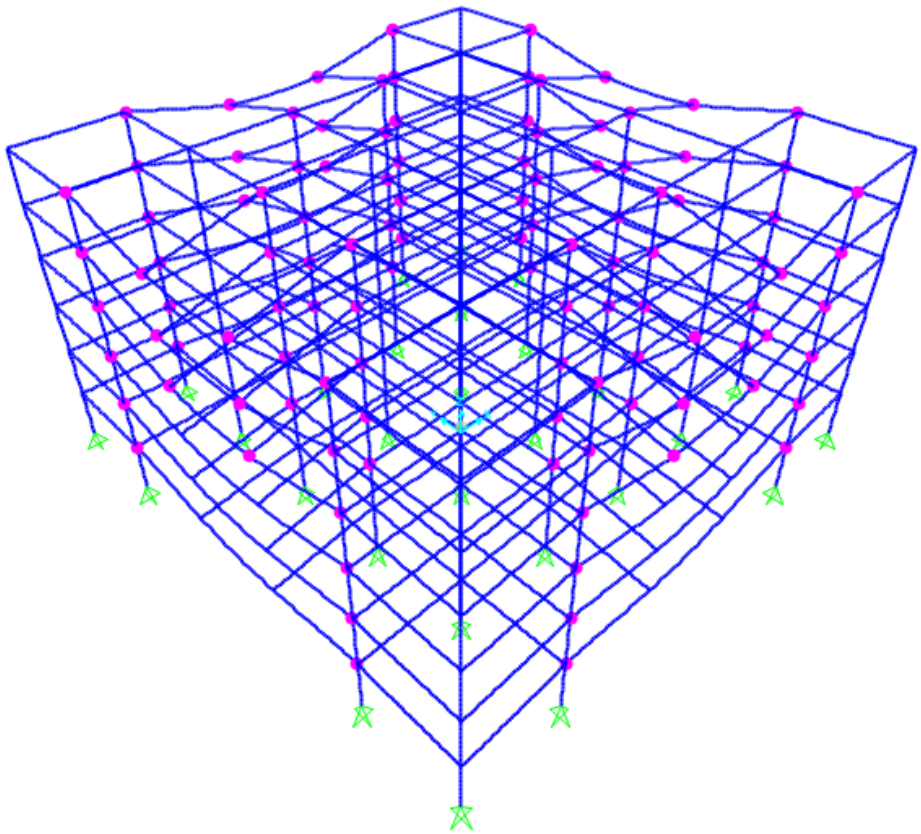

Figure App.4 Plastic Hinge Formation of Push-Y Load Case for Model 6-D-PA

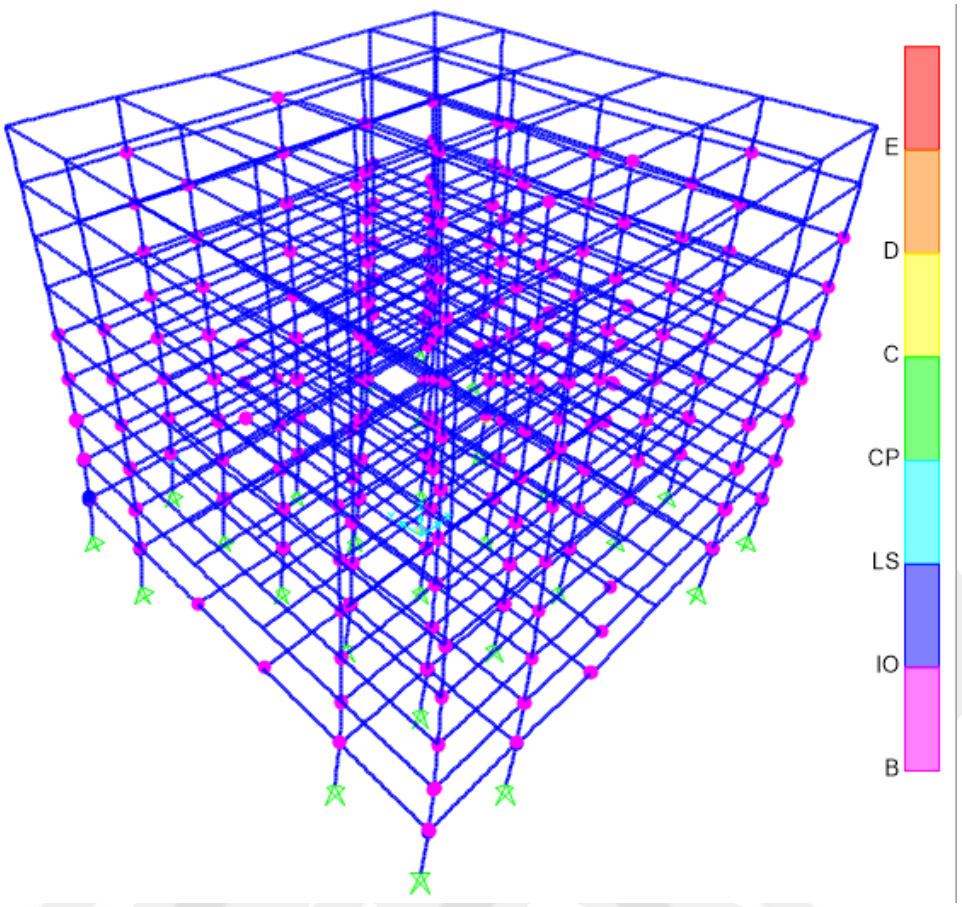

Figure App.5 Plastic Hinge Formation of Push-X Load Case for Model 9-D-PA

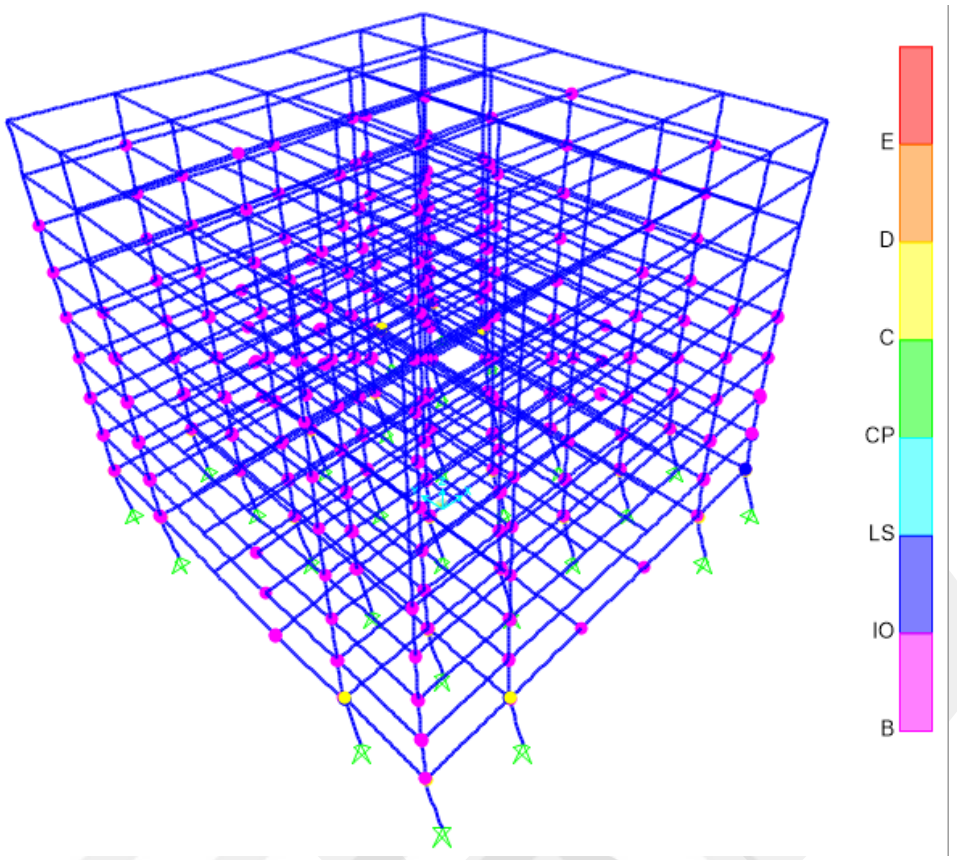

Figure App.6 Plastic Hinge Formation of Push-Y Load Case for Model 9-D-PA

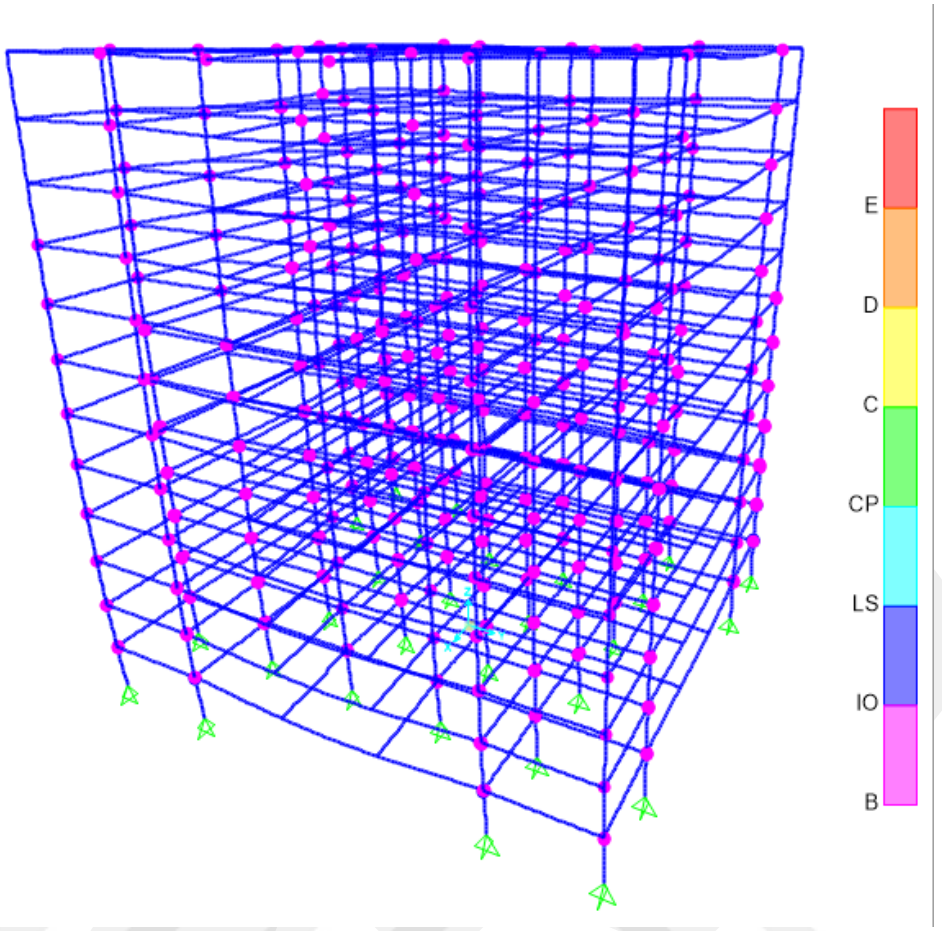

Figure App.7 Plastic Hinge Formation of Push-X Load Case for Model 12-D-PA

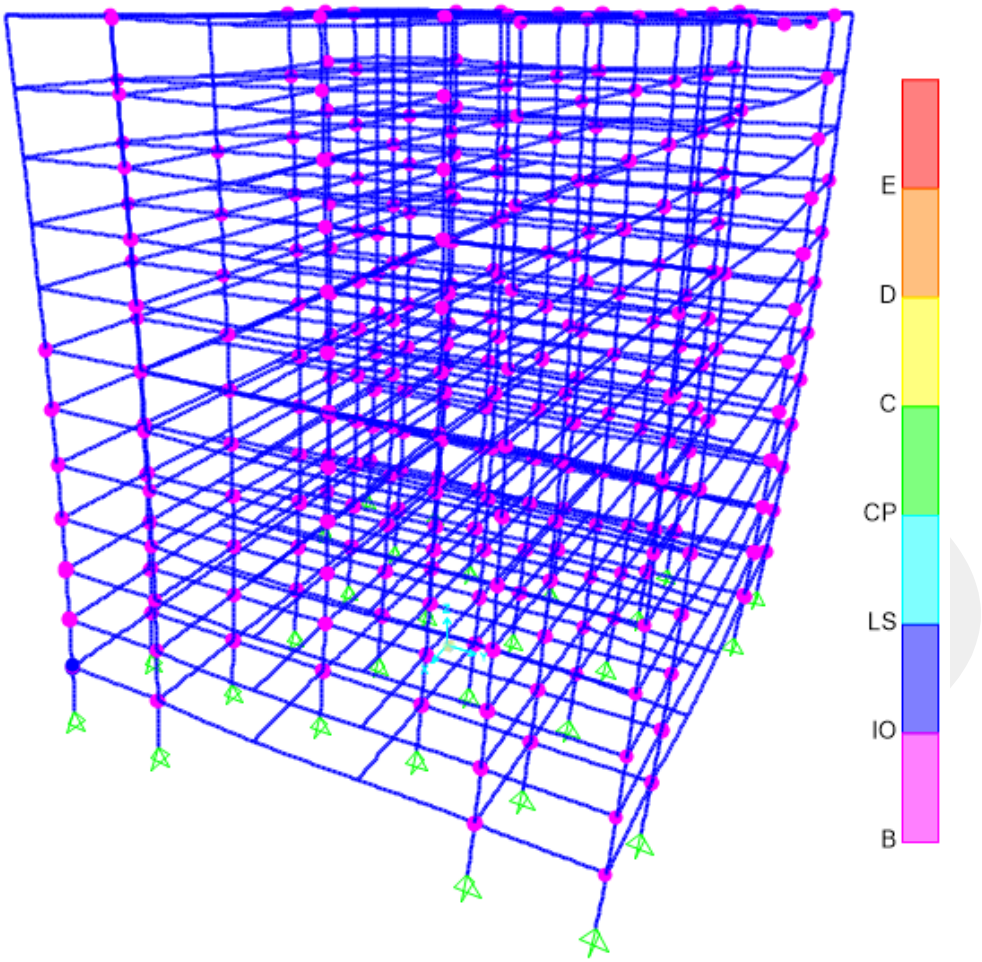

Figure App.8 Plastic Hinge Formation of Push-Y Load Case for Model 12-D-PA

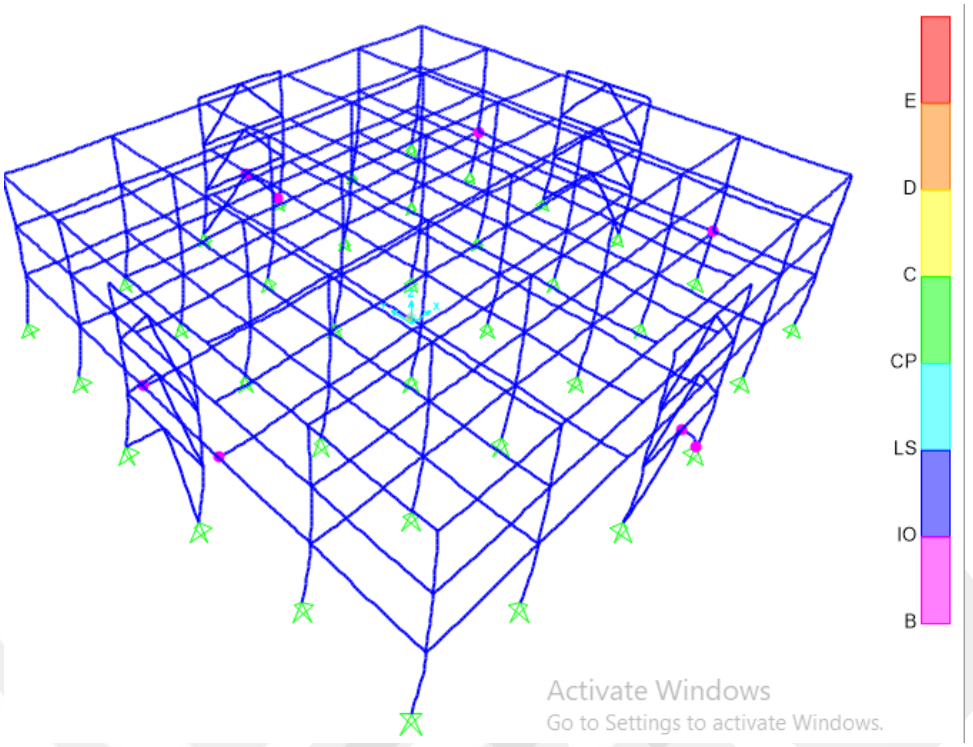

Figure App.9 Plastic Hinge Formation of Push-X Load Case for Model 3-SV-PA

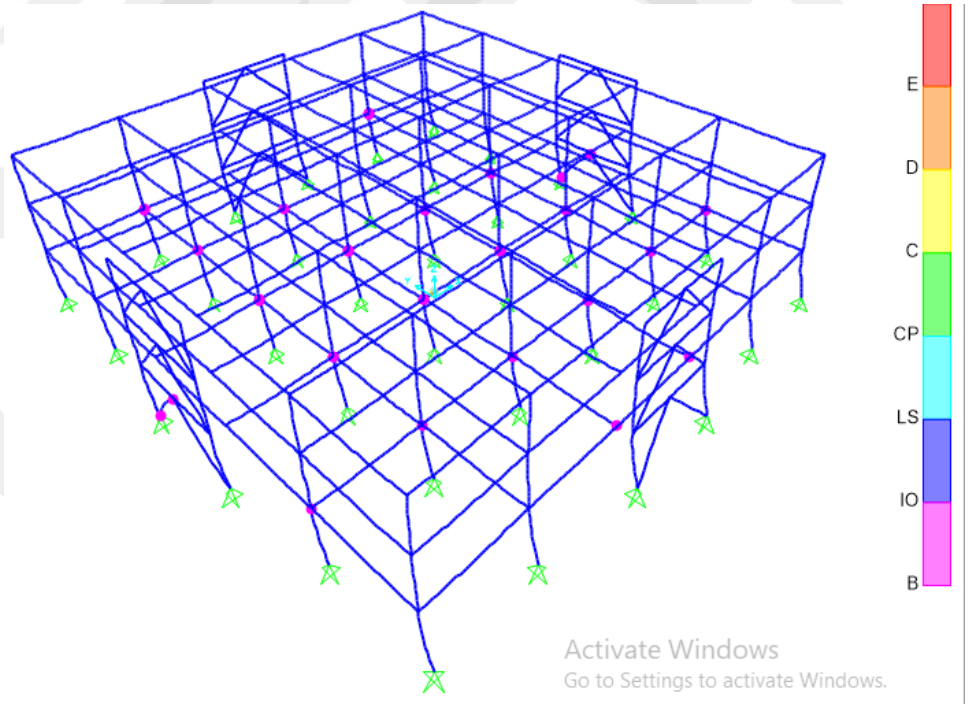

Figure App.10 Plastic Hinge Formation of Push-Y Load Case for Model 3-SV-PA

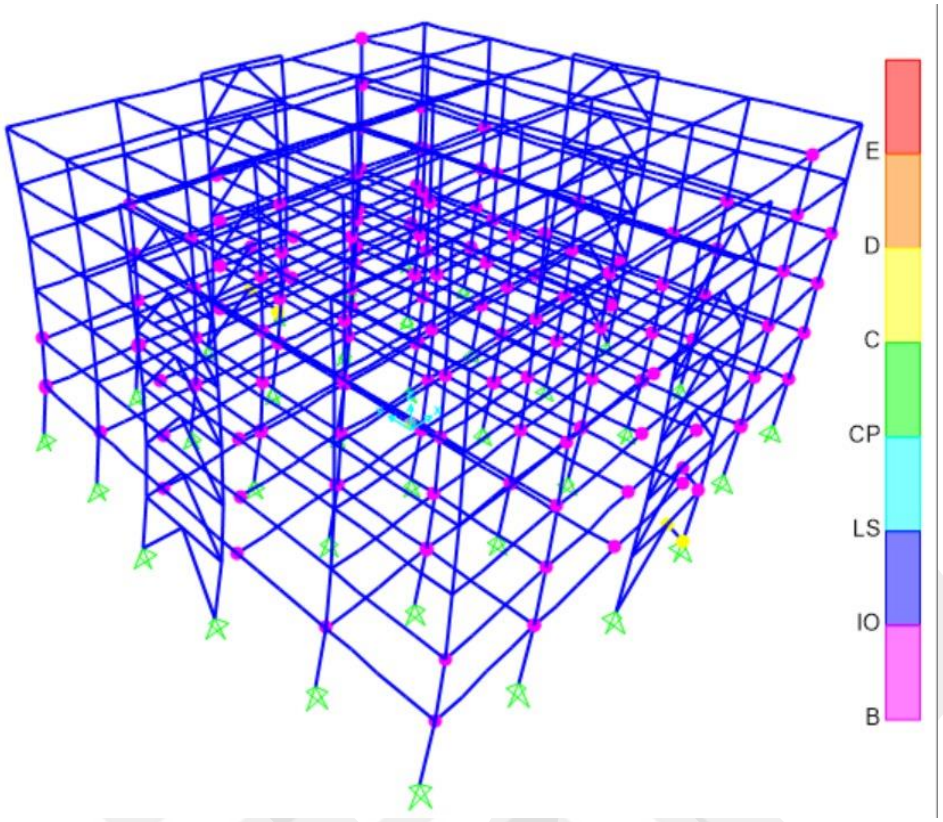

Figure App.11 Plastic Hinge Formation of Push-X Load Case for Model 6-SV-PA

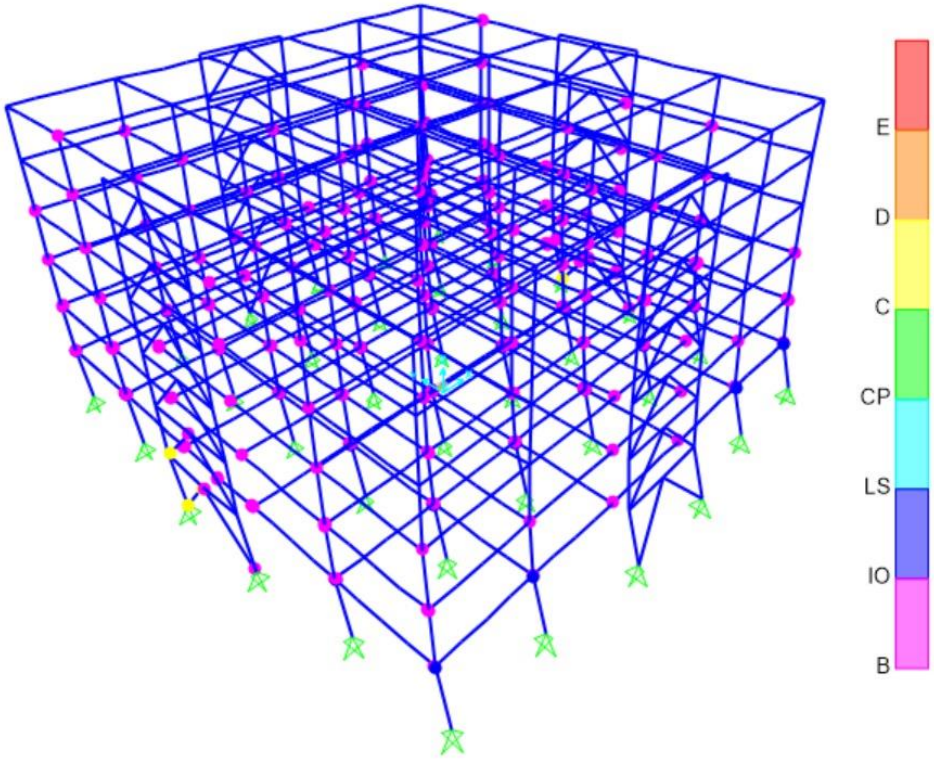

Figure App.12 Plastic Hinge Formation of Push-Y Load Case for Model 6-SV-PA

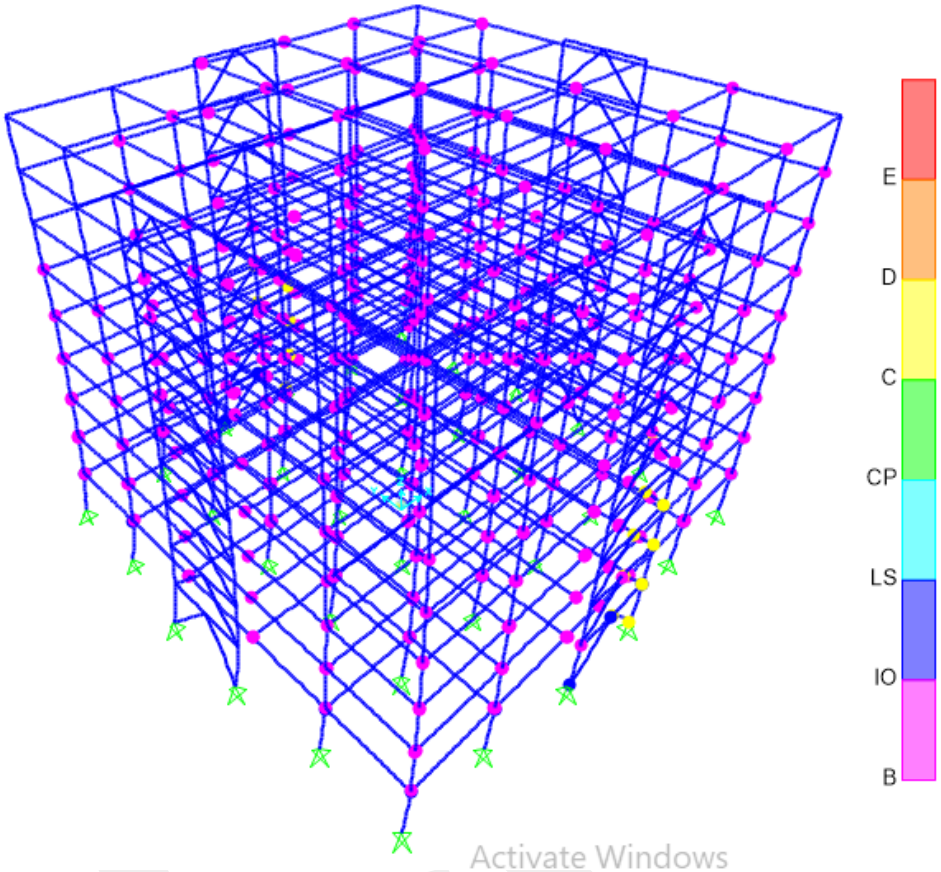

Figure App.13 Plastic Hinge Formation of Push-X Load Case for Model 9-SV-PA

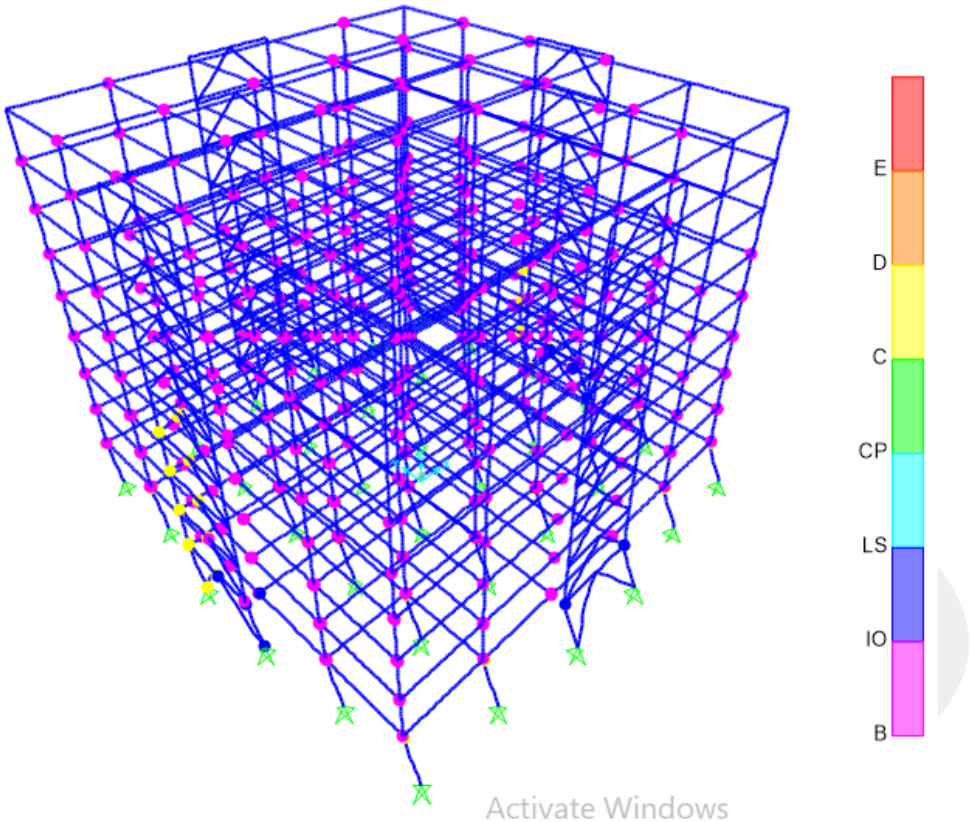

Figure App.14 Plastic Hinge Formation of Push-Y Load Case for Model 9-SV-PA

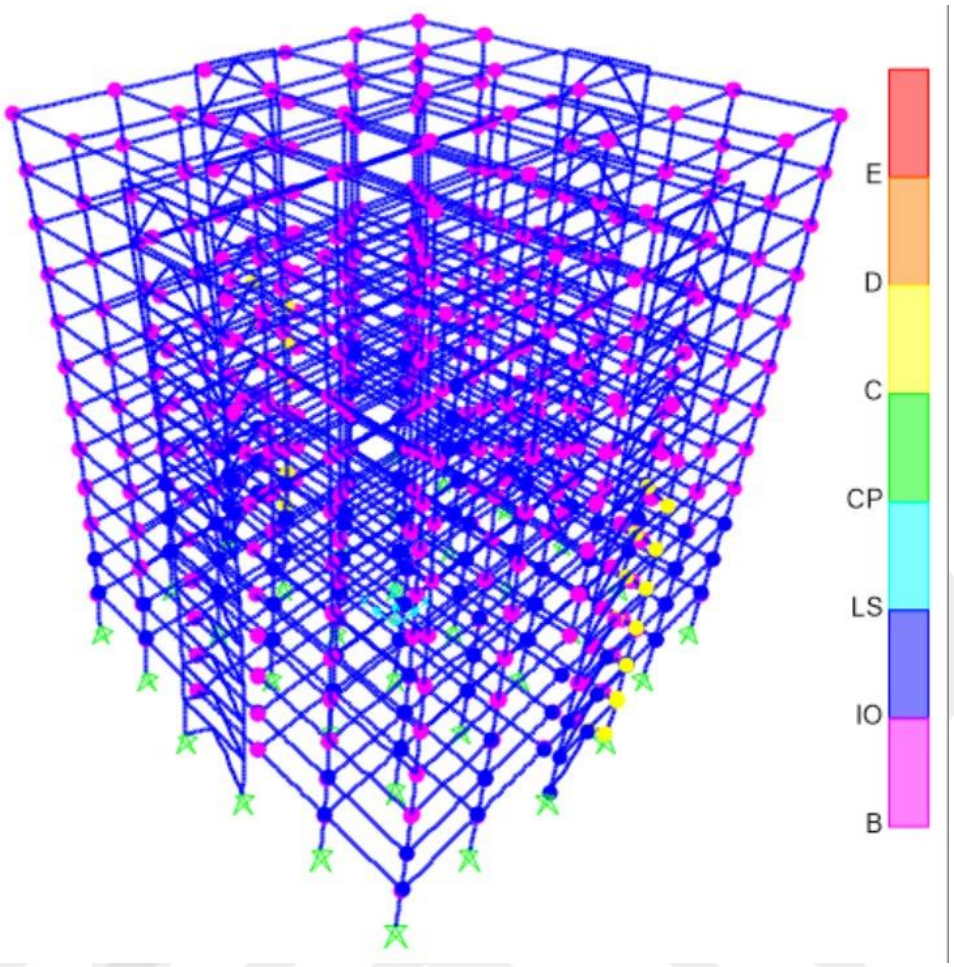

Figure App.15 Plastic Hinge Formation of Push-X Load Case for Model 12-SV-PA

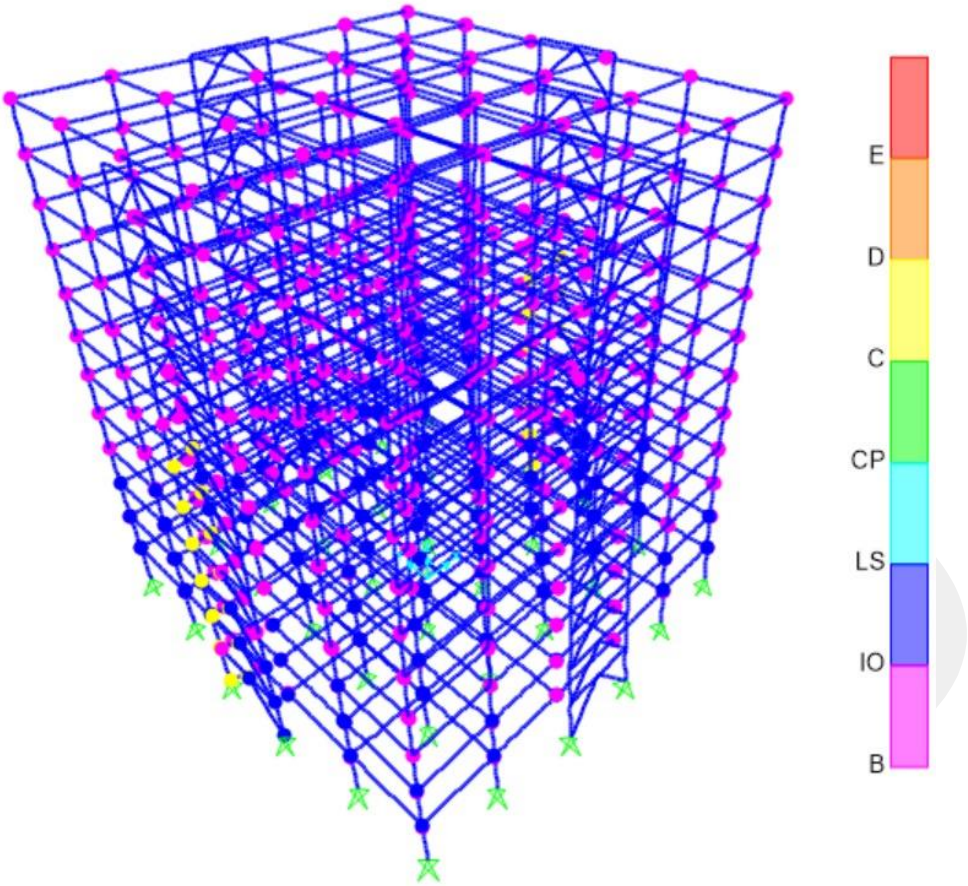

Figure App.16 Plastic Hinge Formation of Push-Y Load Case for Model 12-SV-PA

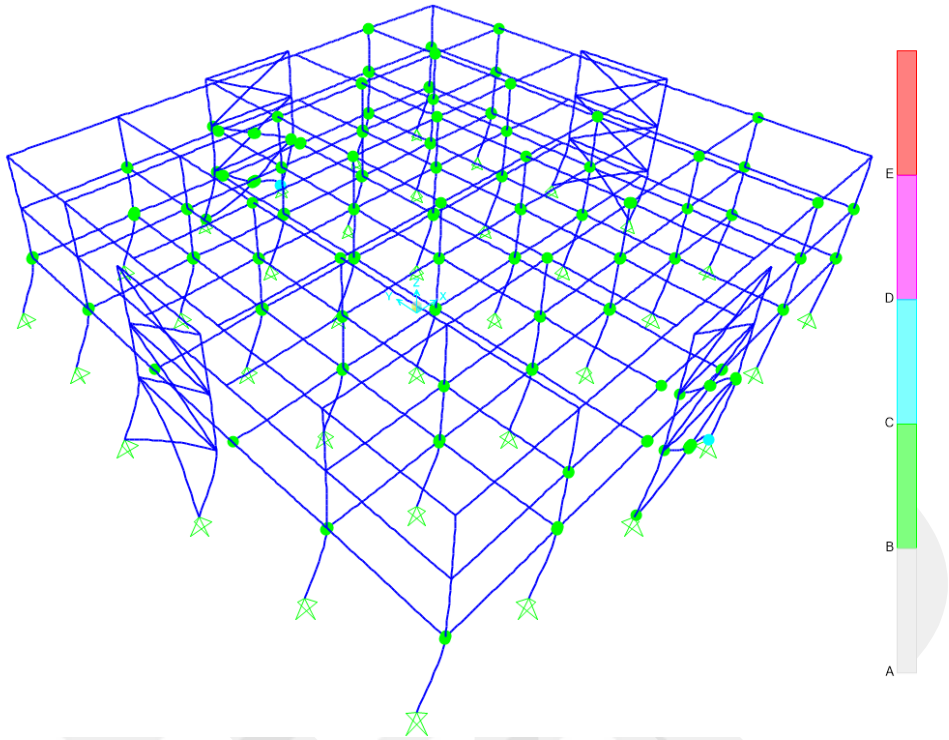

Figure App.17 Plastic Hinge Formation of Push-X Load Case for Model 3-SX-PA

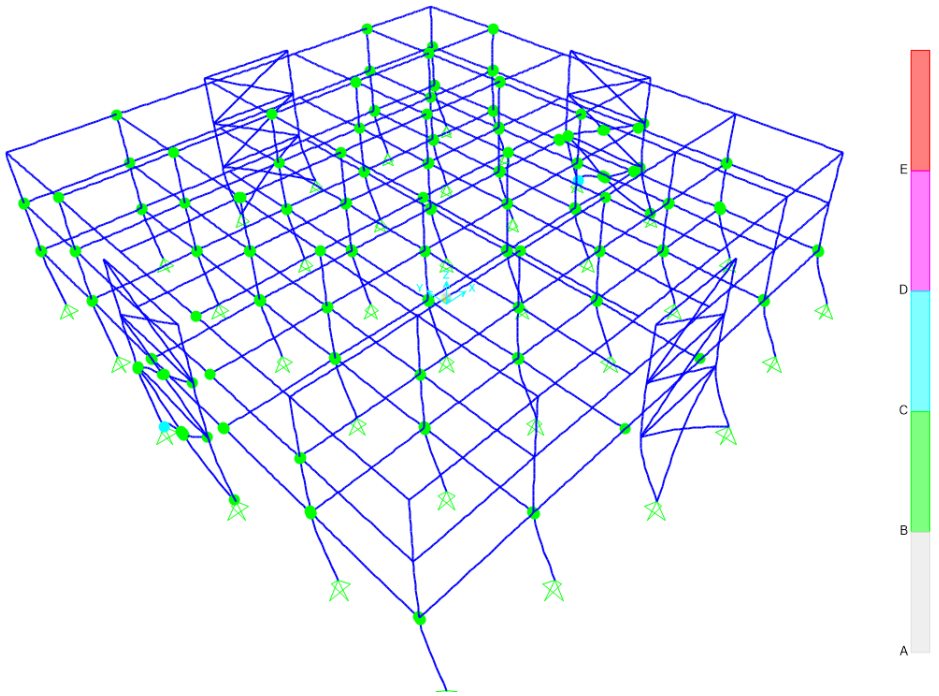

Figure App.18 Plastic Hinge Formation of Push-Y Load Case for Model 3-SX-PA

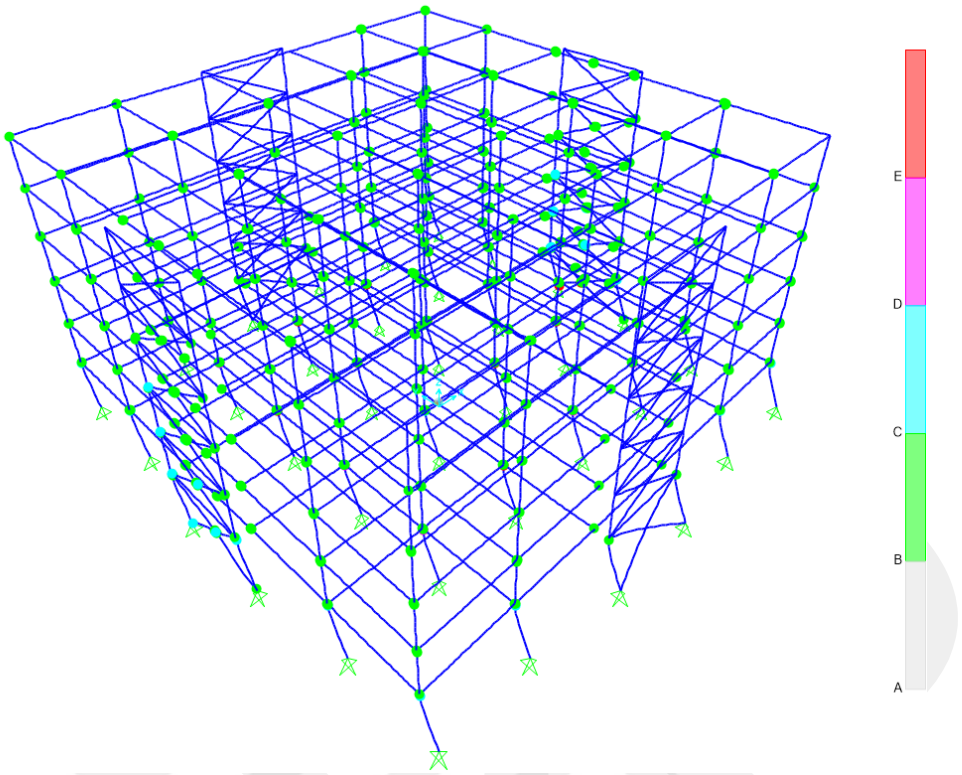

Figure App.19 Plastic Hinge Formation of Push-X Load Case for Model 6-SX-PA

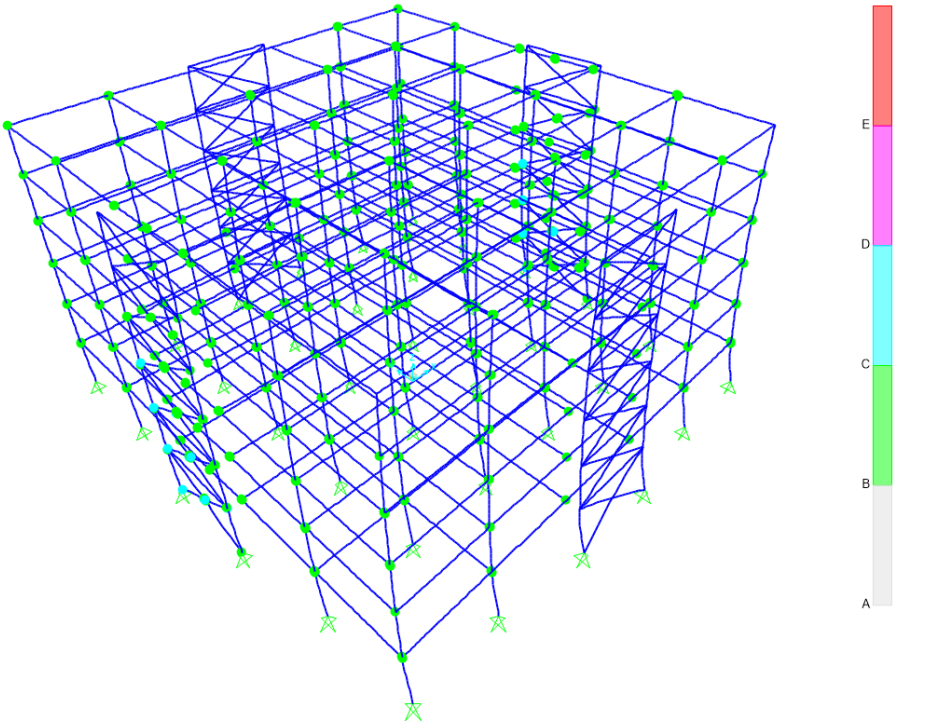

Figure App.20 Plastic Hinge Formation of Push-Y Load Case for Model 6-SX-PA

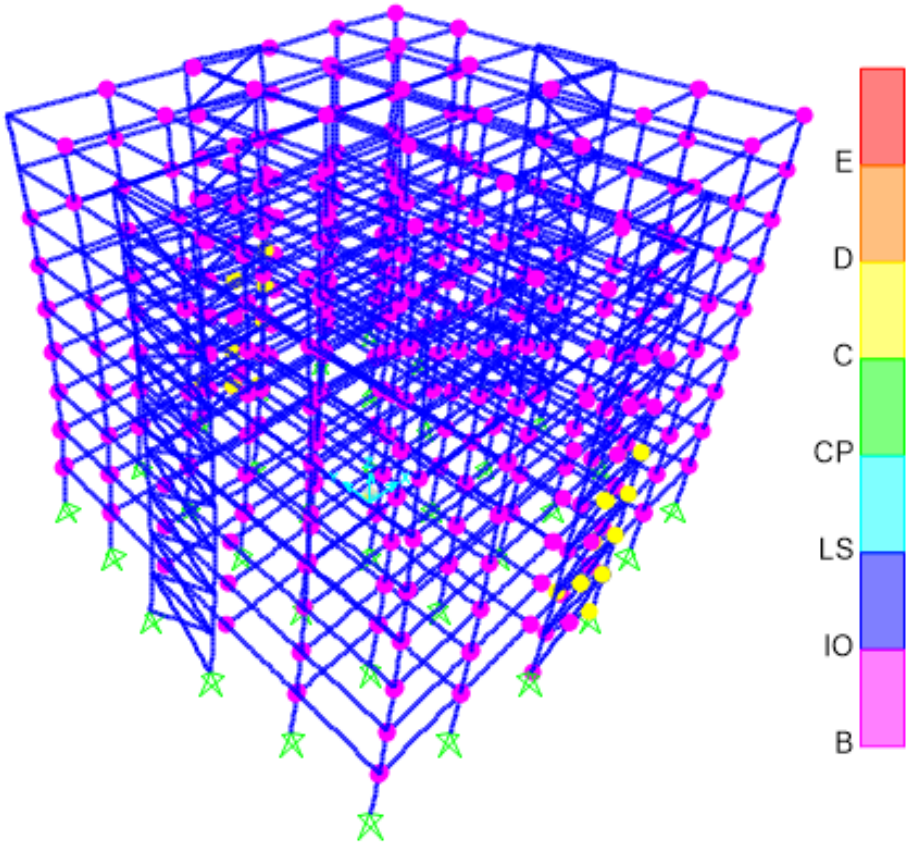

Figure App.21 Plastic Hinge Formation of Push-X Load Case for Model 9-SX-PA

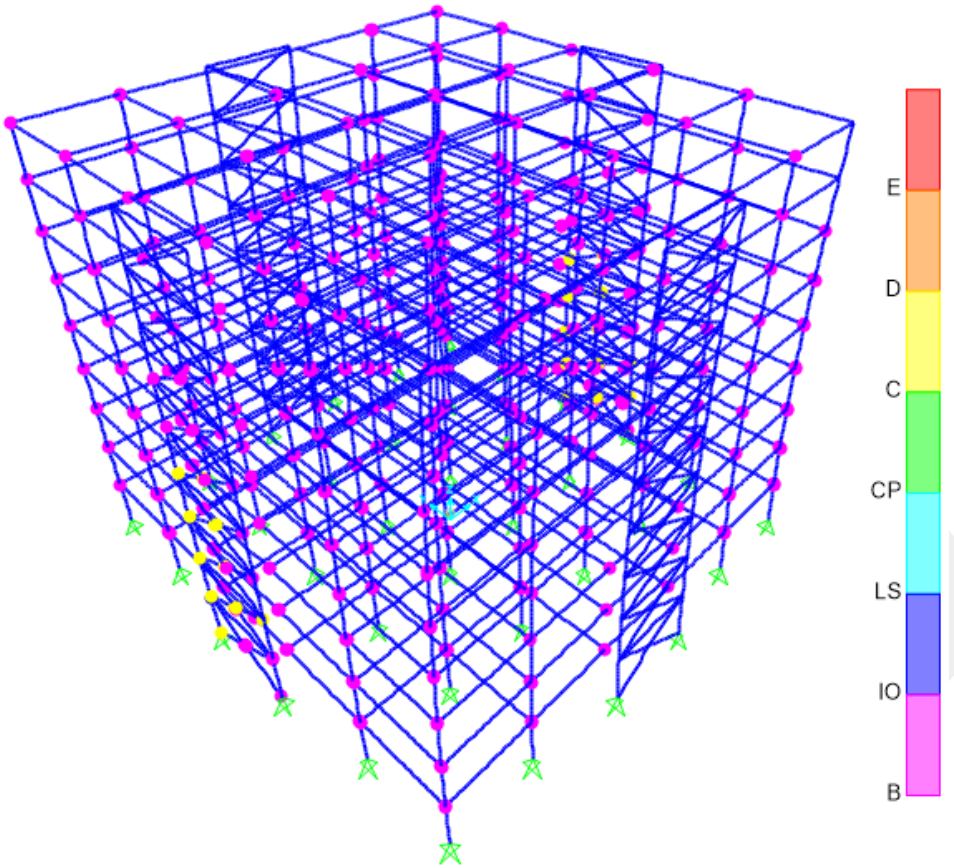

Figure App.22 Plastic Hinge Formation of Push-Y Load Case for Model 9-SX-PA

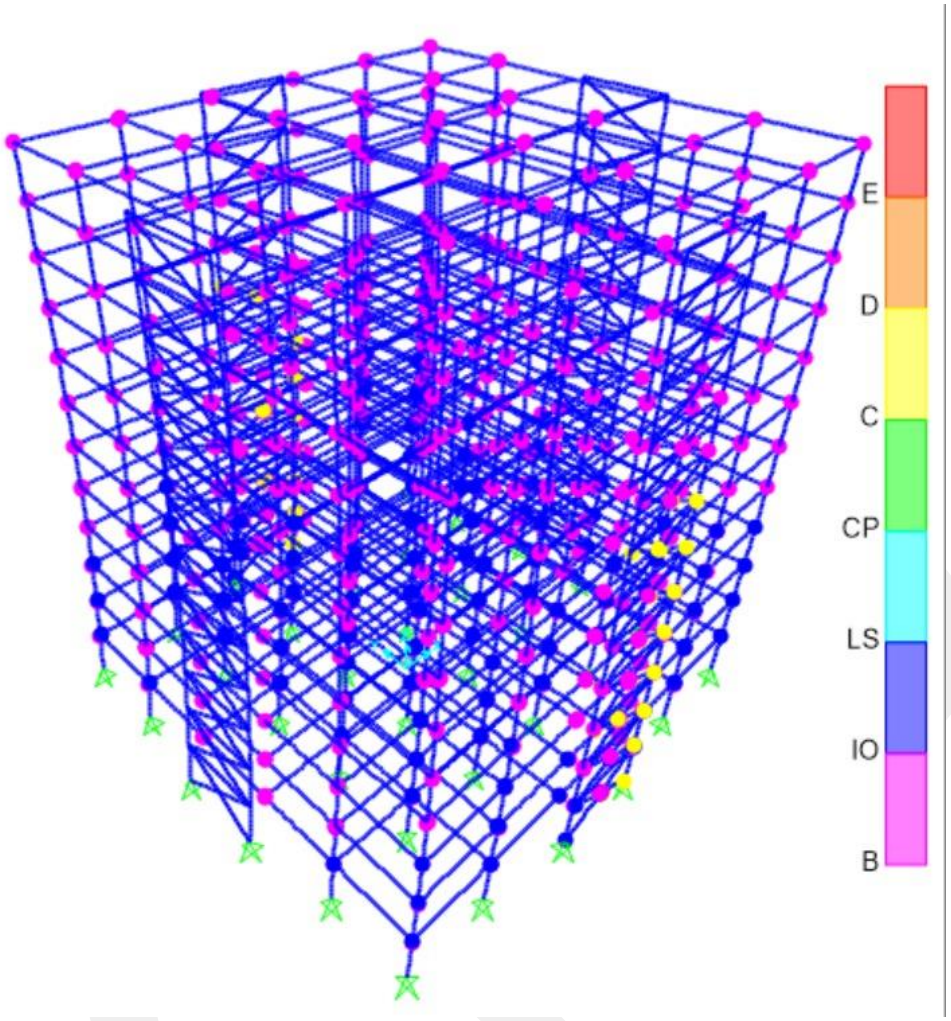

Figure App.23 Plastic Hinge Formation of Push-X Load Case for Model 12-SX-PA

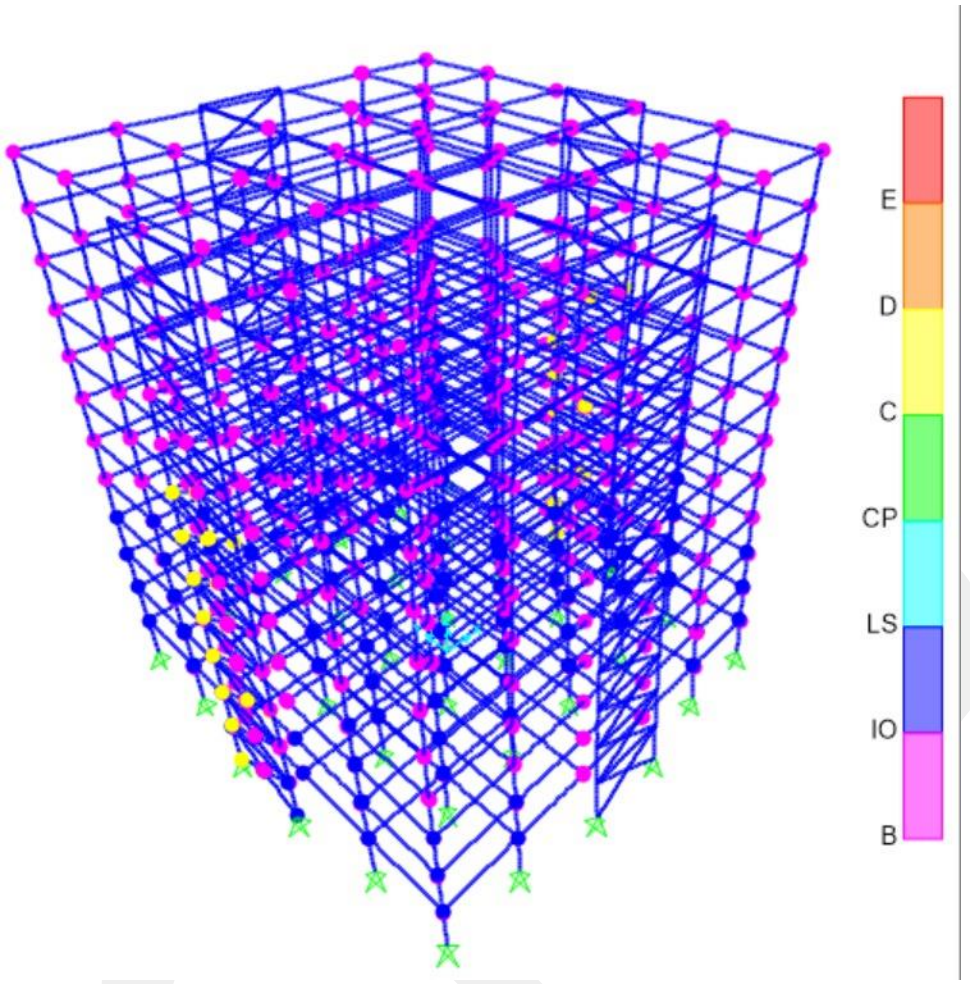

Figure App.24 Plastic Hinge Formation of Push-Y Load Case for Model 12-SX-PA

C - Design Results of Structural Elements

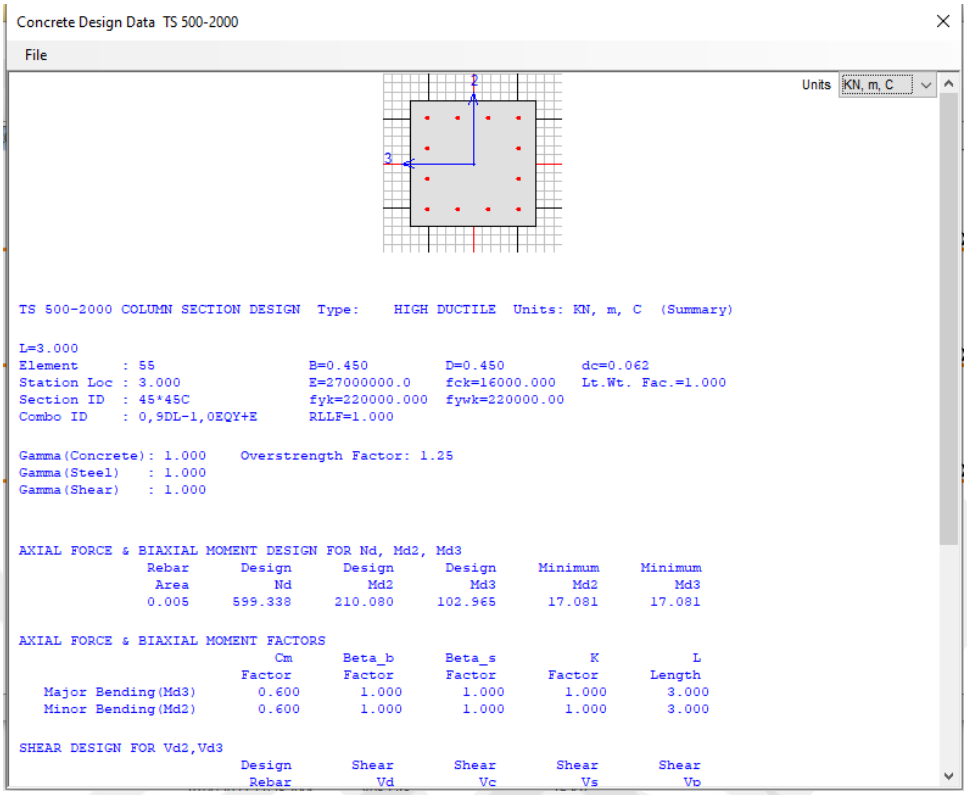

Figure App.25 RC Column Design Results of Model 3-ND-EE

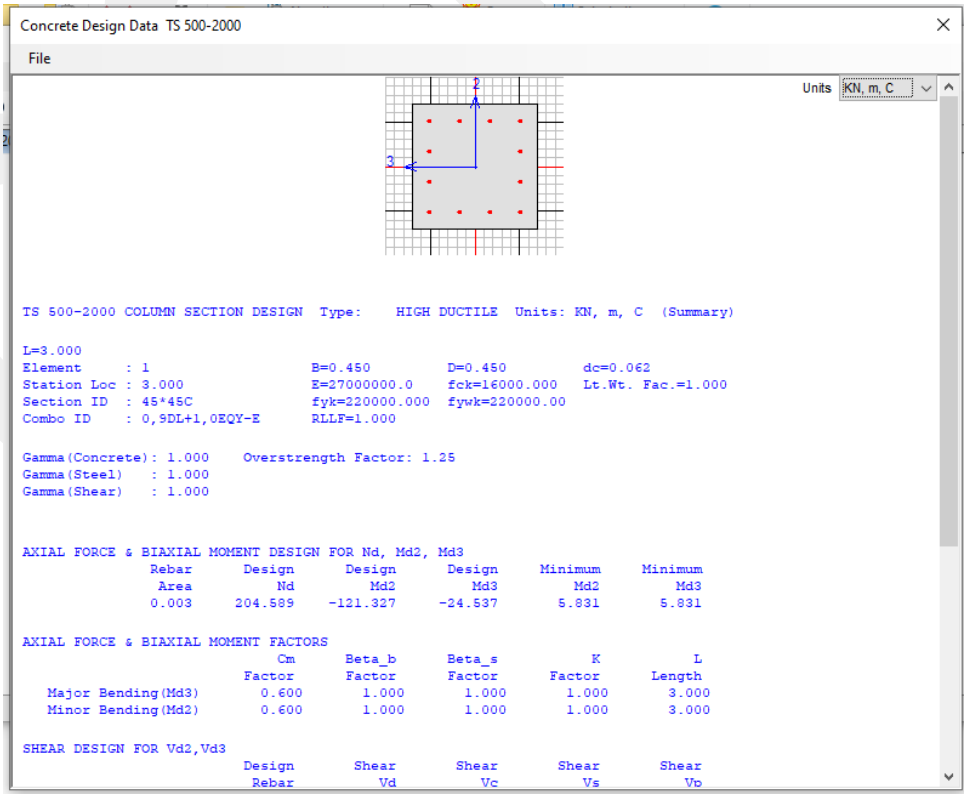

Figure App.26 RC Column Design Results of Model 6-ND-EE

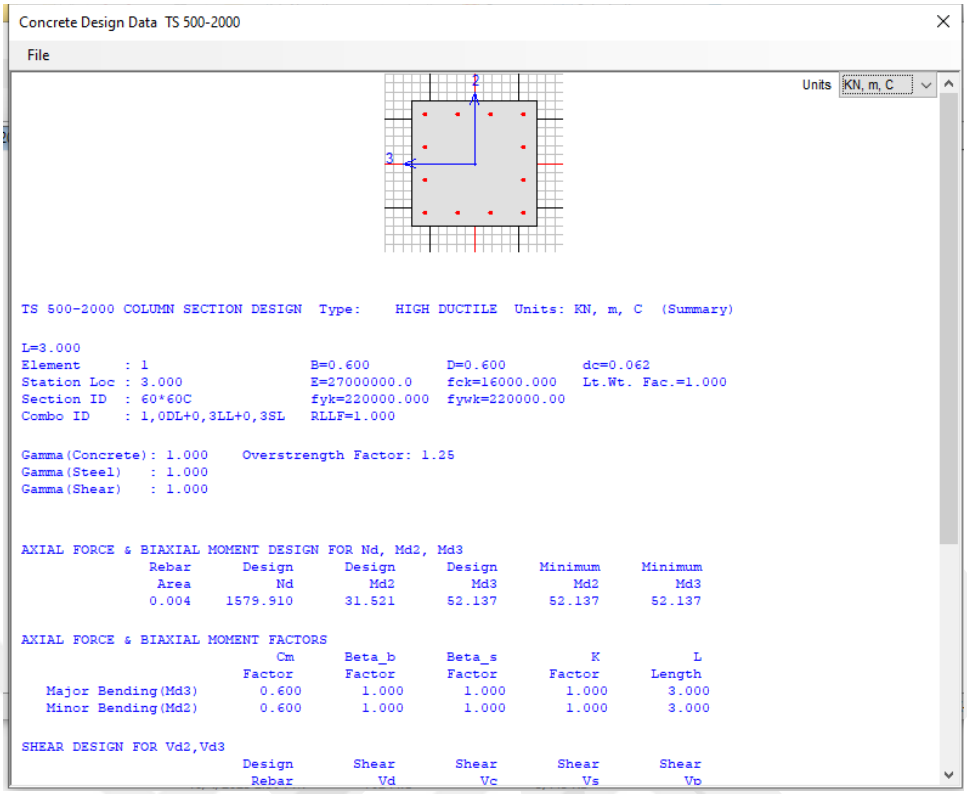

Figure App.27 RC Column Design Results of Model 9-ND-EE

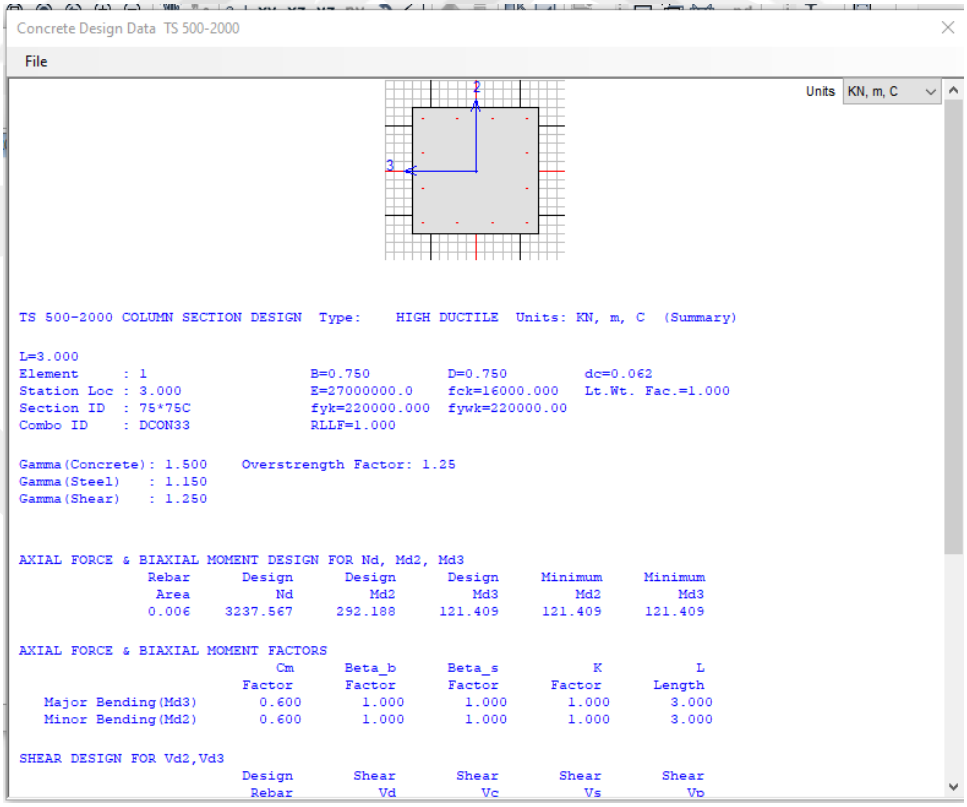

Figure App.28 RC Column Design Results of Model 12-ND-EE

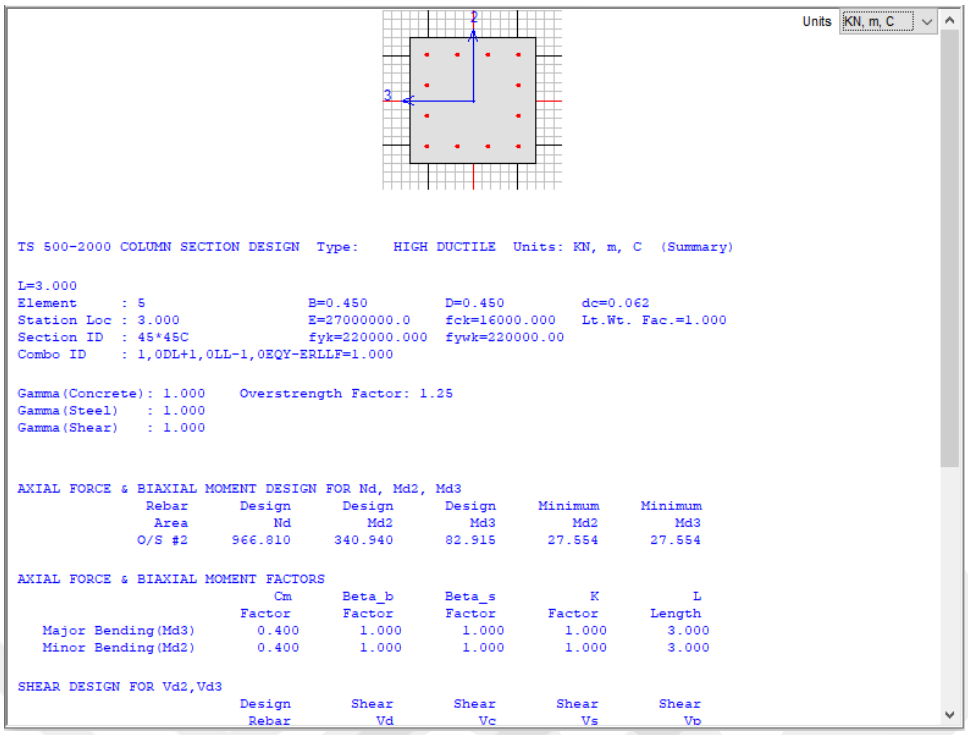

Units KN, m, C

TS 500-2000 COLUMN SECTION DESIGN Type: HIGH DUCTILE Units: KN, m, C (Summary)

L=3.000
Element : 5 B=0.450 D=0.450 dc=0.062
Station Loc : 3.000 E=27000000.0 fck=16000.000 Lt.Wt. Fac.=1.000
Section ID : 45*45C fyk=220000.000 fywk=220000.00
Combo ID : 1,0DL+1,0LL-1,0EQY-ERLLF=1.000

Gamma(Concrete): 1.000 Overstrength Factor: 1.25
Gamma(Steel) : 1.000
Gamma(Shear) : 1.000

AXIAL FORCE & BIAXIAL MOMENT DESIGN FOR Nd, Md2, Md3

	Rebar Area	Design Nd	Design Md2	Design Md3	Minimum Md2	Minimum Md3
	O/S #2	966.810	340.940	82.915	27.554	27.554

AXIAL FORCE & BIAXIAL MOMENT FACTORS

	Cm Factor	Beta_b Factor	Beta_s Factor	K Factor	L Length
Major Bending(Md3)	0.400	1.000	1.000	1.000	3.000
Minor Bending(Md2)	0.400	1.000	1.000	1.000	3.000

SHEAR DESIGN FOR Vd2,Vd3

	Design Rebar	Shear Vd	Shear Vc	Shear Vs	Shear Vp

Figure App.29 RC Column Design Results of Model 3-D-EE

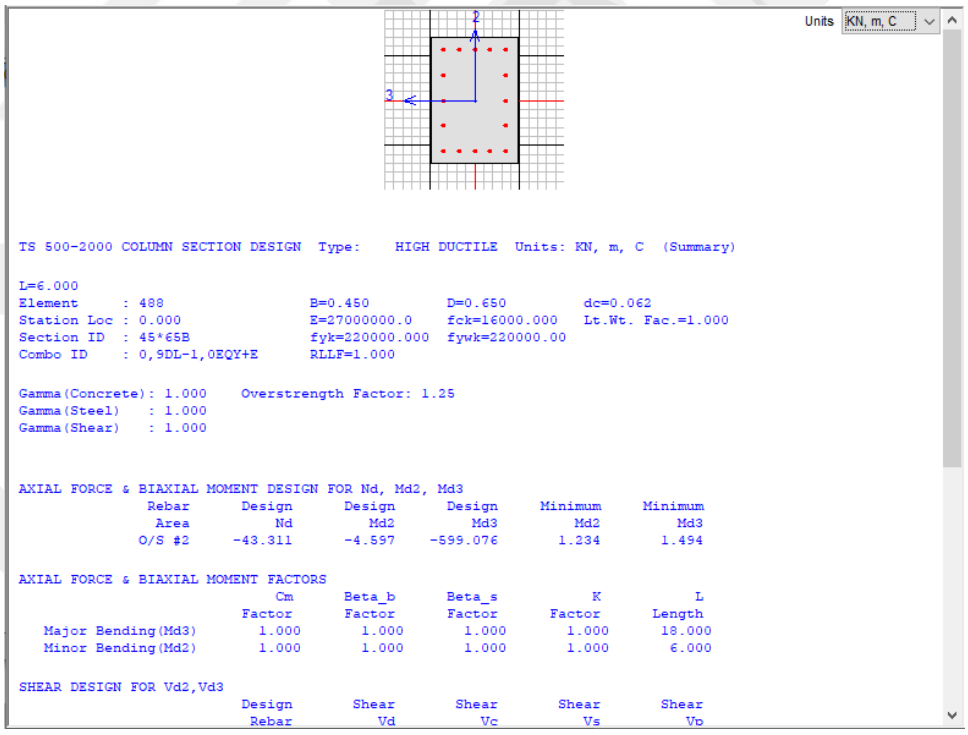

Units KN, m, C

TS 500-2000 COLUMN SECTION DESIGN Type: HIGH DUCTILE Units: KN, m, C (Summary)

L=6.000
Element : 488 B=0.450 D=0.650 dc=0.062
Station Loc : 0.000 E=27000000.0 fck=16000.000 Lt.Wt. Fac.=1.000
Section ID : 45*65B fyk=220000.000 fywk=220000.00
Combo ID : 0,9DL-1,0EQY+E RLLF=1.000

Gamma(Concrete): 1.000 Overstrength Factor: 1.25
Gamma(Steel) : 1.000
Gamma(Shear) : 1.000

AXIAL FORCE & BIAXIAL MOMENT DESIGN FOR Nd, Md2, Md3

	Rebar Area	Design Nd	Design Md2	Design Md3	Minimum Md2	Minimum Md3
	O/S #2	-43.311	-4.597	-599.076	1.234	1.494

AXIAL FORCE & BIAXIAL MOMENT FACTORS

	Cm Factor	Beta_b Factor	Beta_s Factor	K Factor	L Length
Major Bending(Md3)	1.000	1.000	1.000	1.000	18.000
Minor Bending(Md2)	1.000	1.000	1.000	1.000	6.000

SHEAR DESIGN FOR Vd2,Vd3

	Design Rebar	Shear Vd	Shear Vc	Shear Vs	Shear Vp

Figure App.30 RC Column Design Results of Model 6-D-EE

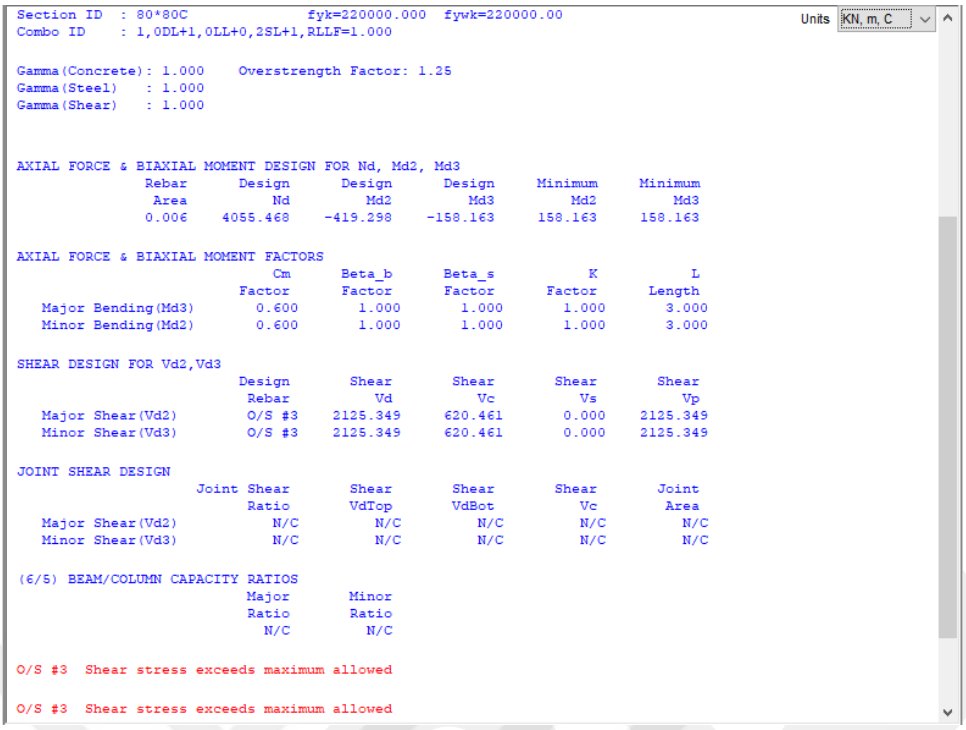

```
Section ID   : 80*80C              fyk=220000.000  fywk=220000.00
Combo ID     : 1,0DL+1,0LL+0,2SL+1,RLLF=1.000

Gamma(Concrete): 1.000    Overstrength Factor: 1.25
Gamma(Steel)   : 1.000
Gamma(Shear)   : 1.000


AXIAL FORCE & BIAXIAL MOMENT DESIGN FOR Nd, Md2, Md3
               Rebar      Design      Design      Design     Minimum     Minimum
               Area          Nd         Md2         Md3         Md2         Md3
              0.006    4055.468    -419.298    -158.163     158.163     158.163

AXIAL FORCE & BIAXIAL MOMENT FACTORS
                           Cm      Beta_b      Beta_s           K           L
                       Factor      Factor      Factor      Factor      Length
   Major Bending(Md3)   0.600       1.000       1.000       1.000       3.000
   Minor Bending(Md2)   0.600       1.000       1.000       1.000       3.000

SHEAR DESIGN FOR Vd2,Vd3
                       Design       Shear       Shear       Shear       Shear
                       Rebar          Vd          Vc          Vs          Vp
   Major Shear(Vd2)    O/S #3    2125.349     620.461       0.000    2125.349
   Minor Shear(Vd3)    O/S #3    2125.349     620.461       0.000    2125.349

JOINT SHEAR DESIGN
                    Joint Shear       Shear       Shear       Shear       Joint
                          Ratio       VdTop       VdBot          Vc        Area
   Major Shear(Vd2)         N/C         N/C         N/C         N/C         N/C
   Minor Shear(Vd3)         N/C         N/C         N/C         N/C         N/C

(6/5) BEAM/COLUMN CAPACITY RATIOS
                       Major       Minor
                       Ratio       Ratio
                         N/C         N/C

O/S #3  Shear stress exceeds maximum allowed

O/S #3  Shear stress exceeds maximum allowed
```

Figure App.31 RC Column Design Results of Model 9-D-EE

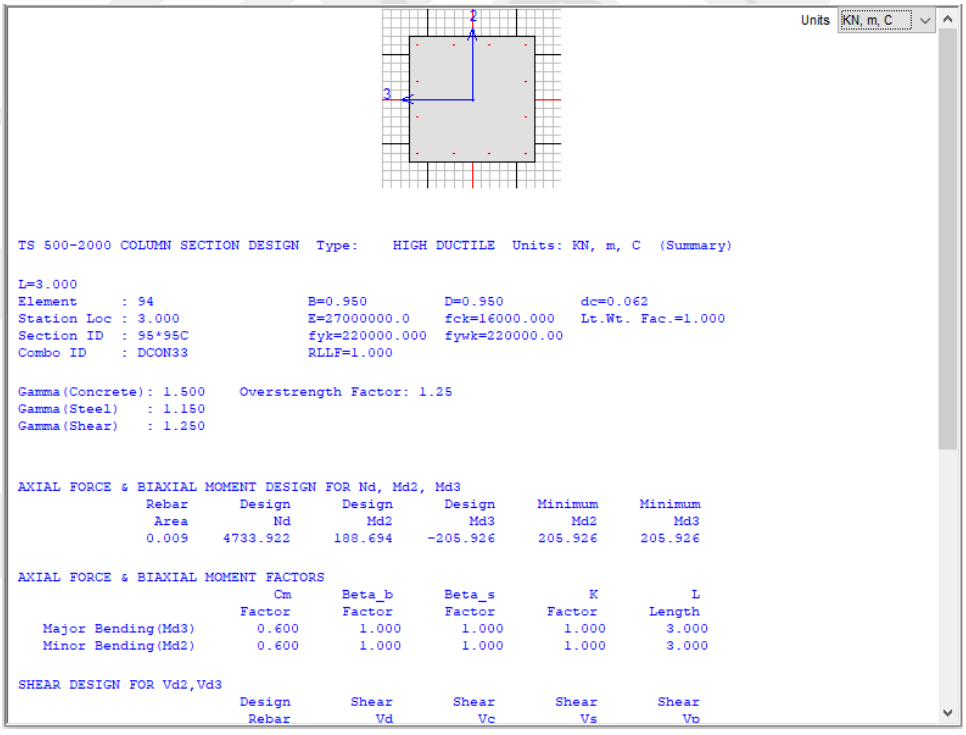

```
TS 500-2000 COLUMN SECTION DESIGN  Type:    HIGH DUCTILE  Units: KN, m, C  (Summary)

L=3.000
Element     : 94                B=0.950         D=0.950         dc=0.062
Station Loc : 3.000             E=27000000.0    fck=16000.000   Lt.Wt. Fac.=1.000
Section ID  : 95*95C            fyk=220000.000  fywk=220000.00
Combo ID    : DCON33            RLLF=1.000

Gamma(Concrete): 1.500    Overstrength Factor: 1.25
Gamma(Steel)   : 1.150
Gamma(Shear)   : 1.250


AXIAL FORCE & BIAXIAL MOMENT DESIGN FOR Nd, Md2, Md3
               Rebar      Design      Design      Design     Minimum     Minimum
               Area          Nd         Md2         Md3         Md2         Md3
              0.009    4733.922     188.694    -205.926     205.926     205.926

AXIAL FORCE & BIAXIAL MOMENT FACTORS
                           Cm      Beta_b      Beta_s           K           L
                       Factor      Factor      Factor      Factor      Length
   Major Bending(Md3)   0.600       1.000       1.000       1.000       3.000
   Minor Bending(Md2)   0.600       1.000       1.000       1.000       3.000

SHEAR DESIGN FOR Vd2,Vd3
                       Design       Shear       Shear       Shear       Shear
                       Rebar          Vd          Vc          Vs          Vp
```

Figure App.32 RC Column Design Results of Model 12-D-EE

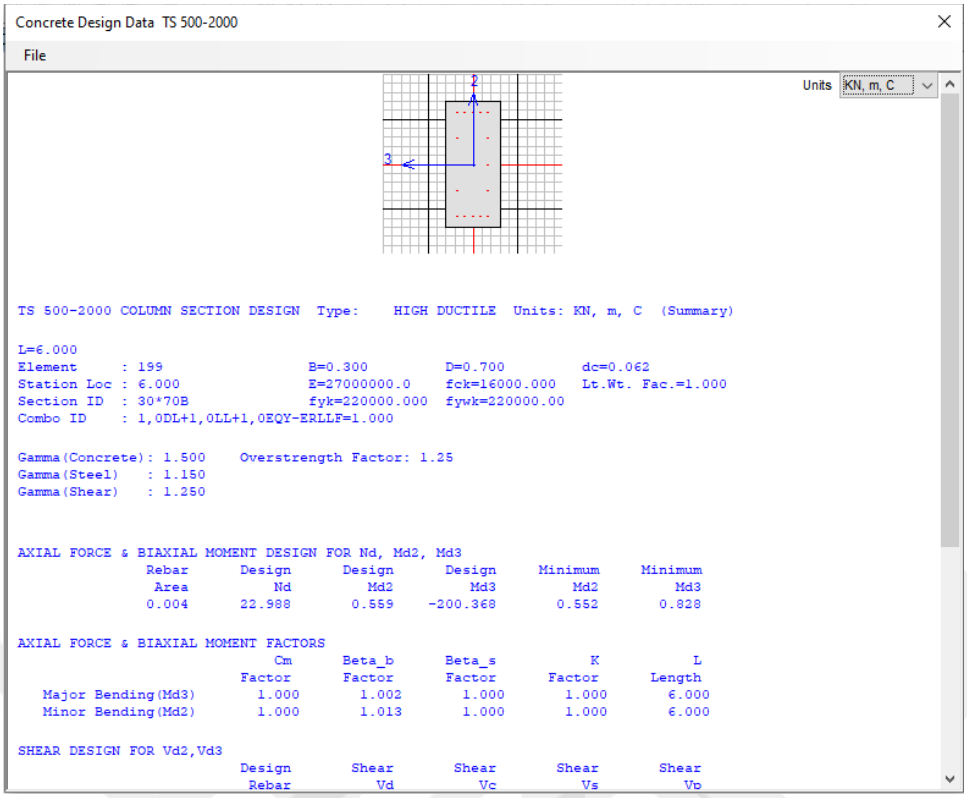

Figure App.33 RC Column Design Results of Model 3-SV-EE

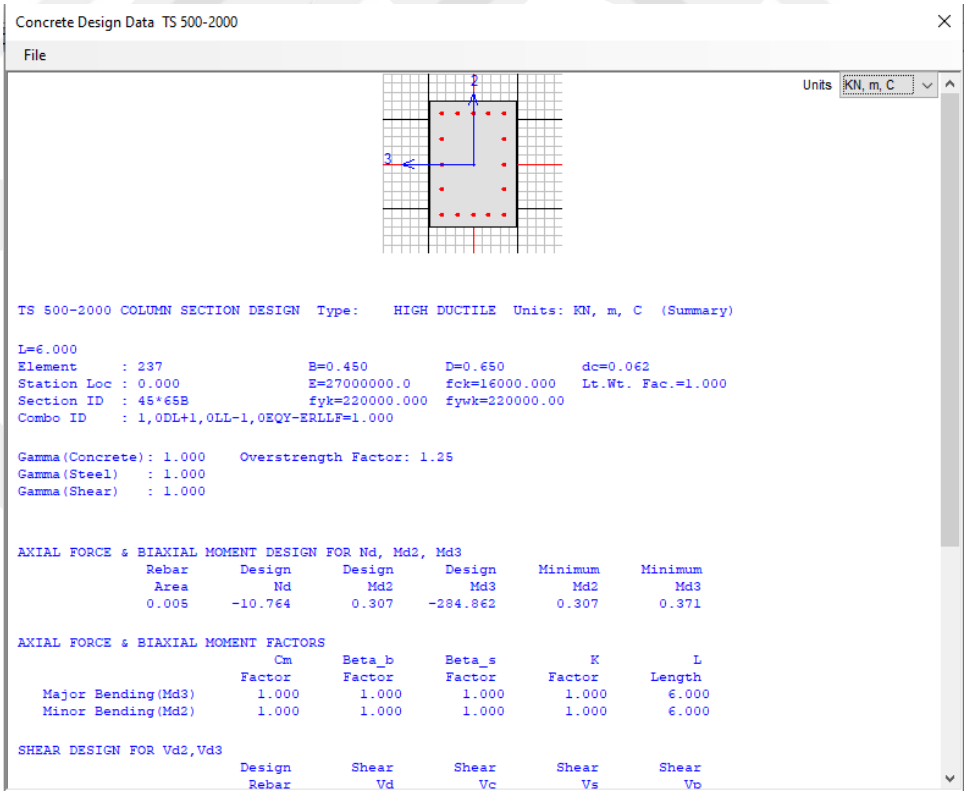

Figure App.34 RC Column Design Results of Model 6-SV-EE

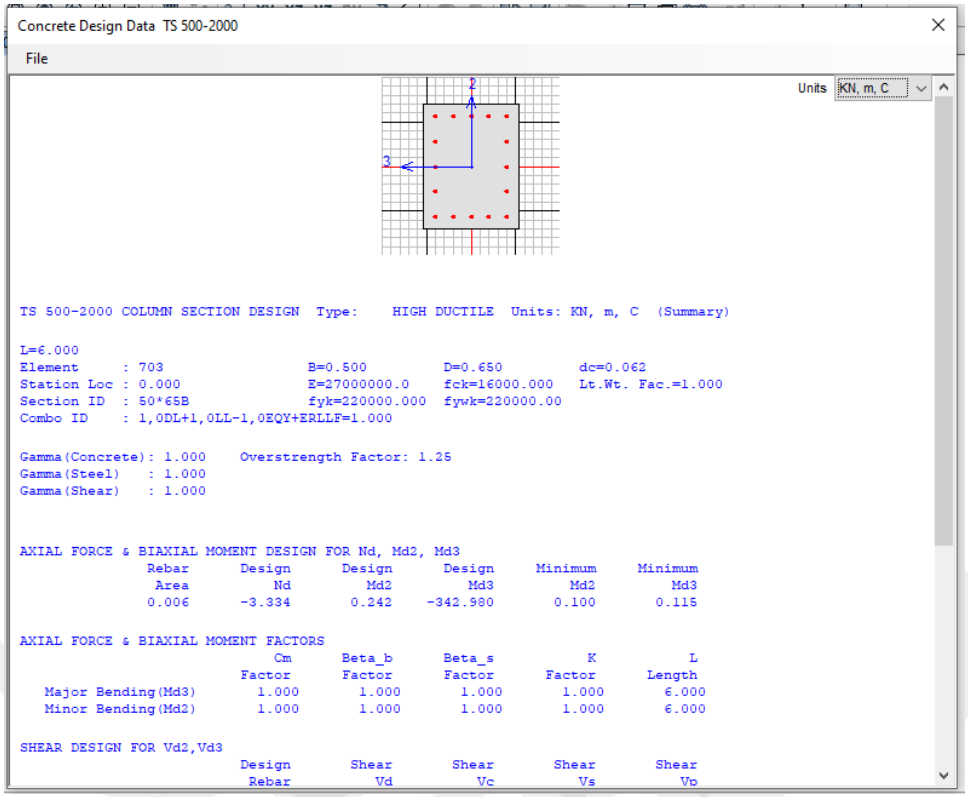

Figure App.35 RC Column Design Results of Model 9-SV-EE

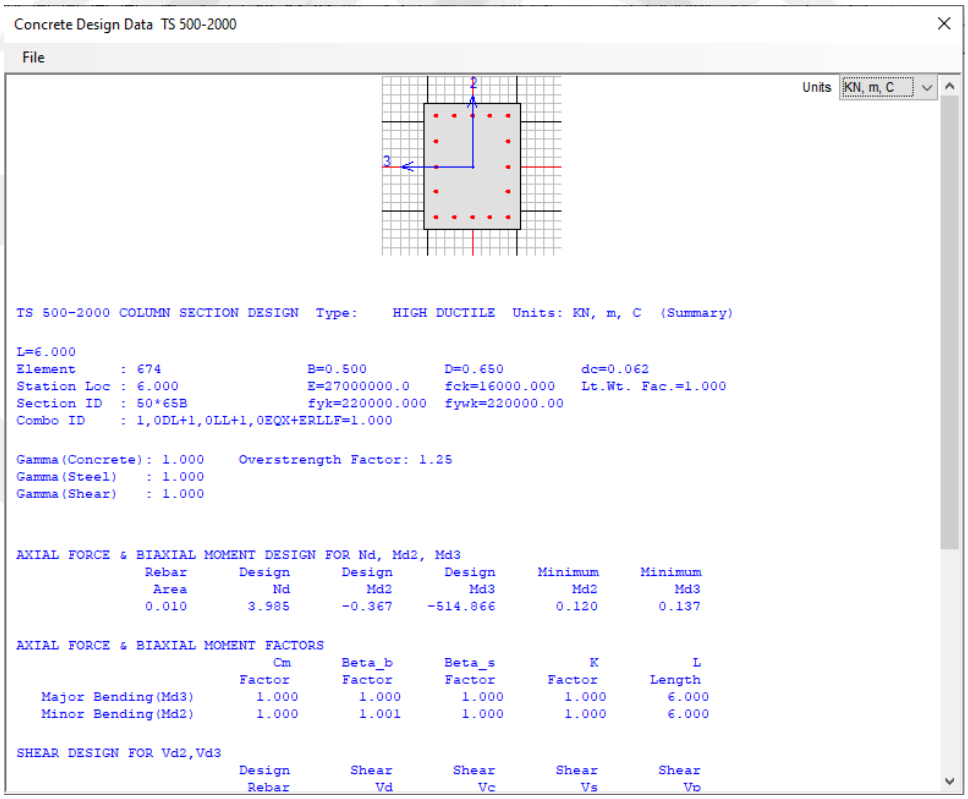

Figure App.36 RC Column Design Results of Model 12-SV-EE

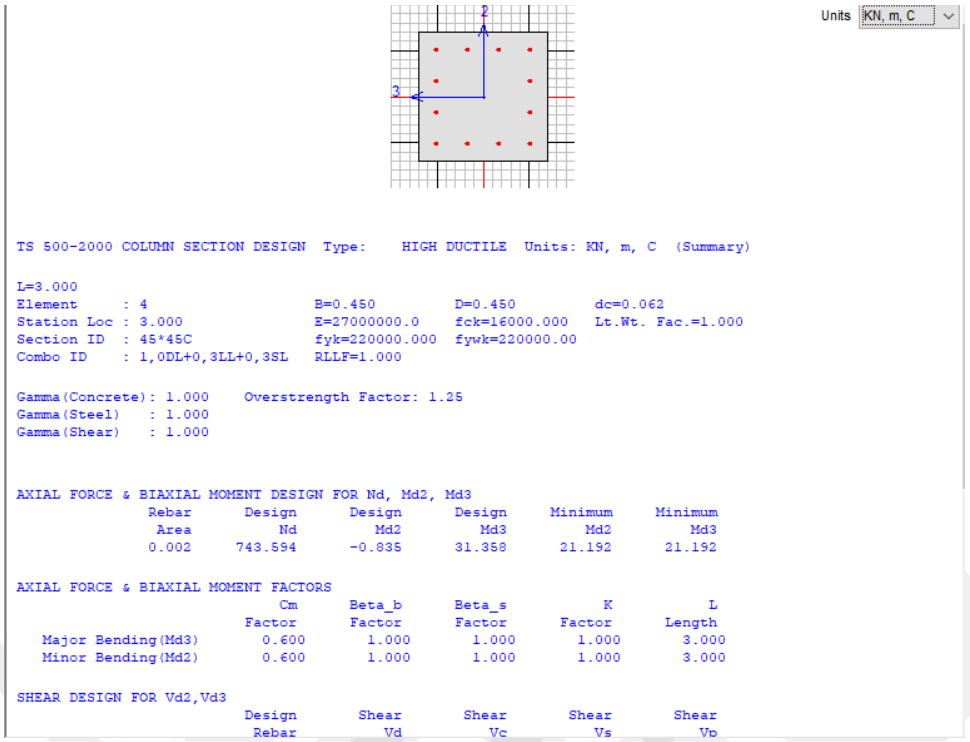

Units KN, m, C

TS 500-2000 COLUMN SECTION DESIGN Type: HIGH DUCTILE Units: KN, m, C (Summary)

L=3.000
Element : 4 B=0.450 D=0.450 dc=0.062
Station Loc : 3.000 E=27000000.0 fck=16000.000 Lt.Wt. Fac.=1.000
Section ID : 45*45C fyk=220000.000 fywk=220000.00
Combo ID : 1,0DL+0,3LL+0,3SL RLLF=1.000

Gamma(Concrete): 1.000 Overstrength Factor: 1.25
Gamma(Steel) : 1.000
Gamma(Shear) : 1.000

AXIAL FORCE & BIAXIAL MOMENT DESIGN FOR Nd, Md2, Md3

Rebar Area	Design Nd	Design Md2	Design Md3	Minimum Md2	Minimum Md3
0.002	743.594	-0.835	31.358	21.192	21.192

AXIAL FORCE & BIAXIAL MOMENT FACTORS

	Cm Factor	Beta_b Factor	Beta_s Factor	K Factor	L Length
Major Bending(Md3)	0.600	1.000	1.000	1.000	3.000
Minor Bending(Md2)	0.600	1.000	1.000	1.000	3.000

SHEAR DESIGN FOR Vd2,Vd3

Design Rebar	Shear Vd	Shear Vc	Shear Vs	Shear Vp

Figure App.37 RC Column Design Results of Model 3-SX-EE

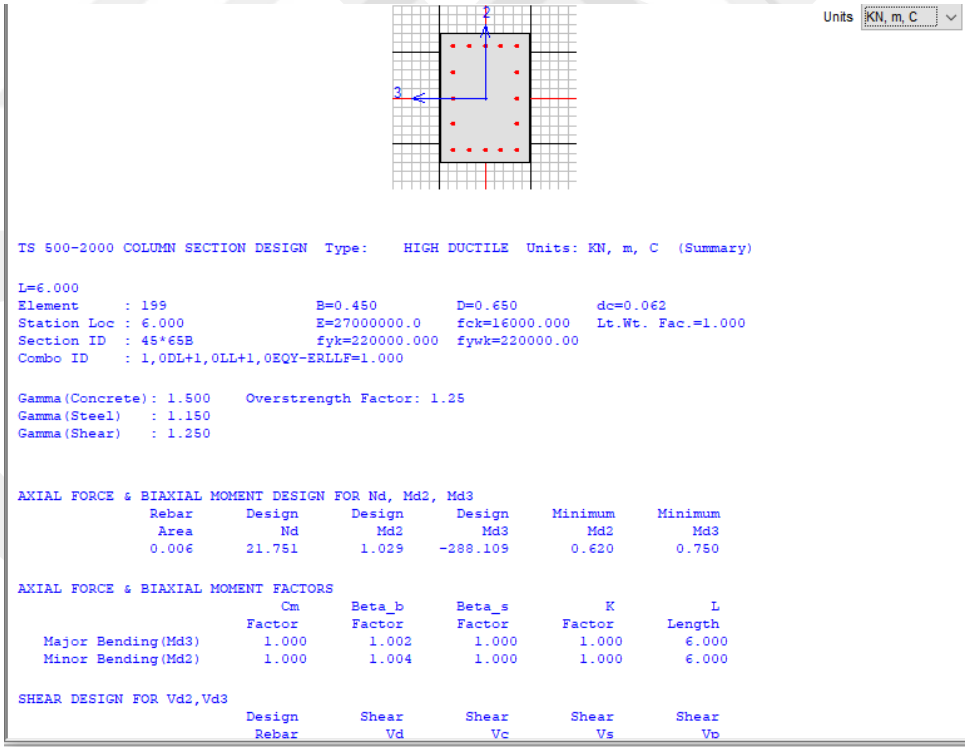

Units KN, m, C

TS 500-2000 COLUMN SECTION DESIGN Type: HIGH DUCTILE Units: KN, m, C (Summary)

L=6.000
Element : 199 B=0.450 D=0.650 dc=0.062
Station Loc : 6.000 E=27000000.0 fck=16000.000 Lt.Wt. Fac.=1.000
Section ID : 45*65B fyk=220000.000 fywk=220000.00
Combo ID : 1,0DL+1,0LL+1,0EQY-ERLLF=1.000

Gamma(Concrete): 1.500 Overstrength Factor: 1.25
Gamma(Steel) : 1.150
Gamma(Shear) : 1.250

AXIAL FORCE & BIAXIAL MOMENT DESIGN FOR Nd, Md2, Md3

Rebar Area	Design Nd	Design Md2	Design Md3	Minimum Md2	Minimum Md3
0.006	21.751	1.029	-288.109	0.620	0.750

AXIAL FORCE & BIAXIAL MOMENT FACTORS

	Cm Factor	Beta_b Factor	Beta_s Factor	K Factor	L Length
Major Bending(Md3)	1.000	1.002	1.000	1.000	6.000
Minor Bending(Md2)	1.000	1.004	1.000	1.000	6.000

SHEAR DESIGN FOR Vd2,Vd3

Design Rebar	Shear Vd	Shear Vc	Shear Vs	Shear Vp

Figure App.38 RC Column Design Results of Model 6-SX-EE

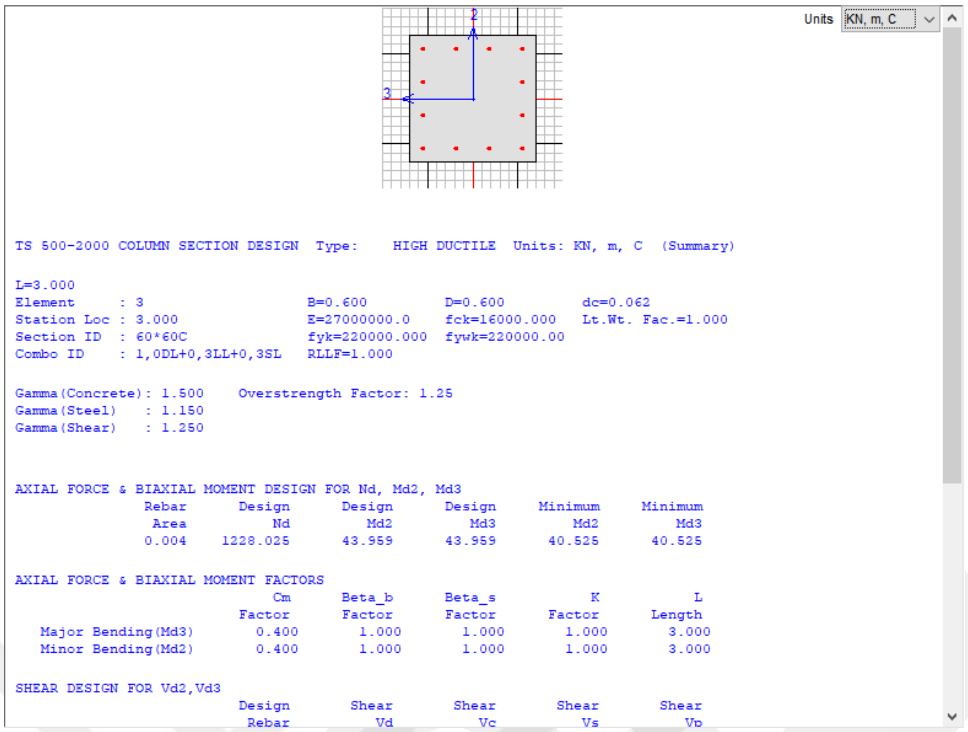

Units KN, m, C

TS 500-2000 COLUMN SECTION DESIGN Type: HIGH DUCTILE Units: KN, m, C (Summary)

L=3.000
Element : 3 B=0.600 D=0.600 dc=0.062
Station Loc : 3.000 E=27000000.0 fck=16000.000 Lt.Wt. Fac.=1.000
Section ID : 60*60C fyk=220000.000 fywk=220000.00
Combo ID : 1,0DL+0,3LL+0,3SL RLLF=1.000

Gamma(Concrete): 1.500 Overstrength Factor: 1.25
Gamma(Steel) : 1.150
Gamma(Shear) : 1.250

AXIAL FORCE & BIAXIAL MOMENT DESIGN FOR Nd, Md2, Md3

Rebar Area	Design Nd	Design Md2	Design Md3	Minimum Md2	Minimum Md3
0.004	1228.025	43.959	43.959	40.525	40.525

AXIAL FORCE & BIAXIAL MOMENT FACTORS

	Cm Factor	Beta_b Factor	Beta_s Factor	K Factor	L Length
Major Bending(Md3)	0.400	1.000	1.000	1.000	3.000
Minor Bending(Md2)	0.400	1.000	1.000	1.000	3.000

SHEAR DESIGN FOR Vd2,Vd3

	Design Rebar	Shear Vd	Shear Vc	Shear Vs	Shear Vp

Figure App.39 RC Column Design Results of Model 9-SX-EE

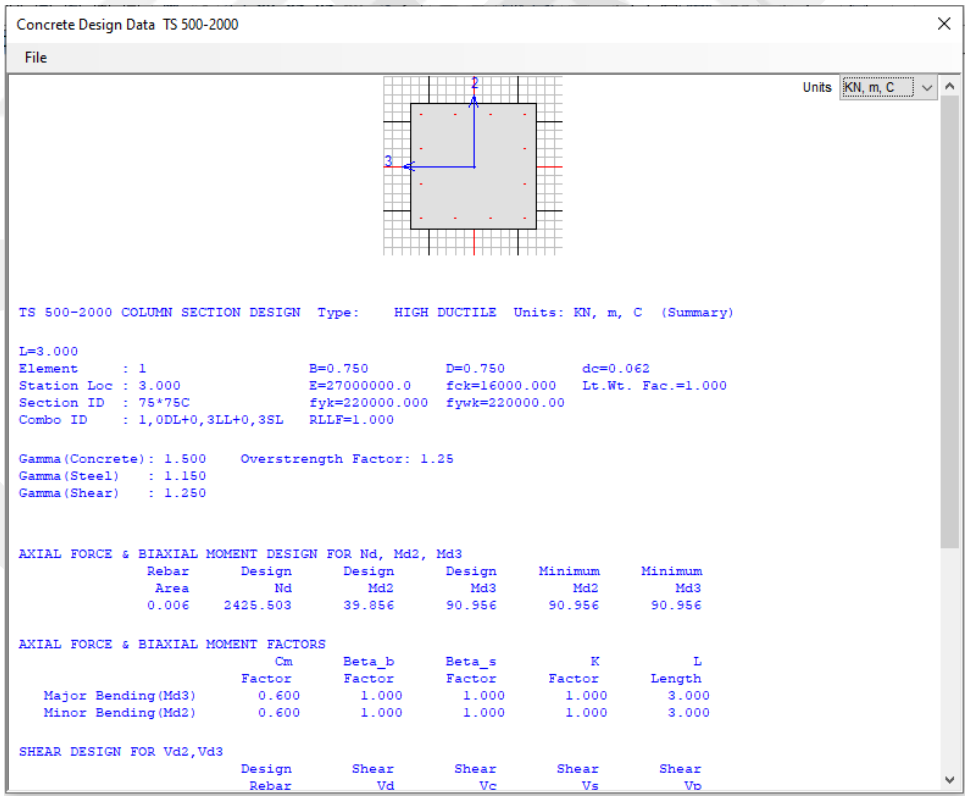

Concrete Design Data TS 500-2000

File

Units KN, m, C

TS 500-2000 COLUMN SECTION DESIGN Type: HIGH DUCTILE Units: KN, m, C (Summary)

L=3.000
Element : 1 B=0.750 D=0.750 dc=0.062
Station Loc : 3.000 E=27000000.0 fck=16000.000 Lt.Wt. Fac.=1.000
Section ID : 75*75C fyk=220000.000 fywk=220000.00
Combo ID : 1,0DL+0,3LL+0,3SL RLLF=1.000

Gamma(Concrete): 1.500 Overstrength Factor: 1.25
Gamma(Steel) : 1.150
Gamma(Shear) : 1.250

AXIAL FORCE & BIAXIAL MOMENT DESIGN FOR Nd, Md2, Md3

Rebar Area	Design Nd	Design Md2	Design Md3	Minimum Md2	Minimum Md3
0.006	2425.503	39.856	90.956	90.956	90.956

AXIAL FORCE & BIAXIAL MOMENT FACTORS

	Cm Factor	Beta_b Factor	Beta_s Factor	K Factor	L Length
Major Bending(Md3)	0.600	1.000	1.000	1.000	3.000
Minor Bending(Md2)	0.600	1.000	1.000	1.000	3.000

SHEAR DESIGN FOR Vd2,Vd3

	Design Rebar	Shear Vd	Shear Vc	Shear Vs	Shear Vp

Figure App.40 RC Column Design Results of Model 12-SX-EE

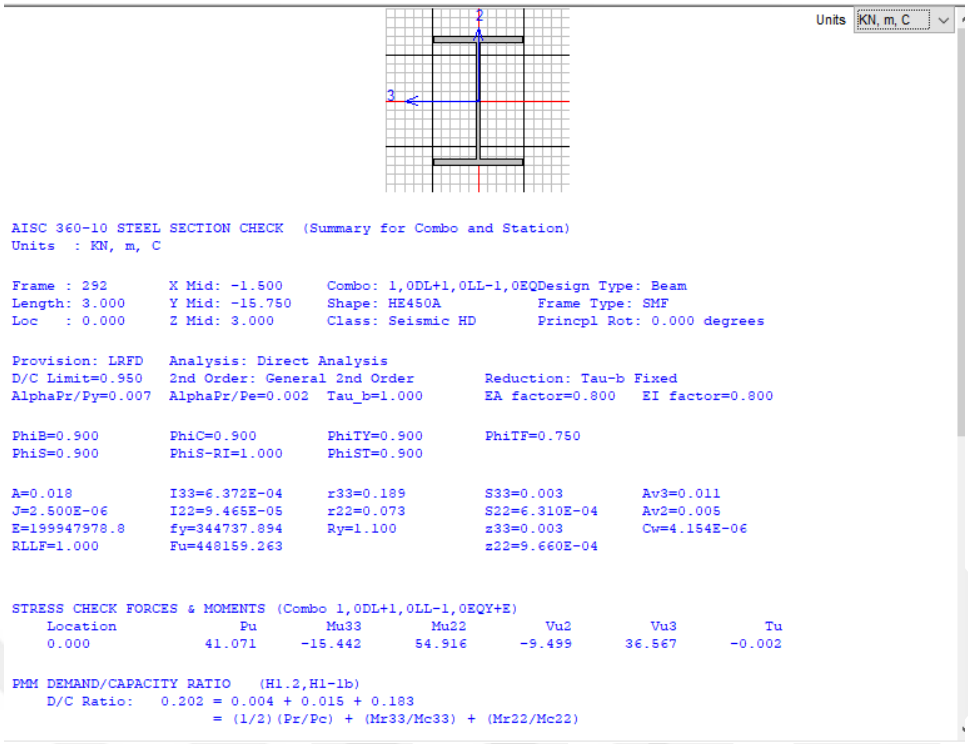


```
AISC 360-10 STEEL SECTION CHECK  (Summary for Combo and Station)
Units  : KN, m, C

Frame : 292       X Mid: -1.500     Combo: 1,0DL+1,0LL-1,0EQDesign Type: Beam
Length: 3.000     Y Mid: -15.750    Shape: HE450A          Frame Type: SMF
Loc   : 0.000     Z Mid: 3.000      Class: Seismic HD      Princpl Rot: 0.000 degrees

Provision: LRFD   Analysis: Direct Analysis
D/C Limit=0.950   2nd Order: General 2nd Order        Reduction: Tau-b Fixed
AlphaPr/Py=0.007  AlphaPr/Pe=0.002  Tau_b=1.000      EA factor=0.800   EI factor=0.800

PhiB=0.900        PhiC=0.900        PhiTY=0.900      PhiTF=0.750
PhiS=0.900        PhiS-RI=1.000     PhiST=0.900

A=0.018           I33=6.372E-04     r33=0.189        S33=0.003         Av3=0.011
J=2.500E-06       I22=9.465E-05     r22=0.073        S22=6.310E-04     Av2=0.005
E=199947978.8     fy=344737.894     Ry=1.100         z33=0.003         Cw=4.154E-06
RLLF=1.000        Fu=448159.263                      z22=9.660E-04


STRESS CHECK FORCES & MOMENTS (Combo 1,0DL+1,0LL-1,0EQY+E)
    Location          Pu         Mu33        Mu22         Vu2         Vu3          Tu
    0.000         41.071      -15.442      54.916      -9.499      36.567      -0.002

PMM DEMAND/CAPACITY RATIO   (H1.2,H1-1b)
    D/C Ratio:   0.202 = 0.004 + 0.015 + 0.183
                       = (1/2)(Pr/Pc) + (Mr33/Mc33) + (Mr22/Mc22)
```

Figure App.41 Steel Bracing Design Results of Model 3-SX-EE

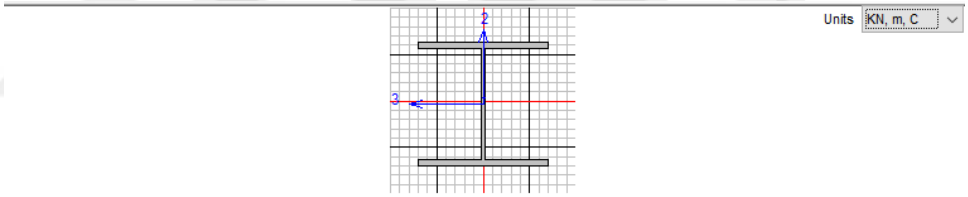


```
AISC 360-10 STEEL SECTION CHECK  (Summary for Combo and Station)
Units  : KN, m, C

Frame : 487       X Mid: -15.850    Combo: 1,0DL+1,0LL+1,0EQDesign Type: Brace
Length: 3.354     Y Mid: 1.500      Shape: HE200A          Frame Type: SMF
Loc   : 0.000     Z Mid: 3.750      Class: Non-Compact     Princpl Rot: 0.000 degrees

Provision: LRFD   Analysis: Direct Analysis
D/C Limit=0.950   2nd Order: General 2nd Order        Reduction: Tau-b Fixed
AlphaPr/Py=0.155  AlphaPr/Pe=0.491  Tau_b=1.000      EA factor=0.800   EI factor=0.800

PhiB=0.900        PhiC=0.900        PhiTY=0.900      PhiTF=0.750
PhiS=0.900        PhiS-RI=1.000     PhiST=0.900

A=0.005           I33=3.692E-05     r33=0.083        S33=3.886E-04     Av3=0.003
J=0.000           I22=1.336E-05     r22=0.050        S22=1.336E-04     Av2=0.001
E=199947978.8     fy=344737.894     Ry=1.100         z33=4.290E-04     Cw=0.000
RLLF=1.000        Fu=448159.263                      z22=2.040E-04


STRESS CHECK FORCES & MOMENTS (Combo 1,0DL+1,0LL+1,0EQY-E)
    Location          Pu         Mu33        Mu22         Vu2         Vu3          Tu
    0.000       -287.731      -1.244       0.801      -1.479       0.234       0.004

PMM DEMAND/CAPACITY RATIO   (H1-1a)
    D/C Ratio:   0.642 = 0.622 + 0.008 + 0.012
                       = (Pr/Pc) + (8/9)(Mr33/Mc33) + (8/9)(Mr22/Mc22)
```

Figure App.42 Steel Bracing Design Results of Model 6-SX-EE

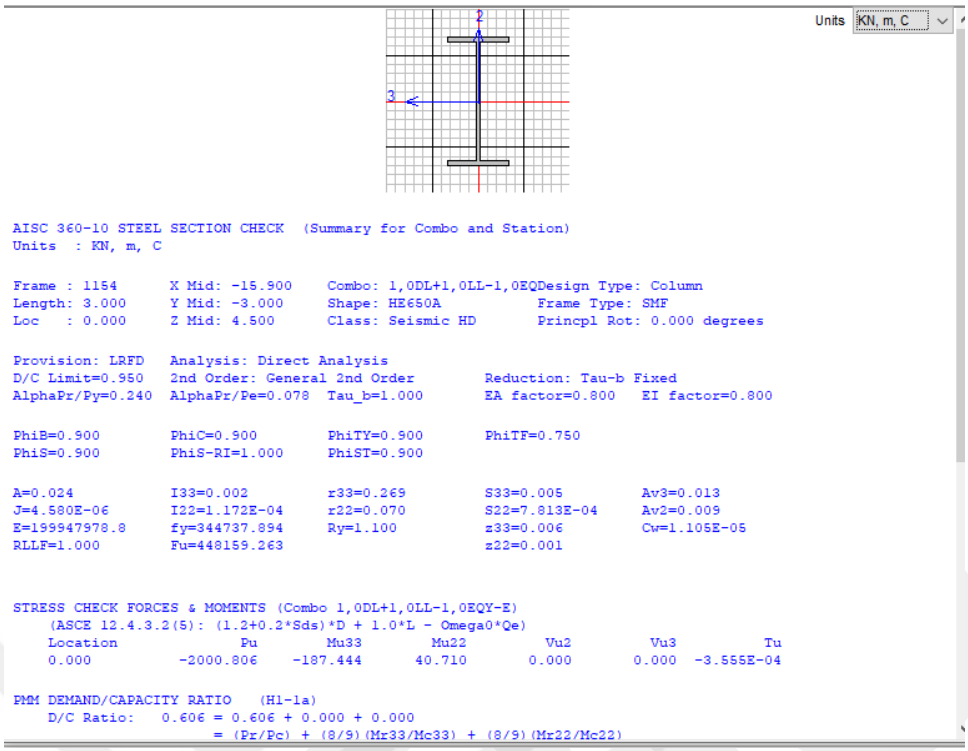

Figure App.43 Steel Bracing Design Results of Model 9-SX-EE

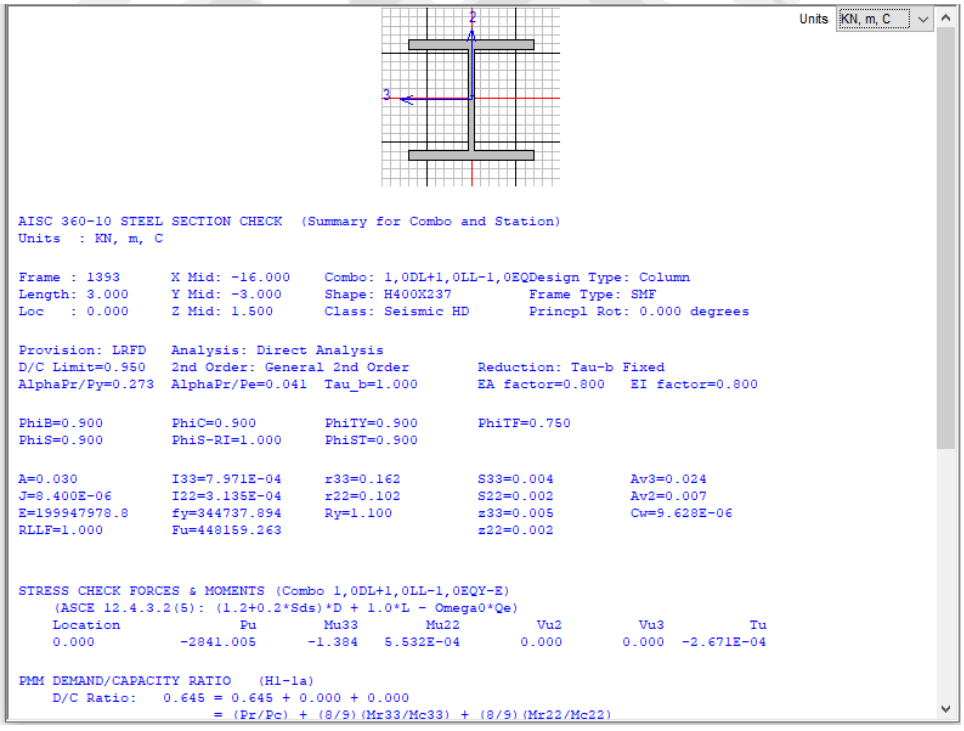

Figure App.44 Steel Bracing Design Results of Model 12-SX-EE